UC Berkeley
UC Berkeley Electronic Theses and Dissertations

Title

Functional Polymer Architectures for Solution Processed Organic Light Emitting Diodes

Permalink

https://escholarship.org/uc/item/7wz809z9

Author

Poulsen, Daniel Andrew

Publication Date

2010

Peer reviewed|Thesis/dissertation

Functional Polymer Architectures for
Solution Processed Organic Light Emitting Diodes

By

Daniel Andrew Poulsen

A dissertation submitted in partial satisfaction of the

requirements for the degree of

Doctor of Philosophy

in

Chemistry

in the

Graduate Division

of the

University of California, Berkeley

Committee in charge:

Professor Jean M. J. Fréchet
Professor Jeffrey R. Long
Professor Michael F. Crommie

Spring 2010

Functional Polymer Architectures for Solution Processed Organic Light Emitting Diodes

Copyright 2010

By

Daniel Andrew Poulsen

Abstract

Functional Polymer Architectures for
Solution Processed Organic Light Emitting Diodes

by

Daniel Andrew Poulsen

Doctor of Philosophy in Chemistry

University of California, Berkeley

Professor Jean M. J. Fréchet, Chair

Organic light emitting diodes (OLED) prepared from electroactive materials show great potential for multicolor display and white light source applications. Unfortunately, the commercialization of multilayer OLEDs has been slow. This can be attributed in part to the vapor deposition technique used to assemble small molecule thin films. The process is not amenable to large area displays and is relatively costly. An attractive alternative solution to this problem is to replace small molecules with organic polymers, which could be solution processed in an efficient and economical manner. Polymeric materials also offer the unique potential to achieve nanoscale self-assembled structures through their functional architecture. These materials can be solution processed and mimic multilayered small molecule devices to achieve improved performance and/or balanced color. Design and synthesis and OLED testing of functional polymers which can achieve defined multilayer or nanostructured film characteristics through simple solution processing is the focus of this thesis.

In Chapter 1, the history of OLED materials as well as the device mechanism and key organic electronic characteristics necessary for high performance devices is introduced. There is also a discussion on the methods for device testing and characterization.

The design and synthesis of novel dendronized linear polymer host materials is presented in Chapter 2. These polymers should possess a rigid linear rod like architecture which had not been investigated for its potential to order a thin film in an assembly of cylindrical structures. This host material was desired in order to optimize the interface of hole and electron transporting material to achieve improved recombination in the thin film.

Similarly, in Chapter 3 a diblock copolymer architecture is studied as host material in OLED devices. In this work the differences between nanoscale self assembled diblock copolymers of hole and electron transporting units and random copolymers of the same composition are studied. These materials show a high external quantum efficiency of 5.6 % for a

simply prepared single layer device which is enabled by the self-assembly of the functional diblock copolymer architecture.

In Chapter 4, these diblock copolymers are exploited not only to create nanoscale domains of hole and electron transporting domains but also to organize the site isolation of two different colored phosphorescent emitters. Polymerizable heteroleptic iridium complexes of different color were developed and covalently incorporated into separate blocks of the diblock copolymer. Following the self assembly of thin film morphology through simple spin coating, the energy transfer from blue to red emitters was greatly reduced enabling synergistic dual emission for white electroluminescence.

Chapter 5 discusses the design and synthesis of electroactive crosslinked polymer nanoparticles with nanoscale size that can achieve the site isolation of emitters. Using different polymerizable iridium complexes, batches of different colored polymer nanoparticles can be simply prepared and mixed at the device preparation stage in any ratio to yield tunable colored devices. These nanoparticles dispersions behave as light emitting inks which can be simply solution processed with predictable and stable electroluminescent color.

In Chapter 6, difunctional polymerizable iridium complexes are used to achieve multilayer structures of electron blocking layers and phosphorescent emissive layers. These small molecules can be solution processed to yield thin films which can be crosslinked through simple heating step. A subsequent layer can then be deposited on top to build up all solution processed multilayered devices. A select high triplet energy crosslinkable iridium complex was shown to perform well as an electron blocker and hole transporting layer in OLEDs with improved performance over the standard water soluble hole transporting layer poly(3,4-ethylenedioxythiophene) poly(styrenesulfonate) (PEDOT:PSS).

This dissertation is dedicated to my mother, Erika Rempel Poulsen.
For all the love, guidance and support in everything I have ever done.

Table of Contents

Acknowledgments

Over the course of my graduate career I have been helped along by many important people. These individuals contributed greatly in shaping me as a scientist and charting the direction of my research. I would like to acknowledge their impact on my life and the work in this dissertation.

My sincere thanks goes to the members of my qualifying exam and dissertation committee; Prof. Jeffrey Long, Prof. Marcin Majda, Prof. Peter Vollhardt, Prof. Michael Crommie and lastly my advisor Prof. Jean M. J. Fréchet. Prof. Fréchet your encouragement, guidance and support as an advisor over the past five years has benefitted me immensely. I've grown as a scientist and a leader under your supervision. I want to thank you for giving me the opportunity to be a part of the Fréchet lab. I consider it a privilege to have worked with and learned from such an inspiring individual.

After moving to California from Canada in 2005 to start these studies there were certain individuals that made the transition much easier for me. Justin "Scoobie" Mynar, Frank Lauterwasser, Marian Snauko and Sridhar Rajaram acted as informal mentors for me in lab. It was always a great resource to know I could come to any of you for advice about anything. I am sincerely grateful to each of you for taking the time to teach me and for the friendships which have made moving far from home much more bearable. Although we may now be separated by distance, I hope I can repay you all in some way for taking the time to help me.

I am also in great debt to my most close collaborators in this work; Dr. Biwu Ma, Dr. Bumjoon Kim and Dr. Haifeng Gao. Biwu, your wealth of creativity and ideas was the spark that set many of these projects into motion. There is no doubt I would not be where I am without you. Bumjoon, your work ethic and drive helped push many of these projects to completion. On top of this, you were always a very humble person and an excellent teacher. Haifeng, your attention to detail, the scientific process and pure hard work has taught me how to be a better scientist. Brainstorming ideas and solving problems with you was one of the most fulfilling parts of coming to lab each day. Without each of you this work would never have been completed and I thank you for this and your friendship.

Apart from those who contributed directly to this work, I would also like to acknowledge several others who have made my time here memorable. The great friendships and good times spent outside of lab made my life more fulfilling. Thank you Clayton Mauldin, Paul Armstrong, Andrew Cramer, Tristan Beaudette, Brian Pujanauski, Tyler Holden, Derek van der Poll and all the other members of the Fréchet lab that have come and gone over the time I have been here.

On a more personal note, I would like to thank my family for supporting me over my entire journey in science and academics. Your encouragement and unconditional love has pushed me to towards this accomplishment. To my mother, you have always been there for me. There is nothing I can say that can express the love and gratitude I have for everything you have done for me. Being so far from home for the last five years has been hard, but hearing family news or

Chapter 1

An Introduction to Organic Light Emitting Diode Materials and Devices

Introduction

Historical Development

The first demonstration of an organic material undergoing electroluminescence was in 1950 by Bernanose et al.[1-5] They observed electroluminescence of acridine orange and quinacrine when placed in an alternating current field. Organic electroluminescence of anthracene single crystals through ohmic contact of electrodes was then demonstrated in 1963 by Pope et al.[6] This work used $10 - 20$ µm thick crystals with electrodes attached in epoxy that required 400 V direct current in order to observe electroluminescence. More work in this area led to devices with much lower voltages in 1982 by Vincett et. al.[7] The difference in this work was the use of much thinner anthracene films (~ 600 nm) that were vacuum deposited. This allowed for much lower device operating voltages (~ 12 V) yielding higher power conversion efficiencies.

The first use of polymers as electroluminescent material was by Partridge et al. in the early 80s.[8-12] This work was the first example of the use of a doped film of polyvinylcarbazole (PVK) as active material. They also highlighted the importance of selecting the work function of the cathode material to matching the electron affinity of the organic.

It was not until later that decade that the true practicality of organic electroluminescent devices was demonstrated by C. W. Tang et al. at Kodak with the preparation of a green organic light emitting diode (OLED) with an external quantum efficiency of 1 % that operated at lower than 10 V.[13-15] As the first report of a diode device, this work demonstrated that a modestly efficient thin film electroluminescent device could be prepared using two or more layers of thin films. It also popularized the use of tris(8-hydroxyquinolinato)aluminium (Alq_3) as a green OLED emitter and indium tin oxide (ITO) as the transparent anode.

In another major advancement, Friend et al. demonstrated in 1990 the first OLED using a conjugated organic polymer.[16-18] In this work a solution processable precursor to the conjugated polymer poly(p-phenylenevinylene) (PPV) was used. The problem of insolubility of PPV was overcome using this precursor to deposit film which was then heated under vacuum to yield the active PPV film. This work was seminal because it brought to light the potential of solution processable materials to make devices simpler, faster and easier to prepare. Cambridge Display Technology (CDT) was formed in 1992 to exploit this technique.

In 1998, the efficiency of OLED devices was greatly increased by the discovery of Thompson et al. that phosphorescent metal complexes could be used as emissive species to greatly increase their efficiencies.[19] To improve on fluorescent devices, which were limited to singlet electrogenerated charges (25 %) by spin-symmetry conservation, low concentrations of cyclometalated iridium or platinum were used to harvest electrogenerated triplet excitons through strong spin-orbit coupling of heavy metal complexes.[20-22] This enabled devices to approach a theoretical 100 % internal quantum efficiency by harvesting all electrogenerated

excitons. Universal Display Corporation (UDC) was formed in 1994 to exploit new phosphorescent organic light emitting diode (PHOLED) materials.

Light emitting diodes prepared from electroactive organic materials show great potential as a practical method for producing devices for multicolor display and white light source applications. The progression of OLED technology has reached a point where highly efficient thin film devices which rival other lighting and display technologies are attainable. In 2004 Sony introduced the first commercial device to use an OLED screen (Sony CLIÉ PEG-VZ90) and followed this with the first commercial OLED TV (Sony XEL-1) in 2007. Samsung SDI is currently the largest manufacturer of OLED displays. There are numerous companies developing new OLED displays and lighting devices with products close to commercial products. The US Department of Energy has set a goal of 150 lm/W commercial white OLED light sources by 2015 to replace incandescent bulbs at 15 lm/W and fluorescent bulbs at 60 – 90 lm/W. Although becoming more commonplace, OLEDs are still overshadowed in the marketplace with other more well established lighting and display technologies. This can be attributed to their complicated device architectures and high cost of manufacturing.

The focus of this thesis is in the area of developing new polymer architectures which enable OLED devices with easier solution processing techniques. The underlying goal was to exploit polymer architectures to obtain self-assembled or simply processed films that mimic multilayered device architectures to yield the same performance at reduced fabrication costs.

Principles of Operation

To date, multilayer electrophosphorescent small molecule devices have yielded the highest external quantum efficiencies.[23] Devices are typically multiple layers of organics sandwiched between the transparent anode (typically indium tin oxide, ITO) and the cathode (typically Al, Ca or Mg). The two or more layers of organic material are chosen specifically for their HOMO and LUMO energy levels (Figure 1.1). Holes are injected into the HOMO of the hole transporting layer (HT) material at the anode and electrons are injected into the LUMO of the electron transporting layer (ET) material from the cathode.
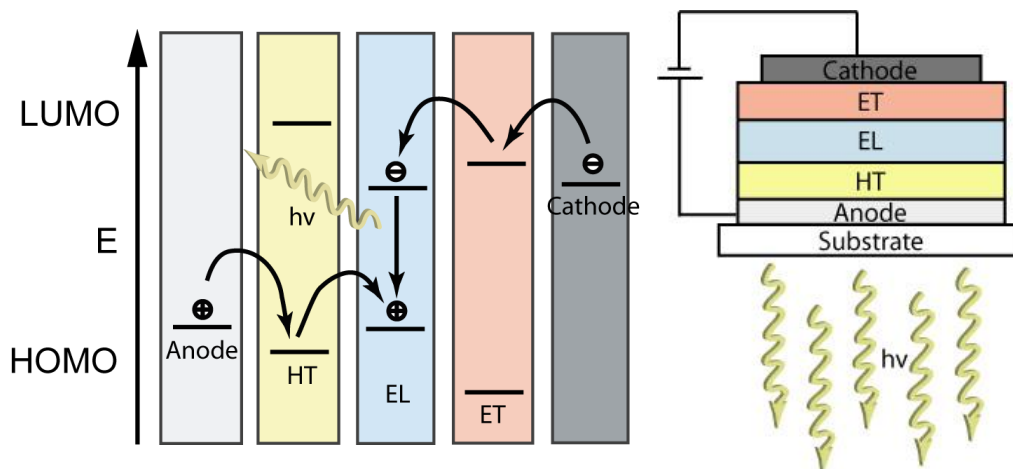
Figure 1.1. Generic energy diagram of a multilayer organic light emitting diode device (left) with corresponding device architecture schematic (right). HT is hole transporting material, EL is the emissive layer and ET is an electron transport layer.

Thus, in order to achieve ohmic contact and low series resistance the work function of the anode and cathode must align well with the ionization potential of the HT and electron affinity of the ET, respectively. Commonly, materials used as hole transporters have high lying HOMOs while electron transporters generally have low lying LUMOs in order to achieve low turn-on voltages. Conversely, electrode materials that have a high work function are optimal for use as anodes and materials with a low work function perform well as cathodes.

Injected charges must traverse the film through charge transfer towards the center of the device. Since essentially all organic solids are bulk insulators this charge transport must occur through either overlapping π-system conjugation electron exchange, or through a charge hopping mechanism. The first requiring close proximity of ordered π-systems, while the second relying on quantum mechanical tunneling between charge carriers in more disordered organic semiconductors. This process is dependent on the temperature and electric field.[24] The fields in a typical thin film OLED are quite high such that the rate of charge transfer follows an Arrhenius-like temperature dependence.

When holes and electrons meet they form a closely associated coulombic ion pair or exciton. One quarter of these electrogenerated excitons are singlets while the remaining three quarters being triplets due to spin-conserved electron-hole recombination statistics.[25] These excitons have some finite lifetime and may energy transfer through Förster or Dexter mechanisms to lower energy states. The probability of an exciton recombining is related to the materials ability to dissipate the resulting energy. Therefore, highly fluorescent or phosphorescent materials are used in OLEDs where the energy dissipation is in light emission. This "harvesting" of excitons should only occur in the emissive layer such that all hole-electron recombinations result in the emission of light.

Energy Transfer Mechanisms

As mentioned, an electrogenerated exciton can be transferred between materials through energy transfer processes. This process becomes significantly important when dealing with OLED devices of multiple colors. An exciton of high energy (blue) will energy transfer to lower energy (red) if given the opportunity. This can occur through two different processes; Dexter or Förster resonance energy transfer (FRET).

Dexter energy transfer is a short range electron transfer process. In order for this transfer to occur it requires intimate contact between the donor and acceptor molecule. The donor and acceptor must be within the distance of their van der Waals radii, as shown in Figure 1.2a where the rate of energy transfer depends on the exponential of the ratio between their distance (R_{DA}) and sum of their van der Waals radii (L). Therefore the distance that this energy transfer process occurs on is ~ 10 – 15 Å. This process involves electron exchange between the donor and acceptor. The excited electron is transferred to the donors LUMO with an electron being back transferred to the donors HOMO. The net result is energy transfer from the donor to the acceptor. This energy transfer can occur for both singlet and triplet excitons.

Förster resonance energy transfer (FRET) is a longer range energy transfer process. This process requires spectral overlap between the emission of the donor and the absorbance of the acceptor. It can be conceptually thought of as the emission of a virtual photon by the donor which is absorbed by the acceptor, although the process is in actuality radiationless. This energy transfer depends on the dipole-dipole interaction between the donor and acceptor ($\mu_D\mu_A$) and importantly the rate is inversely proportional to the distance between them (R_{DA}) to the power of

six (Figure 1.2b). Essentially this indicates that by increasing the distance between donor and acceptor a small amount one can dramatically decrease the amount of energy transfer between them. Generally, FRET can occur in distances on the order of 5 – 10 nm. However it can occur only for singlet excitons since triplet-triplet energy transfer is "forbidden" by the dipole-dipole mechanism.[26,27]

$$k_{ET} \propto e^{-2R_{DA}/L}$$

$$k_{ET} \propto \frac{(\mu_D \mu_A)^2}{R_{DA}{}^6}$$

Dexter energy transfer   Förster resonance energy transfer (FRET)
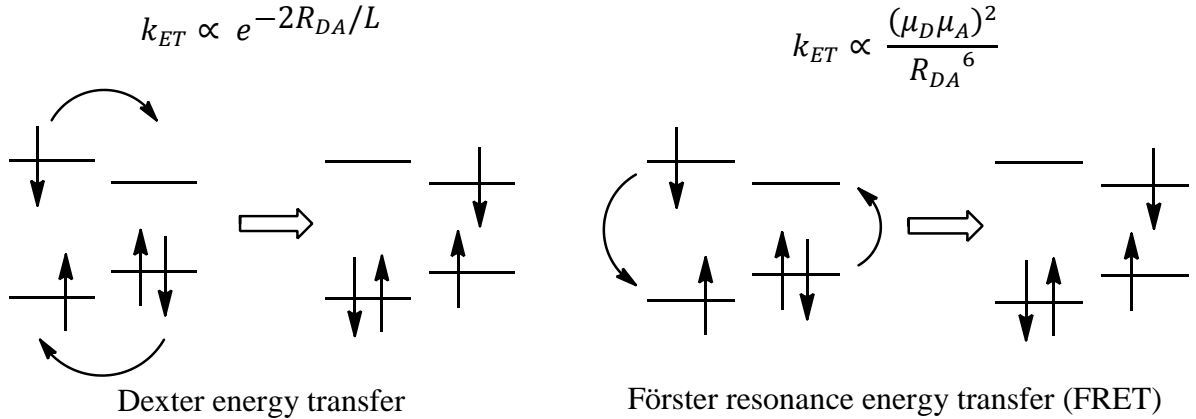
Figure 1.2. An illustration of the two predominant energy transfer processes commonly occurring in OLED devices. a) Dexter energy transfer where k_{ET} is the rate of energy transfer, R_{DA} is the donor acceptor separation and L their van der Waals radii; b) Förster resonance energy transfer where k_{ET} is the rate of energy transfer, μ_D the dipole moment for the donor and μ_A for the acceptor and R_{DA} is the donor acceptor separation.

With these two energy transfer processes in mind, a dual emitter single film device must site isolate donor (blue) from acceptor (red) emitter if they are to emit synergistically. Often times this is highly desirable in order to achieve devices that have electroluminescence that covers the visible spectrum for white lighting. Taking into account the lengthscales of Dexter and Förster energy transfer and the lifetimes of electrogenerated singlet excitons (~ ns) and triplet excitons (~ μs) an organization of emitters which site isolates them in domains larger than 5 – 10 nm is required (Figure 1.3). This goal was targeted with several different strategies in this work.
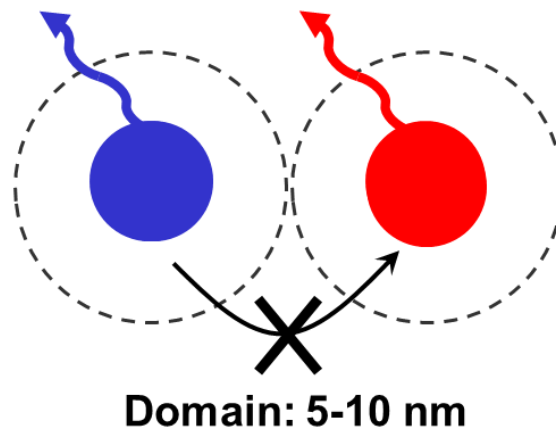
Domain: 5-10 nm

Figure 1.3. For dual synergistic emission of different energy emitters they must be site isolated in domains larger than 5 – 10 nm.

As mentioned briefly, the quantum efficiency of OLED devices was greatly improved in the late 1990's with the discovery that heavy metal complexes function as emitters with much better performance. The use of fluorescent emitters had been the norm with their predicable electroluminescence based on their observed fluorescence. Although high brightness was achievable, the efficiencies of these devices were limited. This was attributed to their inability to harvest triplet excitons.

As a hole and electron recombines to form an exciton it can do so to form either a singlet or a triplet. Considering the vector representation in Figure 1.4, the stable electron spins of the resulting exciton can be generated such that they are opposite and out of phase (-α β), opposite and in phase (α β), both up in phase (α α) or both down in phase (β β). Since each of these spin states are equally likely in an electro-generated exciton, the ratio of singlets to triplets formed will be dictated by the number of possible states of each. Therefore, in an OLED device ¼ or 25 % of the excitons generated are singlets, while ¾ or 75 % are triplets.
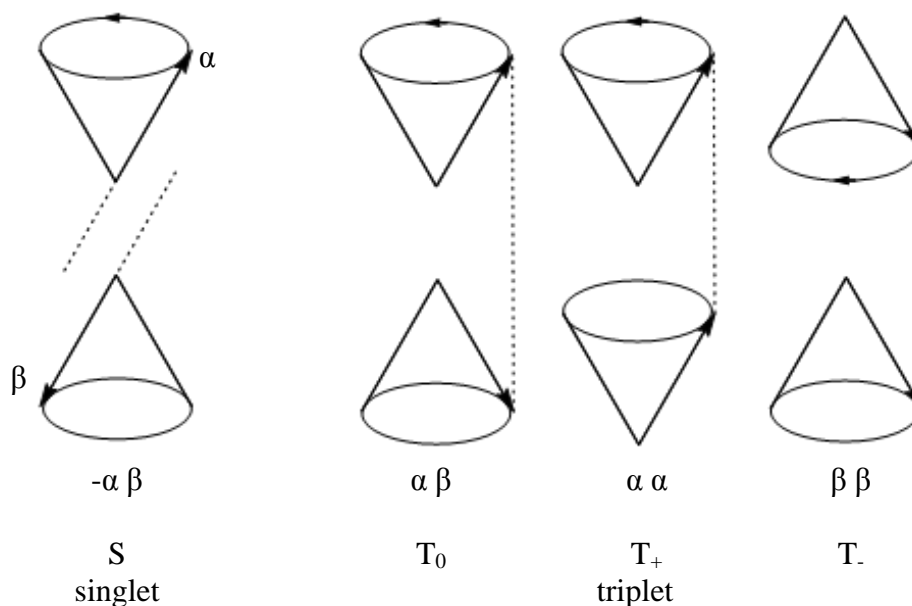
Figure 1.4. Basic vector diagram describing the possible spin states of an exciton. Up electron spin vectors are represented by α while down electron spin vectors are represented by β.[27]

Since the transition from the triplet state is forbidden fluorescent emitters are unable to harvest the generated triplet excitons as OLED emission. This results in a maximum theoretical internal quantum efficiency of 25 %. In order to overcome this, the use of heavy metal phosphors has become prevalent. This is due to their ability to harvest triplet excitons through strong spin-orbit coupling allowing for a maximum internal quantum efficiency of 100 %.

Most inorganic metal complexes that have demonstrated utility in OLEDs as emitters have been platinum[19,21,28] or iridium.[29-32] Metal complexes based on platinum and iridium have been shown to facilitate the harvesting of triplet excitons by mixing of the triplet and singlet states. In these complexes the luminescence originates from the lowest ligand centered triplet

(^{3}LC) with the singlet metal to ligand charge transfer (^{1}MLCT) state mixed through spin-orbit coupling. This allows these complexes to show strong phosphorescent emission with color that is largely dependent on the energy of the ligand. Because of this one can "tune" the color of emission by changing the cyclometalated ligand (Figure 1.5).[28,29,33]

| (dfppy)$_3$Ir | (tpy)$_3$Ir | (pq)$_3$Ir | (dfppy)Ir(acac) | (tpy)Ir(acac) | (pq)Ir(dpm) |
| 468 nm | 510 nm | 578 nm | 466 nm | 485 nm | 555 nm |
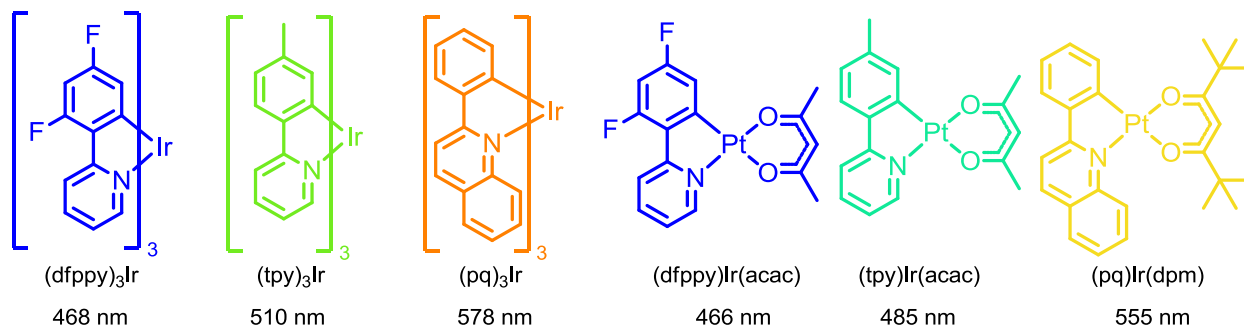
Figure 1.5. Some typical phosphorescent iridium and platinum emitter complexes with emission wavelength maximum (λ_{max}) below. This illustrates that by adjusting the cyclometalating ligand the emission color maximum can be tuned.[30,33]

In order for these phosphorescent metal emitter complexes to be effective in an OLED they must be doped into a host material. Neat films of a single phosphorescent emitter will be subject to quenching and triplet-triplet annihilation (the deactivation of two triplet excitons in close proximity to a singlet exciton and a ground state) resulting in poor efficiency of electroluminescence. In order to overcome these non-radiative losses, phosphorescent emitters are nearly always doped into a host material. Some commonly used host materials for green and red emitters are N,N-dicarbazolyl-4,4'-biphenyl (CBP) and N,N-dicarbazolyl-3,5-benzene (mCP).[21] The requirements of a good host material are that it should effectively transport both holes and electrons (ambipolar) and it must have a sufficiently large HOMO-LUMO gap such that the energy transfer from excitons in the host to the phosphorescent emitter is nearly quantitative. These features are commonly difficult to satisfy in a single material so a combination or mixture of hole and electron transporters can be used. Typically it is difficult to find materials with sufficiently high triplet energy to be suitable hosts for high energy blue phosphorescent materials. Therefore, very wide gap hosts which do not transport charges have been used.[34,35]

In white OLEDs more than one phosphorescent emitter must luminesce simultaneously in order to cover the visible spectrum. Unfortunately, simply mixing two different color phosphorescent emitters into one host, results in emission from the lowest energy phosphor. In this specific case, the energy transfer processes occurring are depicted in Figure 1.6. The host material has a larger triplet and singlet energy than both phosphorescent emitter, therefore energy transfer to both phosphors is efficient. The host material does not intersystem cross (ISC) and therefore no emission should be observed from the host. Singlet excitons can intersystem cross to the triplet state on both phosphors. The problem arises in the energy transfer from high energy phosphor (blue) to low energy (red) by FRET and Dexter, shown in the dashed lines. These energy transfer processes occur efficiently in homogenous mixed films of these materials, so emission should be dominated by the lower energy phosphor. The development of materials that

can minimize these energy transfer processes (dashed lines) while achieving it with a simple solution processed device architecture is a major focus of this thesis.
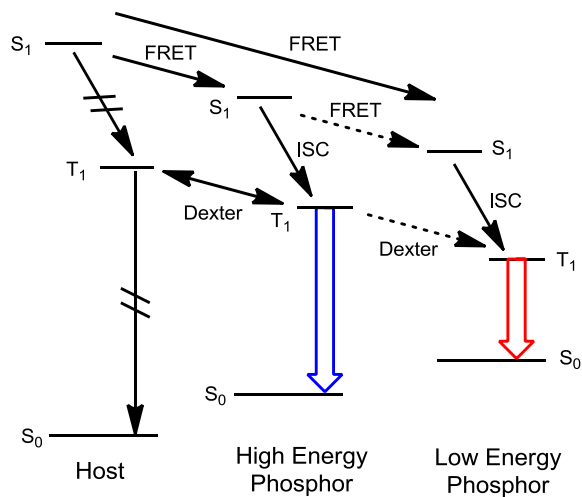
Figure 1.6. Energy transfer processes occurring in double guest-host system with two emitters of different color.

OLED Performance Metrics

The measures of performance in OLEDs have been well established.[36] The most basic of these measurements is the external quantum efficiency (EQE or n_{ext}), which is defined as the number of photons emitted from the device regardless of the wavelength over the number of electrons injected. This fundamental measurement is related directly to the emission properties of the material used in the device though the relationship $n_{ext} = n_{int}n_c$ where the internal quantum efficiency of the material is n_{int} and the device light out-coupling factor in the viewing direction is n_c. Therefore, the internal quantum efficiency value is a result of the characteristic quality of the material used in the device. This value can be related directly to of properties of the material through $n_{int} = \gamma\, n_s\, \Phi_P$ where γ is the charge carrier balance factor (the ratio of electrons/holes at the recombination region),[37] n_s is the efficiency of emissive exciton formation (0.25 for fluorescence, 1 for phosphorescent) and Φ_P is the photoluminescence yield of the material.[38] All these factors are measures of the material and the film structure in a device and therefore are directly related to the resulting external quantum efficiency.

In order to measure the resulting EQE of an OLED device a testing apparatus must measure the current and the resulting brightness of the device. A typical testing setup is depicted in Figure 1.7. This is the preferred configuration since a calibrated photodetector will measure only photons emitted from the front face of the device.[36] Other devices characteristics can then be obtained from these measurements knowing the electroluminescence spectrum such as luminance (cd/m2), luminous efficiency (cd/A) and luminous power efficiency (lm/W).
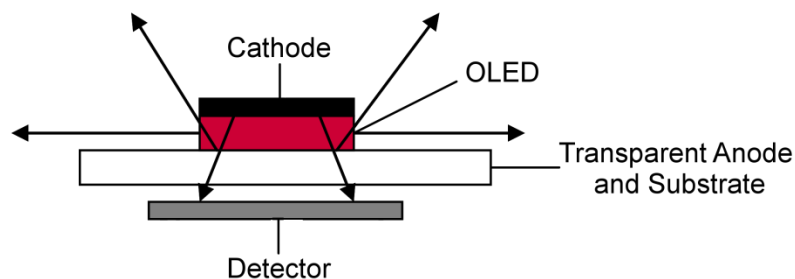
Figure 1.7. The preferred configuration for OLED device testing. The detector should be of larger area than the device and be placed in close proximity to the front face of the device. Using this configuration the external quantum efficiency is simply measured by the device current and the photocurrent of the detector.[36]

Device Preparation Techniques

OLEDs composed of small molecule organics are typically prepared with device architectures of multiple layers sandwiched between electrodes. These multilayer devices are fabricated through layer by layer high vacuum deposition of small molecules. This requires a high vacuum chamber with thermal or e-beam sources in order to deposit the small molecule organics in a controlled manner at pressures less than 10^{-5} torr. Essentially all of the currently available commercial devices are manufactured using some form of this method. Generally, this type of device fabrication is costly since it is not high throughput and the chamber must be large enough to hold and deposit over the entire area of the device substrate. It is likely for this reason that current commercial OLED devices are small area displays. This manufacturing technique does however offer a several advantages. The ability to build layered devices of essentially a limitless number of layers with defined composition and thickness provides a large variable space in which to tune device engineering and achieve very high performance. This method also allows the use of masks and patterning to create individual pixels or substructures in the device. Lastly, the materials being deposited can be of extremely high purity since they do not come in contact with solvent or air during fabrication, thereby minimizing quenching and charge trapping sites which result in degraded performance. These advantages have enabled the preparation of very efficient devices with EQE greater than 20 %.

A simpler and potentially more economical method of device preparation is solution processing. An inkjet printed or roll to roll processed device could be manufactured at much lower cost since these methods can be easily rendered high throughput. It could also overcome limitations on the size of an OLED device since the vacuum chamber may not be required. Solution processed OLEDs are indeed an attractive method of device preparation however it generally requires the design and synthesis of polymeric materials which are more easily cast into thin films. It also presents several challenges in obtaining high performance devices. A particularly significant problem is the difficulty in achieving the typical multilayer device architecture. Solution cast layers of polymers cannot simply be built up layer by layer as in the previous case. Subsequent deposition of layers will disturb the previously deposited one. Therefore, each layer must be cast from orthogonal solvents or the previous layer must be rendered insoluble through some chemical modification like crosslinking. The second major problem with solution processed devices is the inability to pattern pixels or substructures in the film. This may be achieved to some extent with inkjet printing but the feature sizes are not as

8

small as those obtained by masked vacuum deposition and this technique is not straightforward to implement. Therefore, site isolation of different colored emitters to create individual pixels or minimize energy transfer for white lighting is still a challenge.

        The specific aim of this thesis was to overcome the limitations of solution processed devices through design and synthesis of novel polymers with functional architectures. The target polymers synthesized within exhibit the ability to achieve site isolation through self-assembled nanostructured films or the ability to enable multilayer devices with simple solution processing steps. Ultimately, the goal was to exploit well designed polymeric materials which enable solution processed multicolor or white OLEDs with device performance that rivals small molecule based devices prepared by vacuum deposition.

References

(1)   Bernanose, A.; Vouaux, P. *J. Chim. Phys.* **1953**, *50*, 261.
(2)   Bernanose, A.; Comte, M.; Vouaux, P. *J. Chim. Phys.* **1953**, *50*, 64.
(3)   Bernanose, A. *J. Chim. Phys.* **1955**, *52*, 396.
(4)   Bernanose, A.; Vouaux, P. *J. Chim. Phys.* **1955**, *52*, 509.
(5)   Bernanose, A. *Br. J. Appl. Phys.* **1955**, *6*, S54-S55.
(6)   Pope, M.; Kallmann, H. P.; Magnante, P. *J. Chem. Phys.* **1963**, *38*, 2042-2043.
(7)   Vincett, P.; Barlow, W.; Hann, R.; Roberts, G. *Thin Solid Films* **1982**, *94*, 171-183.
(8)   Partridge, R. H. Radiation sources. U.S. Patent 3,995,299, November 30, 1976.
(9)   Partridge, R. *Polymer* **1983**, *24*, 733-738.
(10)   Partridge, R. *Polymer* **1983**, *24*, 739-747.
(11)   Partridge, R. *Polymer* **1983**, *24*, 748-754.
(12)   Partridge, R. *Polymer* **1983**, *24*, 755-762.
(13)   Tang, C. W. Organic electroluminescent cell. U.S. Patent 4,356,429, October 26, 1982.
(14)   Tang, C. W.; VanSlyke, S. A. *Appl. Phys. Lett.* **1987**, *51*, 913.
(15)   Tang, C. W.; VanSlyke, S. A.; Chen, C. H. *J. Appl. Phys.* **1989**, *65*, 3610.
(16)   Burroughes, J. H.; Bradley, D. D. C.; Brown, A. R.; Marks, R. N.; Mackay, K.; Friend, R. H.; Burns, P. L.; Holmes, A. B. *Nature* **1990**, *347*, 539-541.
(17)   Friend, R. H.; Burroughes, J. H.; Bradley, D. D. Electroluminescent devices. U.S. Patent 5,247,190, September 21, 1993.
(18)   Friend, R. H.; Gymer, R. W.; Holmes, A. B.; Burroughes, J. H.; Marks, R. N.; Taliani, C.; Bradley, D. D. C.; Santos, D. A. D.; Bredas, J. L.; Logdlund, M.; Salaneck, W. R. *Nature* **1999**, *397*, 121-128.
(19)   Baldo, M. A.; O'Brien, D. F.; You, Y.; Shoustikov, A.; Sibley, S.; Thompson, M. E.; Forrest, S. R. *Nature* **1998**, *395*, 151-154.
(20)   Kawamura, Y.; Goushi, K.; Brooks, J.; Brown, J. J.; Sasabe, H.; Adachi, C. *Appl. Phys. Lett.* **2005**, *86*, 071104.
(21)   Adamovich, V.; Brooks, J.; Tamayo, A.; Alexander, A. M.; Djurovich, P. I.; D'Andrade, B. W.; Adachi, C.; Forrest, S. R.; Thompson, M. E. *New J. Chem.* **2002**, *26*, 1171-1178.
(22)   O'Brien, D. F.; Baldo, M. A.; Thompson, M. E.; Forrest, S. R. *Appl. Phys. Lett.* **1999**, *74*, 442.
(23)   Adachi, C.; Thompson, M.; Forrest, S. *IEEE J. Sel. Top. Quant.* **2002**, *8*, 372-377.
(24)   Li, L.; Meller, G.; Kosina, H. *Microelectr. J.* **2007**, *38*, 47-51.
(25)   Pope, M.; Swenberg, C. E. *Electronic Processes in Organic Crystals and Polymers*; Oxford University Press, 1999.

(26)   Forster, T. *Discuss. Faraday Soc.* **1959**, *27*, 7-17.

(27)   Turro, N. J. *Modern Molecular Photochemistry*; University Science Books: Sausalito, CA, 1991.

(28)   Ma, B.; Li, J.; Djurovich, P. I.; Yousufuddin, M.; Bau, R.; Thompson, M. E. *J. Am. Chem. Soc.* **2005**, *127*, 28-29.

(29)   Li, J.; Djurovich, P. I.; Alleyne, B. D.; Yousufuddin, M.; Ho, N. N.; Thomas, J. C.; Peters, J. C.; Bau, R.; Thompson, M. E. *Inorg. Chem.* **2005**, *44*, 1713-1727.

(30)   Tamayo, A. B.; Alleyne, B. D.; Djurovich, P. I.; Lamansky, S.; Tsyba, I.; Ho, N. N.; Bau, R.; Thompson, M. E. *J. Am. Chem. Soc.* **2003**, *125*, 7377-7387.

(31)   Lamansky, S.; Djurovich, P.; Murphy, D.; Abdel-Razzaq, F.; Kwong, R.; Tsyba, I.; Bortz, M.; Mui, B.; Bau, R.; Thompson, M. E. *Inorg. Chem.* **2001**, *40*, 1704-1711.

(32)   Lamansky, S.; Djurovich, P.; Murphy, D.; Abdel-Razzaq, F.; Lee, H.; Adachi, C.; Burrows, P. E.; Forrest, S. R.; Thompson, M. E. *J. Am. Chem. Soc.* **2001**, *123*, 4304-4312.

(33)   Brooks, J.; Babayan, Y.; Lamansky, S.; Djurovich, P. I.; Tsyba, I.; Bau, R.; Thompson, M. E. *Inorg. Chem.* **2002**, *41*, 3055-3066.

(34)   Ren, X.; Li, J.; Holmes, R. J.; Djurovich, P. I.; Forrest, S. R.; Thompson, M. E. *Chem. Mater.* **2004**, *16*, 4743-4747.

(35)   Holmes, R. J.; D'Andrade, B. W.; Forrest, S. R.; Ren, X.; Li, J.; Thompson, M. E. *Appl. Phys. Lett.* **2003**, *83*, 3818.

(36)   Forrest, S.; Bradley, D.; Thompson, M. *Adv. Mater.* **2003**, *15*, 1043-1048.

(37)   Scott, J. C.; Malliaras, G. G.; Salem, J. R.; Brock, P. J.; Bozano, L.; Carter, S. A. In *Organic Light-Emitting Materials and Devices II*; Kafafi, Z. H., Ed.; SPIE: San Diego, CA, USA, 1998; Vol. 3476, pp. 111-122.

(38)   Kafafi, Z. H. *Organic electroluminescence*; CRC Press, 2005.

Chapter 2

Dendronized Linear Polymers as Bipolar Host Material in Electroluminescent Devices

Abstract

In this chapter the utility of a dendronized linear polymer architecture was explored as a bipolar host material in OLED devices. This architecture provides a radial bipolar transport gradient that mimics the multilayer nature of a traditional OLED within a single macromolecule. The targets incorporated oxadiazole (electron transporter) and triarylamine (hole transporter) as the linear polymer core and as the dendron exterior, respectively. Two synthetic routes were explored: divergent bis-hydroxymethyl propionic acid (bis-HMPA) dendron growth from a linear polymer and convergent grafting of a functionalized Fréchet type dendron through "click" chemistry. These dendronized linear polymers were evaluated as the host material in single layer OLED devices doped with a green phosphorescent iridium emitter (tpy)$_2$Ir(acac). Device results for this series of polymers showed respectable efficiencies of up to 3 % external quantum efficiency for a single layer device in air. However, it was determined that higher generation dendronized polymers showed decreased efficiencies and not the desired enhancement in performance due to dendronized linear polymer assembly characteristics. The problems with this system are likely due to the incorporation of larger quantities of electro-inert dendron scaffold.
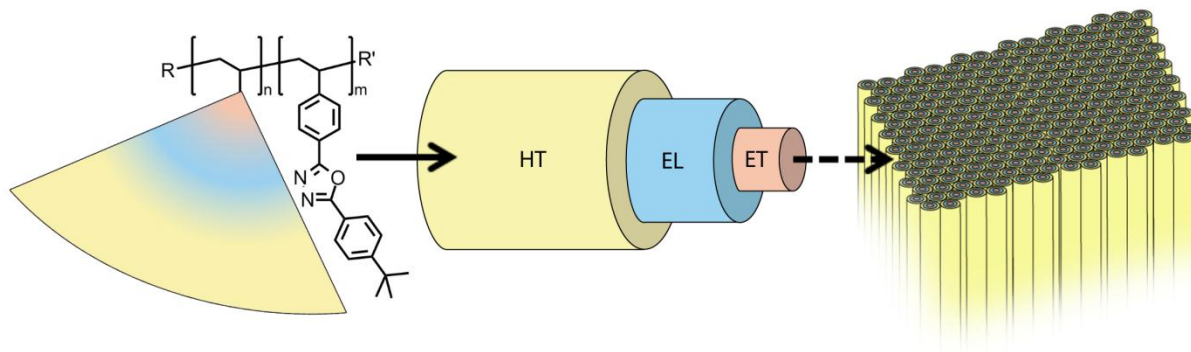
Introduction

Commercialization of small molecule multilayer OLEDs has been slow. This can be attributed in part to the vapor deposition technique used to assemble small molecule thin films. The process is not amenable to large area displays and is relatively costly. An attractive alternative solution to this problem is to replace small molecules with organic polymers, which could be solution processed in an efficient and economical manner. Block copolymers, an approach that is discussed in Chapter 3, have been explored as a means to achieve a self-assembled structure that mimics these multi-layer structures. A potential drawback of the block copolymer architecture is the reliance on the polymer film to arrange into an optimal morphology. A diblock copolymer of bipolar materials can organize into a variety of 3-dimensional arrangements (Figure 2.1). Presumably, a morphology that allows for efficient recombination of excitons at the interface of the two electroactive transporting domains while enabling efficient charge injection at the electrodes would be ideal. Since obtaining a desired morphology and maintaining it over the lifetime of a device is not trivial, this architecture may be limited in its reproducibility and lifetime. With this in mind, an attractive target architecture is a dendronized linear polymer which has the potential to overcome these limitations.
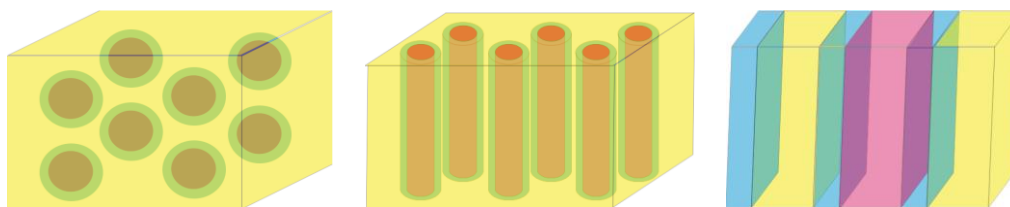
Figure 2.1. Domain segregation into several film morphologies (from left to right) spherical, cylindrical or lamellar.

A dendronized linear polymer introduces the ability to implement a radial functionality gradient.[1] They can be synthesized such that the core has a different functional characteristic than the exterior. In a similar fashion, one could envision using the functional gradient to mimic the multilayer nature of an OLED device within a single macromolecule. This would entail implementing a structure with a bipolar radial transport gradient. The well-defined covalent nature of a dendronized linear polymer would lock the morphology of the domain interface. A target for OLED use could employ electron transport character at the cylinder core and hole transport at the exterior (Figure 2.2). Dendronized polymers have previously found use in light harvesting applications[2] and dendronized polyfluorene polymers have been studied extensively in OLEDs to prevent excimer formation and prolong the lifetime of blue emission.[3-6]
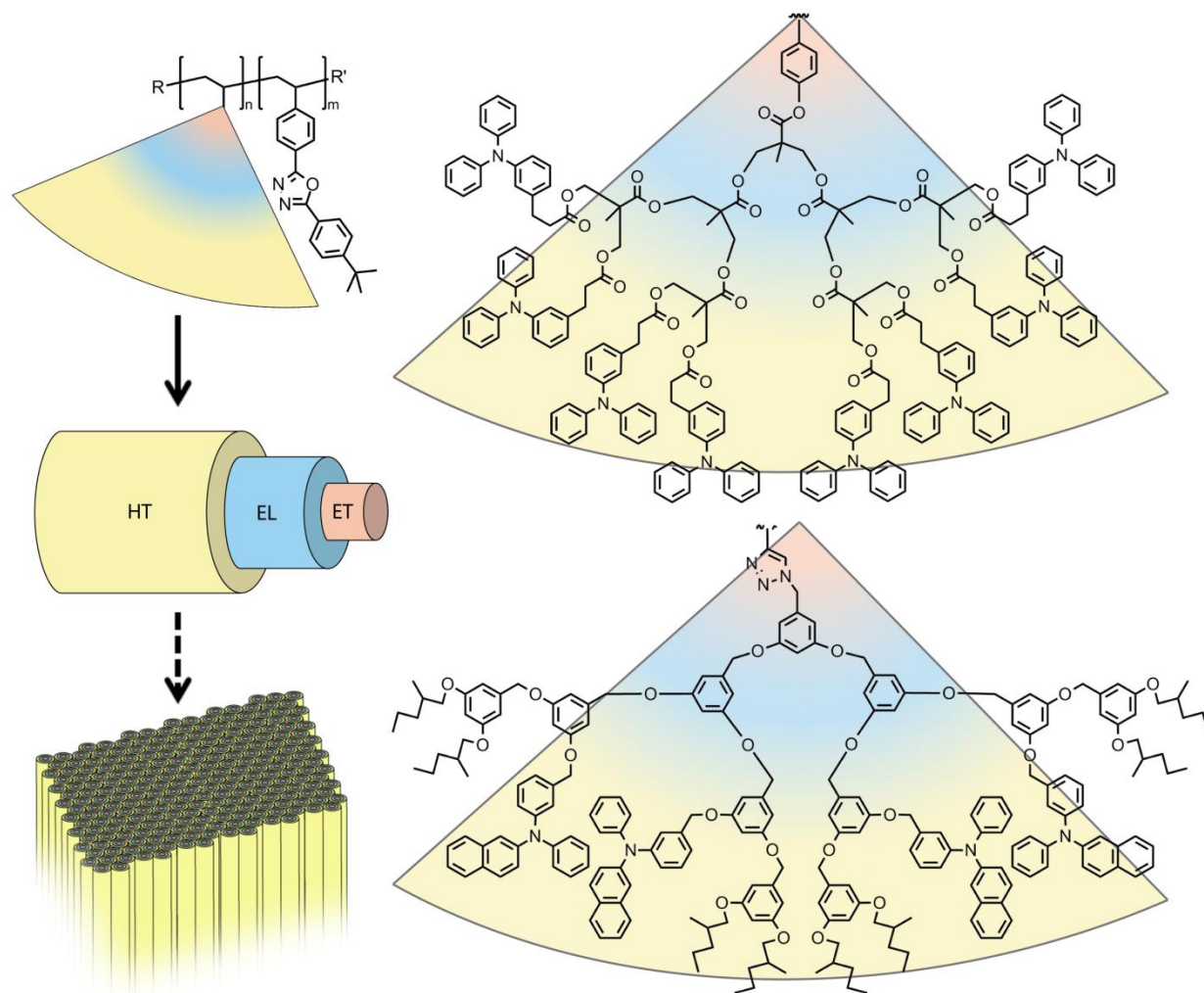
Figure 2.2. Dendronized linear polymer synthetic targets both illustrating a radial functionality gradient. The rigid rod nature of a sterically bulky dendronized linear polymer yields a gradient of electron transporting (ET) to emissive (EL) to hole transporting (HT) material from the center outward radially. A divergently grown polymer (top right) and a convergent "clicked" polymer (bottom right).

This chapter presents a new approach towards polymer OLEDs using dendronized linear polymers containing a bipolar radial transport gradient as host material. The well-defined covalent architecture and structural stability of dendronized linear polymers may present benefits in efficiency and in device lifetimes by limiting bulk phase separation.

A potential limitation to this design strategy is the introduction of insulating dendrons. At higher generations the benefits of the dendronized linear polymer architecture may be offset by a decrease in charge mobility due to an increased amount of dendritic benzyl ether or aliphatic ester segregating the hole and electron transport domains. This may not necessarily result in poor performance since it is not desired for charges to migrate through the emissive region, but to recombine and result is emission. The ideal structure should be one that balances these influences on device efficiency and is why several generations of dendronized linear polymers have been investigated.

13

Results and Discussion

The preparation of non-conjugated polymers composed of oxadiazole and triaryl amine as electron transporting and hole transporting materials, respectively, has been previously reported.[7,8] In this study, similar monomeric subunits exhibiting desirable transport characteristics have been used, but in a novel dendronized linear polymer structure intended to allow for the tuning of the interface between electron and hole transporting material to obtain maximum recombination efficiency. Dendronized linear polymers have traditionally been prepared by three general techniques; the grafting approach,[9] macromonomer polymerization[10] and divergent growth.[11] Two forms of dendronized linear polymer have been explored; a post polymerization divergently grown aliphatic ester dendron and a convergently grown benzylic ether dendron clicked to the polymer backbone post polymerization using a "graft to" approach. This chapter discusses the synthesis of two dendronized polymer targets; the first achieved through the divergent approach and the second through a convergent "graft to" approach.

Divergent dendronized polymer

In recent years, "living" radical polymerizations have received much attention leading to the development of stable alkoxyamine initiators which facilitate controlled nitroxide mediated polymerizations with low polydispersities and predictable molecular weights.[12,13] This initiator was chosen to synthesize the linear backbone for these reasons as well as its high functional group tolerance. In order to obtain a linear backbone core with electron transport characteristics a *para* substituted styrenic oxadiazole, which possessed a pendant *tert*-butyl group to improve polymer solubility, was chosen. This monomer was synthesized through formation of the tetrazole from 4-bromobenzonitrile in *N,N*-dimethylformamide (DMF).[7,14] This compound is stable under ambient conditions but reacts readily with acid chlorides at reflux to yield the oxadiazole.[7] Finally, the vinyl group was added to generate desired monomer under standard Stille coupling conditions with tributyl(vinyl)tin.

Linear polymer backbone **1** was synthesized by random "living" radical co-polymerization of oxadiazole monomer and 4-acetoxystyrene using 0.7 mol% alkoxyamine initiator (Scheme 2.1) at 125 °C for 14 h. The extent of monomer incorporation was determined by ^{1}H NMR spectroscopy (Figure 2.3) and is summarized in Table 2.1 at each dendronization step. NMR results indicate that these monomers polymerize at relatively similar rates to produce polymers with a nearly random statistical distribution, as confirmed by their incorporation into test polymers for which conversion was limited to 50%.

To facilitate efficient hole and electron recombination similar numbers of hole and electron transport monomers per cross sectional area of polymer is desired. As such, a low ratio of n/m is desired since dendron growth from the hydroxyl group provides double the number of sites for hole transporter attachment per generation. However, at very low incorporation of dendron focal point (low n/m), the space between dendrons may be too large to provide the steric congestion required to induce a conformational change from random coil to rigid rod even at high generations. Therefore, a ratio of 0.5 for n/m was chosen as an intermediate of these two competing factors. At this level of acetoxystyrene backbone incorporation the ratio of oxadiazole to triarylamine is 1:1, 1:2 and 1:4 in the final polymers **1-[G1]-TPA₂**, **1-[G2]-TPA₄** and **1-[G3]-TPA₈** respectively.
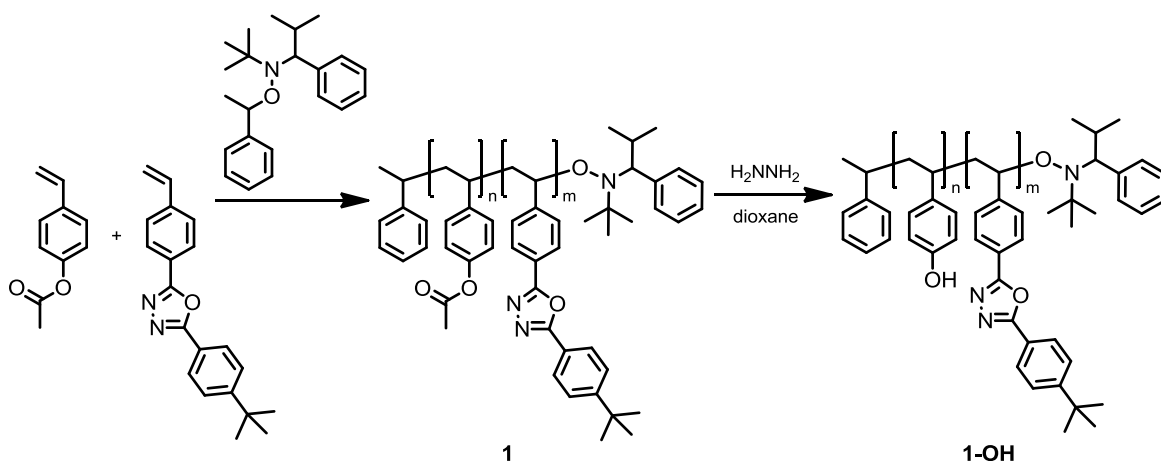
Scheme 2.1. Synthetic scheme for synthesis of an electron transporting linear polymer backbone with phenolic dendron focal points.

Removal of the acetyl group from the initial linear backbone polymer was achieved through hydrazinolysis in dioxane at room temperature over 19 hours, yielding the hydroxy terminus prepared for divergent dendron growth.[15] This initial linear polymer was used for all the subsequent product polymers.

Table 2.1.

Polymer	^{1}H NMR n/m	UV$_{ps}$ M$_w$ ^{a}	MALS M$_w$^{b}	Theoretical MW ^{c}	PDI ^{d}
1	0.45	45 000	71 000	70 000	1.4
1-OH	0.50	41 000	65 000	67 300	1.4
1-[G1]-A	0.47	46 000	77 000	81 300	1.4
1-[G1]-(OH)$_2$	0.47	42 000	72 000	78 700	1.5
1-[G2]-A$_2$	0.50	54 000	101 000	105 800	1.3
1-[G2]-(OH)$_4$	0.42	52 000	99 000	98 400	1.4
1-[G3]-A$_4$	0.51	74 000	149 000	154 600	1.7
1-[G3]-(OH)$_8$	0.51	73 000	136 000	140 200	1.7

^{a} Weight average as determined by size exclusion chromatography using a UV detector based on polystyrene standard elution times. ^{b} Weight average as determined by size exclusion chromatography using a multi angle light scattering detector (dn/dc calculated assuming 100% mass recovery in elution peak). ^{c} Predicted molecular weight based on 100% monomer conversion and complete dendronization. ^{d} Polydispersity index calculated from size exclusion chromatography UV trace.
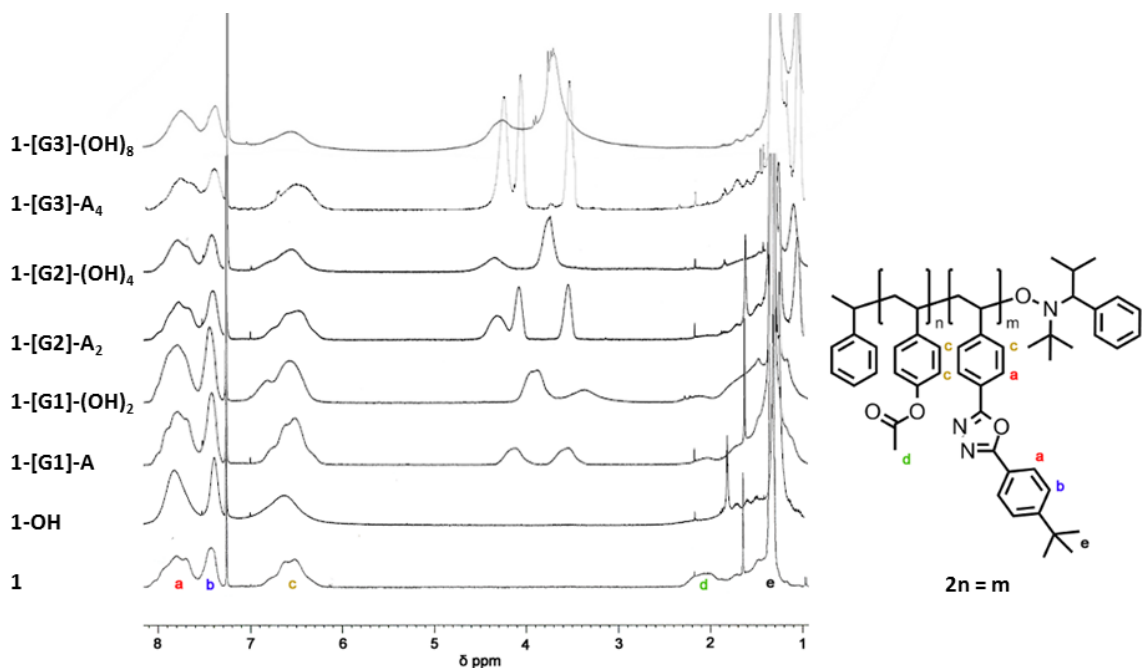
Figure 2.3. ^{1}H NMR spectra showing monomer incorporation assignment for **1** and dendritic ester growth up to **1-[G3]-(OH)$_8$**.

Rapid and efficient dendronization of hydroxystyrene has been demonstrated using isopropylidene-2,2-bis(methoxy)propionic anhydride **3**.[11,16] The advantages of this dendritic material was the simple preparation of the reactive anhydride which can be stored and used at will, as well as the simple dendronization deprotection step achieved by stirring with an acidic ion exchange resin. The isopropylidene-2,2-bis(methoxy)propionic acid **2** was synthesized through acid catalyzed protection with dimethoxypropane.[17,18] Anhydride **3** was prepared through dicyclohexylcarbodiimide (DCC) coupling (Scheme 2.2). A twofold excess of **3** was reacted with the phenolic hydroxyl groups in the linear polymer **1-OH** with catalytic dimethylaminopyridine (DMAP) in pyridine, yielding **1-[G1]-A**. This was followed by simple deprotection with acidic Dowex 50Wx2 to yield **1-[G1]-(OH)$_2$** (Scheme 2.2). A portion of this first generation dendronized linear polymer was dendronized further, and the remainder was kept for triarylamine attachment in order to obtain a series of different generations. Repeated dendronization yielded higher generation polymers **1-[G2]-(OH)$_4$** and **1-[G3]-(OH)$_8$** with four and eight free hydroxyl termini respectively.

16
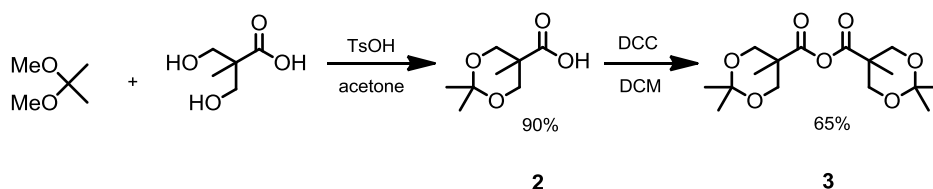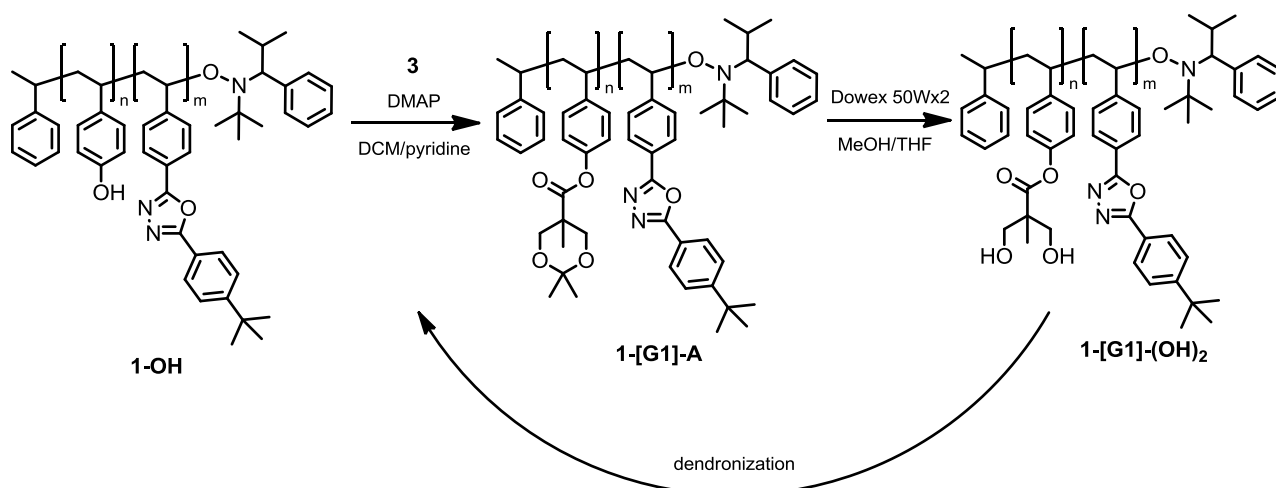
Scheme 2.2. Simple synthesis of the reactive anhydride of isopropylidene-2,2-bis(methoxy)propionic acid. Reiterative dendronization procedure using this material yields various generation bis-HPMA dendronized linear polymers **1-[G1]-(OH)$_2$, 1-[G2]-(OH)$_4$ and 1-[G3]-(OH)$_8$**.

The triphenylamine hole transporting material was designed with a carboxylic acid functional handle for simple esterification attachment to the final polymer dendron exterior. The synthesis of **4** was accomplished by tetrahydropyran (THP) protection of 3-bromobenzyl alcohol followed by palladium catalyzed coupling with diphenylamine. This material was converted to the corresponding bromide through the Appel reaction followed by nucleophilic substitution with an oxazoline protected carboxylic acid. Deprotection of the oxazoline in acid yielded the final triarylamine hole transporting unit **4** in 57 % overall yield. The final step in dendronized linear polymer synthesis was attachment of this triarylamine unit to the dendron hydroxyl exterior through DCC catalyzed esterification followed by simple purification by precipitation (Scheme 2.3). A summary of all the final dendronized polymers synthesized through this method is given in Table 2.2. The final yields for the exterior functionalization step were all above 95 % however is should be expected that with this divergent dendronized linear polymer approach there will be defects at each step leading to the increase in polydispersity. Nevertheless, the molecular weights measured by light scattering detection were reasonably close to the theoretical values.
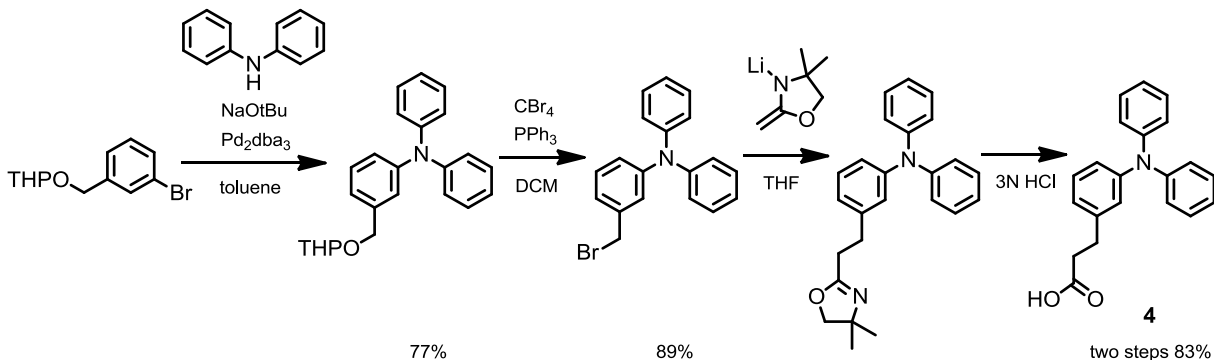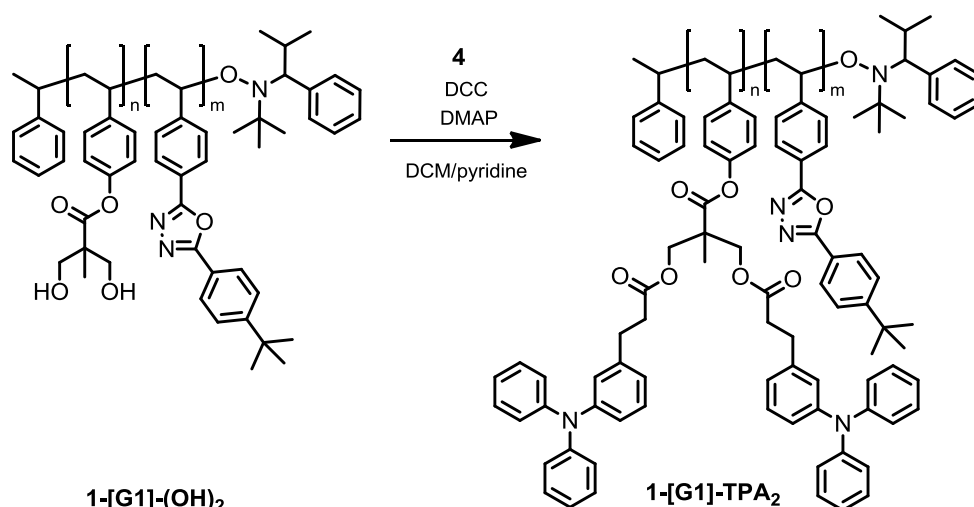
Scheme 2.3. Synthetic scheme for a carboxylc acid functionalized triarylamine. Functionalization of the dendronized polymer exterior with the triarylamine hole transporting unit. This was performed on **1-[G1]-(OH)$_2$**, **1-[G2]-(OH)$_4$** and **1-[G3]-(OH)$_8$** to yield final product polymers **1-[G1]-TPA$_2$**, **1-[G2]-TPA$_4$** and **1-[G3]-TPA$_8$** respectively.

Table 2.2.

Polymer	UV$_{ps}$ M$_w$ [a]	MALS M$_w$ [b]	Theoretical MW [c]	PDI [d]
1-[G1]-TPA$_2$	56 200	139 600	131 600	1.3
1-[G2]-TPA$_4$	58 100	156 800	206 100	1.5
1-[G3]-TPA$_8$	115 200	321 000	355 700	1.7

[a] Weight average as determined by size exclusion chromatography using a UV detector based on polystyrene standard elution times. [b] Weight average as determined by size exclusion chromatography using a multi angle light scattering detector (dn/dc calculated assuming 100% mass recovery in elution peak). [c] Predicted molecular weight based on 100% monomer conversion and complete dendronization. [d] Polydispersity index calculated from size exclusion chromatography UV trace.

^{1}H NMR of these final polymers also indicated the expected coverage of the triarylamine hole transporter exterior. When the ^{1}H NMR spectra were normalized to the oxadiazole aryl peak in the experimental details Figure 2.5a, the peaks corresponding to the triarylamine dendron (Figure 2.5b-e) approximately double in area going from **1-[G1]-TPA$_2$** to **1-[G2]-TPA$_4$** and to **1-[G3]-TPA$_8$** as expected. These final dendronized linear polymers were a suitable material to test the hypothesis that this architecture may aid in charge recombination in an OLED device.

Convergent clicked dendronized polymer.

The second approach taken to obtaining a dendronized linear polymer with OLED transport capabilities was by dendron grafting to a linear backbone. This method was highly attractive because the dendronization steps are performed on a small macromolecule that is

18

easily purified and well defined. The dendritic defects present in the divergently synthesized polymer discussed previously can be minimized. Once the monodisperse desired dendron is obtained, the polydispersity of the final polymer is only affected by the backbone distribution and the efficacy of the grafting step. For this reason the highly selective and high yielding Cu(I)-catalyzed Huisgen [2 + 3] dipolar cycloaddition reaction between an organic azide and a terminal alkyne was and good choice to obtain the target.[9,19-21]
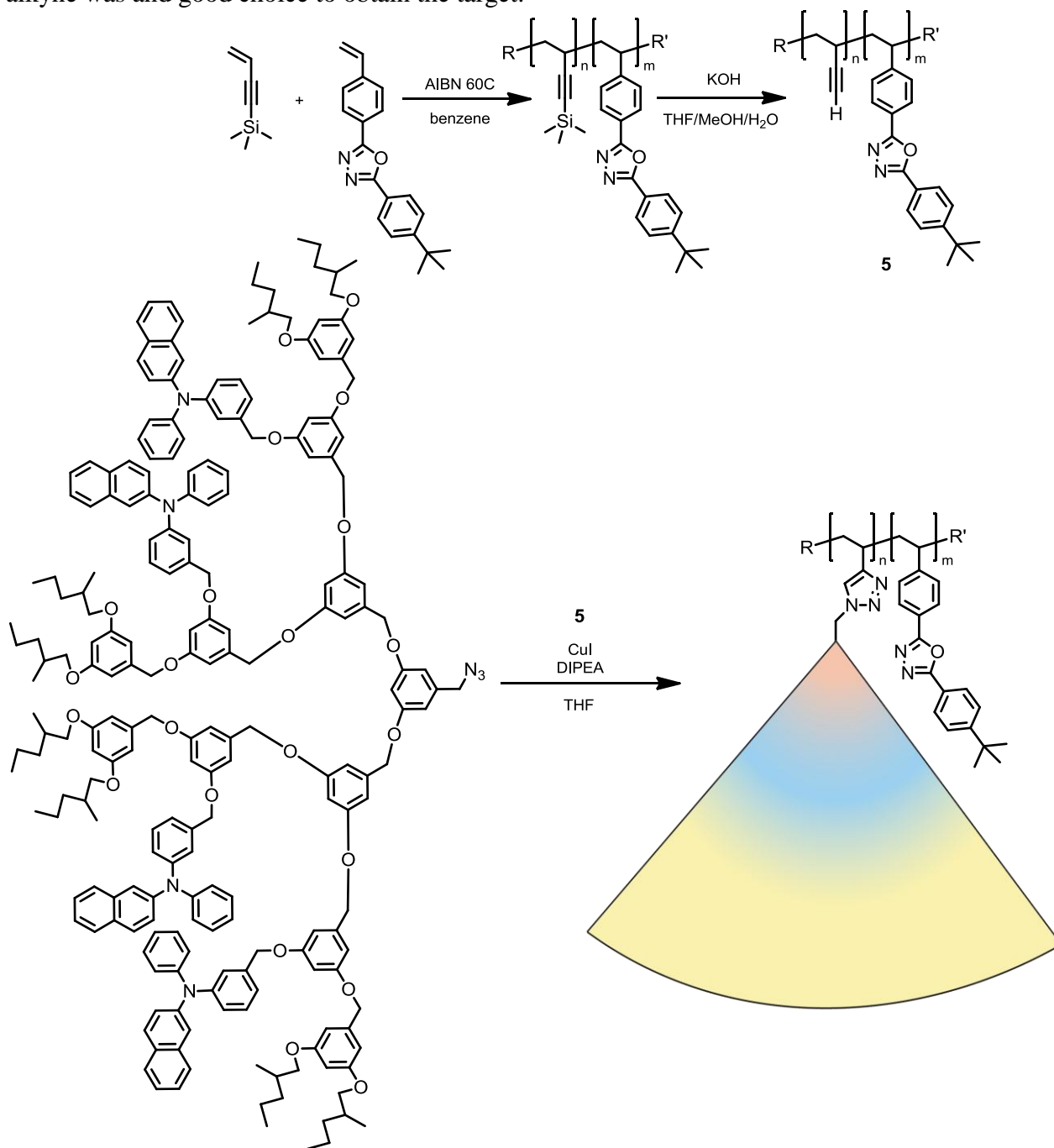
Scheme 2.4. Convergently synthesized dendron which was used to assemble a dendronized linear polymer by a "click" chemistry grafting approach.

Bulk co-polymerization of *p*-oxadiazole and a 4-trimethylsilyl-1-buten-3-yne was performed with AIBN at 60 °C. This yielded a 48 kDa M_w polymer **5-TMS** with PDI of 1.79. The trimethylsilyl (TMS) group was efficiently cleaved with base yielding **5** with free terminal alkynes that can undergo cycloaddition with organic azides to tether triarylamine terminated dendron (Scheme 2.4). The preparation of dendron **6** was accomplished by sodium azide nucleophilic substitution of the benzyl bromide focal point, whose synthesis has been previously reported and used in dendrimer OLEDs for site isolation.[22] Attachment of the dendron was performed under organic "click" conditions in tetrahydrofuran with CuI and Hunig's base to yield **5-[G3]-[TAA]₄**. The final dendronized polymer was purified by repeated precipitation from hexanes.

OLED testing of host dendronized polymers

These polymers were investigated in simple single layer OLED devices as the host material for a phosphorescent iridium emitter. Each polymer, when doped with an emissive metal complex, should implement all the elements of a multilayer device (hole transporter, electron transporter and emitter). Host dendronized polymers were all doped with 8 wt. % (tpy)₂Ir(acac)[23,24] and spun cast from chlorobenzene directly on prepatterned ITO substrates. The cathode material was then evaporated on top of these thin films to yield simple device architectures of ITO/dendronized polymer with 8 wt.% (tpy)₂Ir(acac) dopant (90 nm) /LiF (1 nm)/Al (100 nm). These devices were then tested as OLEDs in air by measuring voltage, current and the brightness of light emitted from the front face.

The resulting device characteristics for the divergently grown dendronized linear polymer are shown in Figure 2.4. The electroluminescence observed from these devices was promising considering the color of emission is characteristic of the phosphorescent complex used (tpy)₂Ir(acac).[23,24] This indicates that the triplet energy of the host dendronized polymer was sufficiently high that energy transfer from the host dendronized polymer to the phosphorescent emitter occurred efficiently and completely, as desired. The turn-on voltages for these devices were 7.7 V, 8.1 V and 9.1 V at 0.1 Cd/m^2 for the G1, G2 and G3 polymers respectively. Although slightly high these values are typical for a single layer polymer device. The interesting point to note is the increasing trend of turn-on voltage for higher generation polymers. Looking at the maximum brightness for these devices, 2823 Cd/m^2 (at 27.8 V), 1073 Cd/m^2 (at 23.6 V) and 53 Cd/m^2 (at 23.6 V) for G1, G2 and G3 polymers respectively, there was clearly a decreasing brightness trend for higher generation polymers. The first two polymers (**1-[G1]-TPA₂** and **1-[G2]-TPA₄**) with brightness > 1000 Cd/m^2 were respectably high however **1-[G3]-TPA₈** was barely visibly on. These results by themselves were not necessarily ruinous but along with the external quantum efficiency results it was not promising for this series of polymers.

The maximum EQE values were 2.98 %, 0.94 % and 0.06 % for G1, G2 and G3 polymers respectively. The generation one polymer was the only host polymer with relatively high efficiency in a thin film device. The trend observed of decreased efficiency with higher generation is the opposite of what was desired for these materials. These results indicate that there is no beneficial effect of the higher generation and presumably more rigid like polymers. In fact there is clearly a detrimental effect which is likely due to the incorporation of increased amounts of electro-inert dendritic ester material or the larger ratio of hole to electron transporting material in higher generation dendronized polymers. Generally, it appears that high generation dendronized polymers do not improve device performance. The **1-[G1]-TPA₂** functions well but

20

essentially very similarly to the simpler to prepare random copolymer of TPA and OXA as described in Chapter 3 with an EQE of 2.0 %.

The resulting device characteristics for the convergently "clicked" dendronized linear polymer are not shown because the devices were non-functional. This dendronized linear polymer was not a good material as a host for phosphorescent emitters. This may be attributed to small amounts of copper catalyst impurity remaining the polymer. This route of synthesis is therefore less desirable since the final step Cu(I)-catalyzed Huisgen [2 + 3] dipolar cycloaddition may introduce small amounts of copper which remain. A similar target may be attainable using strained cyclooctynes which do not require copper catalyst[25] or through a different "click" chemistry such as the thiol-ene,[26,27] however the poor results from the divergently prepared host material did not lend credit towards this polymer architecture target being a desirable one.
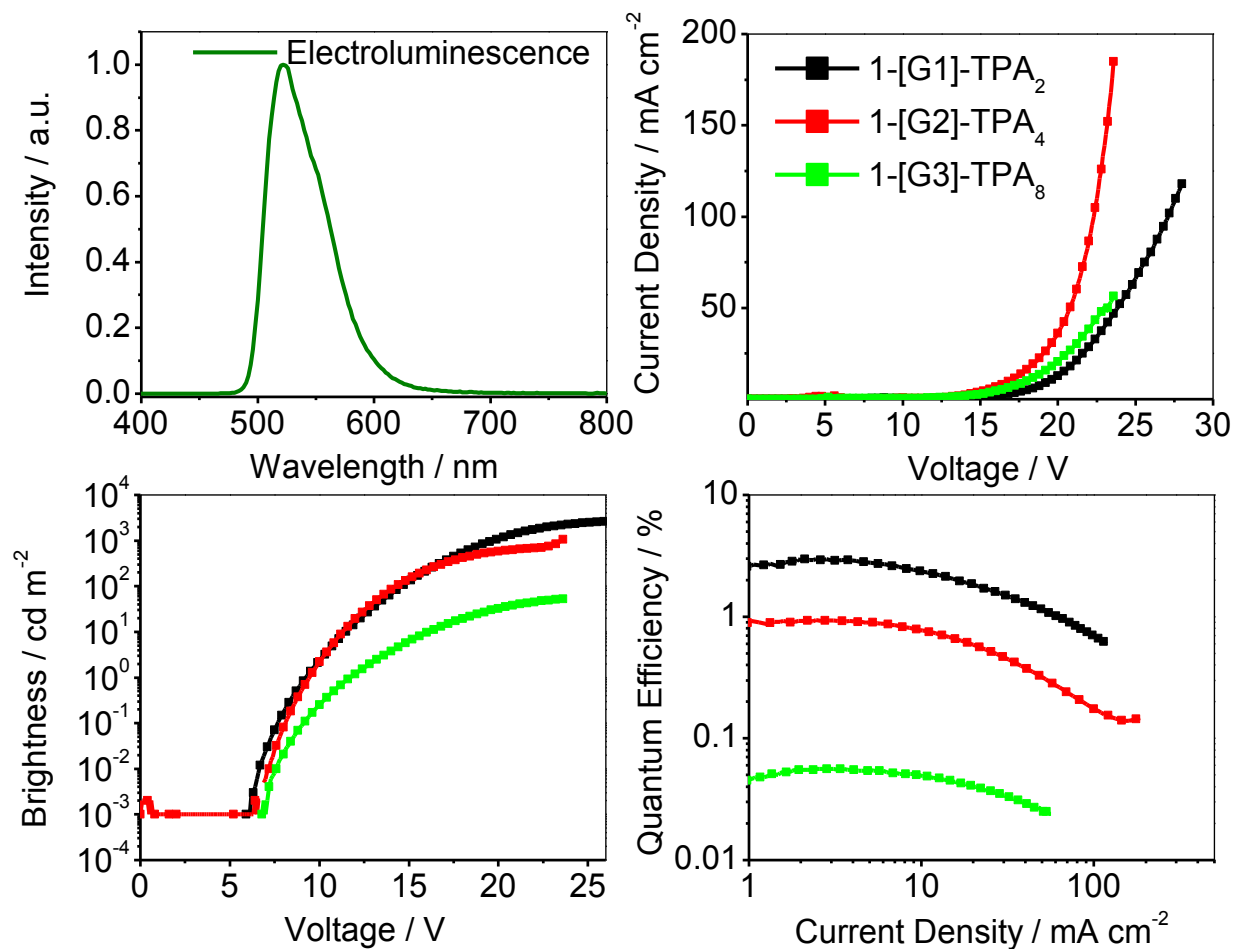
Figure 2.4. Single layer device characteristics with structure ITO/dendronized polymer with 8 wt.% (tpy)$_2$Ir(acac) dopant (90 nm) /LiF(1 nm)/Al(100 nm).

Conclusion

Two synthetic routes have been employed to obtain dendronized linear polymers with a radial charge transport polarity gradient. These polymers have been designed to function as the electroactive material in organic light emitting diodes. The desired benefit of this architecture

21

was the ability to optimize the emissive interface of electron transport and hole transport domains with the covalent linkage of different generation dendrons. As a result, it was expected that they would be good candidates as an efficient single layer device or may be used as the emissive layer in a mutilayer device. The radial bifunctionality was desired to provide increased emissive interface surface area for improved recombination efficiency. Unfortunately, the resulting devices showed decreased performance, as in higher turn-on voltage, lower brightness and lower efficiency, in going to higher generation dendronized linear polymers. This negative effect may be attributed to the increased content of electroinert dendritic ester scaffold or the higher ratio and therefore imbalance of hole to electron transporting moieties. A target dendronized polymer where the dendritic material is itself hole or electron transporting may overcome these challenges.

Experimental

Devices Fabrication and Measurement. Prior to device fabrication, ITO on glass substrates were patterned as 2 mm wide stripes with resistivity of 20 Ω/cm. The substrates were cleaned by sonication in soap solution; rinsed with deionized water; boiled in trichloroethylene, acetone, and ethanol for 5 min each; and dried with nitrogen. Finally, the substrates were treated with UV ozone for 10 min. The organic active layer dendronized linear polymer was prepared by spin-casting of solutions at 3000 rpm for 60s. The solutions were filtered (2 μm poly(vinylidene difluoride) filter) prior to use. The thickness of organic layer was monitored using a Dektak profilometer. After spin casting, a shadow mask with a 2 mm wide stripe was put onto the substrates perpendicular to the ITO stripes. A cathode consisting of 1nm LiF and 100nm aluminium was deposited at a rate of 0.02 Å/s and 4-5 Å/s respectively. OLEDs were formed at the 2×2 mm squares where the ITO (anode) and Al (cathode) stripes intersect.

The devices were tested in air within 2 hours of fabrication. The electrical and optical intensity characteristics of the devices were measured with a Keithly 2400 sourcemeter/2000 multimeter coupled to a Newport 1835-C optical meter, equipped with a UV-818 Si photodetector. Only light emitting from the front face of the device was collected and used in subsequent efficiency calculations. The EL spectra were measured on a USB4000 Miniature Fiber Optic Spectrometer. The emission was found to be uniform throughout the area of each device.

General Synthesis. Unless otherwise noted, all reagents were used as received and without further purification, or were prepared according to literature procedure. Reaction mixtures and chromatography fractions were analyzed using Whatman 250 μm thick 60 Å partisil K6F thin layer chromatography (TLC) plates. Unless otherwise specified, organic extracts were dried over anhydrous $MgSO_4$ and solvents were removed with a rotary evaporator under vacuum by a Fisher MaximaDry single stage pump. Methylene chloride, tetrahydrofuran (THF), toluene, pyridine, *N,N*-dimethylformamide (DMF), and triethylamine were purchased from Fisher and vigorously purged with nitrogen for 1 h. The solvents were further purified by passing them under nitrogen pressure through two packed columns (Glass Contour) of neutral alumina (for THF and methylene chloride), neutral alumina and copper(II) oxide (for toluene), or activated molecular sieves (for DMF).

All NMR spectra were measured in $CDCl_3$ with TMS or solvent signals as the standards. High-resolution mass spectra (HRMS) were obtained with a Micromass ProSpec using fast atom bombardment (FAB). Elemental analyses were performed by the University of California,

Berkeley mass spectrometry facility. Previously prepared compounds were determined to be pure within the limits of NMR analysis, unless otherwise noted.

THF GPC was carried out at 1.0 mL/min. Three PLgel columns (7.5 x 300 mm) were used. The columns had a pore size of 105, 103, and 500 Å, respectively. The particle size was 5 mm. The GPC system consisted of a Waters 510 pump, a Waters 717 autosampler, a Waters 486 UV-Vis detector, a Wyatt DAWN EOS light scattering detector, and a Wyatt Optilab DSP differential refractive index detector. The columns were thermostatted at 35 °C.

DMF GPC was carried out at 1.0 mL/min. Two Plgel mixed-bed C columns (7.5 x 300 mm) were used. The particle size was 5 mm. The GPC system consisted of a Waters 510 pump, a Waters U6K injector, a Waters 486 UV-Vis detector, and a Waters 410 differential refractive index detector. The columns were thermostatted at 70 °C.

The following compounds were synthesized according to literature precedent: *N-tert*-Butyl-α-iso-propylnitrone,[12] 2,2,5-Trimethyl-4-phenyl-3-azahexane-3-nitroxide,[12] 2,2,5-Trimethyl-3-(1'-phenylethoxy)-4-phenyl-3-azahexane,[13] 5-(4-Bromophenyl)tetrazole,[7] 2-(4-*tert*-Butylphenyl)-5-(4-bromophenyl)-1,3,4-oxadiazole,[7] 2-(4-*tert*-Butylphenyl)-5-(4-vinylphenyl)-1,3,4-oxadiazole,[7] Isopropylidene-2,2-bis(methoxy)propionic acid,[18] Isopropylidene-2,2-bis(methoxy)propionic anhydride (**3**),[17] 4-Trimethylsilyl-1-buten-3-yne.[9]

Polymer 1. To a dry Wheaton sealable glass vessel with a stirbar 0.252 g (15.5 mmol) of *p*-acetoxystyrene, 0.946 g (3.11 mmol) of oxadiazole, 1 mL of *tert*-butylbenzene and 5.1 mg (0.017 mmol) of alkoxyamine initiator was added. The vessel was purged of oxygen through 3 freeze, pump, thaw cycles with argon backfill. The glass vessel was flame sealed under argon, and then bulk polymerization was started at 125 °C for 14 h with stirring. The vessel was allowed to cool, and then opened. A small amount of dichloromethane (DCM) was added to the mixture to yield a viscous residue that was precipitated from hexanes. The white polymer precipitate was collected on a medium frit and then dried under vacuum to yield 1.11 g (93%) of **7**. ^{1}H NMR (CDCl$_3$, 400 MHz): δ ppm 1.33 (s, 9), 1.9-2.3 (br, 3n/m), 6.2-6.9 (br, 2+2n/m), 7.3-7.6 (br, 2), 7.6-8.2 (br, 4). Calcd M$_w$ 70 000. Found THF GPC (UV polystyrene standard) M$_w$ 45 000 PDI 1.4. THF GPC (MALS) M$_w$ 71 000 PDI 1.3.

Polymer 1-OH. 15 mL of dioxane was added to a scintillation vial containing 1.07 g of polymer **7**. This solution was stirred while 1.6 mL of hydrazine hydrate (H$_2$NNH$_2$ · xH$_2$O) was added creating a frothy bubbling solution. The solution was stirred at 40 °C for 24 h, and then the solvent was evaporated under reduced pressure. The remaining solid was dissolved in a minimum amount of dichloromethane and precipitated from methanol. The resulting white precipitate was filtered on a medium frit and dried under vacuum yielding 0.990 g of **1-OH**. ^{1}H NMR (CDCl$_3$, 400 MHz): δ ppm 1.33 (br, 9), 2.17 (s, 1n/m), 6.1-7.0 (br, 2+2n/m), 7.3-7.6 (br, 2), 7.6-8.2 (br, 4). Calcd M$_w$ 67 300. Found THF GPC (UV polystyrene standard) M$_w$ 41 000 PDI 1.4. THF GPC (MALS) M$_w$ 65 000 PDI 1.2.

Polymer 1-[G1]-A. To a scintillation vial containing 0.95 g of **1-OH** was added 0.95 mL (12 mmol) of dry pyridine and 38 mg (0.31 mmol) of dimethylaminpyridine (DMAP). While stirring, a mixture of 1.05 g (3.19 mmol) anhydride **3** in 3.4 mL of dry dichloromethane (DCM) was added to the reaction mixture. The resulting solution was stirred for 48 h at room temperature. The solvent was evaporated under reduced pressure and a minimum amount of dichloromethane was added to precipitate from methanol. The white precipitate was filtered on a medium frit and dried under vacuum to yield 1.08 g (93%) **1-[G1]-A**. ^{1}H NMR (CDCl$_3$, 400 MHz): δ ppm 1.33 (s, 9), 3.3-3.8 (br, 2n/m), 3.9-4.3 (br, 2n/m), 6.1-7.0 (br, 2+2n/m), 7.3-7.6 (br,

2), 7.6-8.1 (br, 4). Calcd M_w 81 300. Found THF GPC (UV polystyrene standard) M_w 46 000 PDI 1.4. THF GPC (MALS) M_w 77 000 PDI 1.3.

Polymer 1-[G1]-[OH]$_2$. To a scintillation vial containing 1.03 g of **1-[G1]-A** was added acidic Dowex 50Wx2, 7 mL of methanol (MeOH) and 7 mL of tetrahydrofuran (THF). The solution was stirred slowly at 40 °C for 24 h and then filtered. The solvent was evaporated under reduced pressure and a minimum amount of dichloromethane was added to precipitate from petroleum ether. The white precipitate was filtered on a medium frit and dried under vacuum to yield 0.89 g (90%) of **1-[G1]-[OH]$_2$**. ^{1}H NMR (CDCl$_3$, 400 MHz): δ ppm 1.33 (s, 9), 3.0-3.7 (br, 2n/m), 3.7-4.2 (br, 4n/m), 6.1-7.0 (br, 2+2n/m), 7.3-7.6 (br, 2), 7.6-8.1 (br, 4). Calcd M_w 77 700. Found THF GPC (UV polystyrene standard) M_w 42 000 PDI 1.5. THF GPC (MALS) M_w 72 000 PDI 1.3.

Polymer 1-[G2]-A$_2$. To a scintillation vial containing 0.610 g of **1-[G1]-[OH]$_2$** was added 1.0 mL (12 mmol) of dry pyridine and 40 mg (0.33 mmol) of dimethylaminopyridine (DMAP). A mixture of 0.944 g (2.86 mmol) anhydride **3** in 3.5 mL of dry dichlormethane (DCM) was added to the reaction mixture was stirred for 24 h at room temperature. The solvent was evaporated under reduced pressure and the resulting solid was dissolved in a minimum amount of dichlormethane (DCM). The viscous solution was added dropwise to petroleum ether, and the resulting white precipitate collected by filtration on a medium frit to yield 0.685 g (83%) of **1-[G2]-A$_2$**. ^{1}H NMR (CDCl$_3$, 400 MHz): δ ppm 1.06 (br, 6n/m), 1.32 (s, 9+12n/m), 3.4-3.7 (br, 4n/m), 3.9-4.2 (br, 4n/m), 4.2-4.5 (br, 4n/m), 6.1-7.0 (br, 2+2n/m), 7.3-7.6 (br, 2), 7.6-8.1 (br, 4). Calcd M_w 105 800. Found THF GPC (UV polystyrene standard) M_w 54 000 PDI 1.3. THF GPC (MALS) M_w 101 000 PDI 1.2.

Polymer 1-[G2]-[OH]$_4$. To a scintillation vial containing 0.636 g of **1-[G2]-A$_2$** was added acidic Dowex 50Wx2, 10 mL of methanol (MeOH) and 10 mL of tetrahydrofuran (THF). The solution was stirred slowly at 40 °C for 48 h and then filtered. The solvent was evaporated under reduced pressure and a minimum amount of dichloromethane was added to precipitate from petroleum ether. The white precipitate was filtered on a medium frit and dried under vacuum to yield 0.536 g (81%) of **1-[G2]-[OH]$_4$**. ^{1}H NMR (CDCl$_3$, 400 MHz): δ ppm 1.10 (s, 6n/m), 1.32 (br, 9+3n/m), 3.6-3.9 (br, 8n/m), 4.1-4.6 (br, 4n/m), 6.1-7.0 (br, 2+2n/m), 7.3-7.6 (br, 2), 7.6-8.1 (br, 4). Calcd M_w 98 400. Found THF GPC (UV polystyrene standard) M_w 52 000 PDI 1.4. THF GPC (MALS) M_w 99 000 PDI 1.3.

3-(bromomethyl)-N,N-diphenylaniline. 3-bromobenzyl alcohol was protected with THP under standard procedures to yield 2-((3-bromobenzyl)oxy)tetrahydro-2H-pyran.[28] To a flame dried flask was added 9.2 g (34.3 mmol) 2-((3-bromobenzyl)oxy)tetrahydro-2H-pyran, 9.0 g (54 mmol) diphenylamine, 305 mg (0.33 mmol) tris(dibenzylideneacetone)dipalladium(0), 765 mg (1.4 mmol) 1,1'-bis(diphenylphosphino)ferrocene and 5.2 g (54 mmol) sodium *tert*-butoxide. To this flask was added 90 mL toluene followed by stirring at 90 °C under argon overnight. The product was filtered through celite then purified on a column of silica with 9:1 hexanes:ethyl acetate eluent (Rf = 0.27) to yield 9.4 g (26 mmol, 77%) of N,N-diphenyl-3-(((tetrahydro-2H-pyran-2-yl)oxy)methyl)aniline as a thick yellow oil. This material was stirred in 100 mL ethanol with 1 mol % pyridinium 4-toluenesulfonate at 55 °C for 8 hr then concentrated in vacuo. The resulting oil was purified through a short plug of silica to yield (3-(diphenylamino)phenyl)methanol ^{1}H NMR (CDCl$_3$, 300 MHz): δ ppm 1.63 (s, 1), 4.57 (s, 2), 6.98-7.04 (m, 4), 7.06-7.09 (m, 5), 7.20- 7.38 (m, 5). To a flame dried flask was added 150 mL dry dichloromethane (DCM) followed by cooling in an ice bath. To this cooled flask was added 6.2 g (24 mmol) triphenylphosphine followed by 7.7 g (24 mmol) carbon tetrabromide. The (3-

(diphenylamino)phenyl)methanol was then added dissolved in 50 mL DCM. This mixture was stirred for 6 hours then quenched by addition of H_2O. The resulting organic layer was extracted with a saturated solution of NaBr and concentrated in vacuo. The product was purified on a silica column with 9:1 hexanes:ethyl acetate eluent to yield 7.5 g (22 mmol, 89 % over two steps) of 3-(bromomethyl)-N,N-diphenylaniline as a brown oil. ^{1}H NMR (CDCl$_3$, 400 MHz): δ ppm 4.36 (s, 2), 6.96-7.09 (m, 9), 7.16-7.44 (m, 5). ^{13}C NMR (CDCl$_3$, 400 MHz): δ ppm 33.68, 122.70, 122.70, 123.31, 124.00, 124.70, 129.39, 129.53, 139.04, 147.69, 148.40.

3-(3-(diphenylamino)phenyl)propanoic acid (4). To a flame dried flask was added 1.7 mL (13.3 mmol) 2,4,4-trimethyl-1,3-oxazoline and 20 mL dry THF. This flask was cooled to -78 °C in a dry ice/acetone bath followed by slow dropwise addition of 5.9 mL (14 mmol) *n*-butyl lithium (2.5M in hexanes). To this solution was added dropwise by cannula 1.5 g (4.5 mmol) 3-(bromomethyl)-N,N-diphenylaniline dissolved in 10 mL dry THF. This solution was stirred for 4 hours while warming to room temperature. The mixture was concentrated in vacuo then dissolved in DCM and extracted with sat. NaHCO$_3$. The organic layer was concentrated in vacuo to yield a crude oil. In a flask this oil was heated to reflux in 3N HCl for 3 hours. The resulting mixture was extracted with DCM (3 x 40 mL) and washed with brine. The organic layer was dried over MgSO$_4$ and concentrated in vacuo. The product oil was purified on a column of silica with 20:1 ethyl acetate:methanol (Rf = 0.5) to yield 1.17 g (3.7 mmol, 83%) of 3-(3-(diphenylamino)phenyl)propanoic acid **4** as a light brown solid. ^{1}H NMR (CDCl$_3$, 400 MHz): δ ppm 2.61 (t, 2), 2.73 (t, 2), 6.83-7.08 (m, 9) 7.12-7.26 (m, 5), 8.53 (s, 1). ^{13}C NMR (CDCl$_3$, 400 MHz): δ ppm 30.59, 35.49, 122.00, 122.44, 122.69, 122.73, 123.73, 124.02, 129.29, 141.51, 147.77, 148.00, 172.17.

General procedure for exterior triarylamine attachment. To a small dry flask was added 75 mg of dendronized polymer, 5 mg dimethylamino pyridine and 250 uL of pyridine. To a separate dry flask was added 2 mL DCM, 130 mg dicyclohexylcarbodiimide (2.5x the estimated free dendronized polymer exterior hydroxyl groups) and 160 mg of **4** (2x free hydroxyl groups). This solution was then quickly added to the first and stirred for 24 hours at room temperature. The resulting mixture was precipitated from an excess amount of methanol then washed with hexanes to yield the final triarylamine decorated dendronized linear polymer. ^{1}H NMR shown in Figure 2.5.
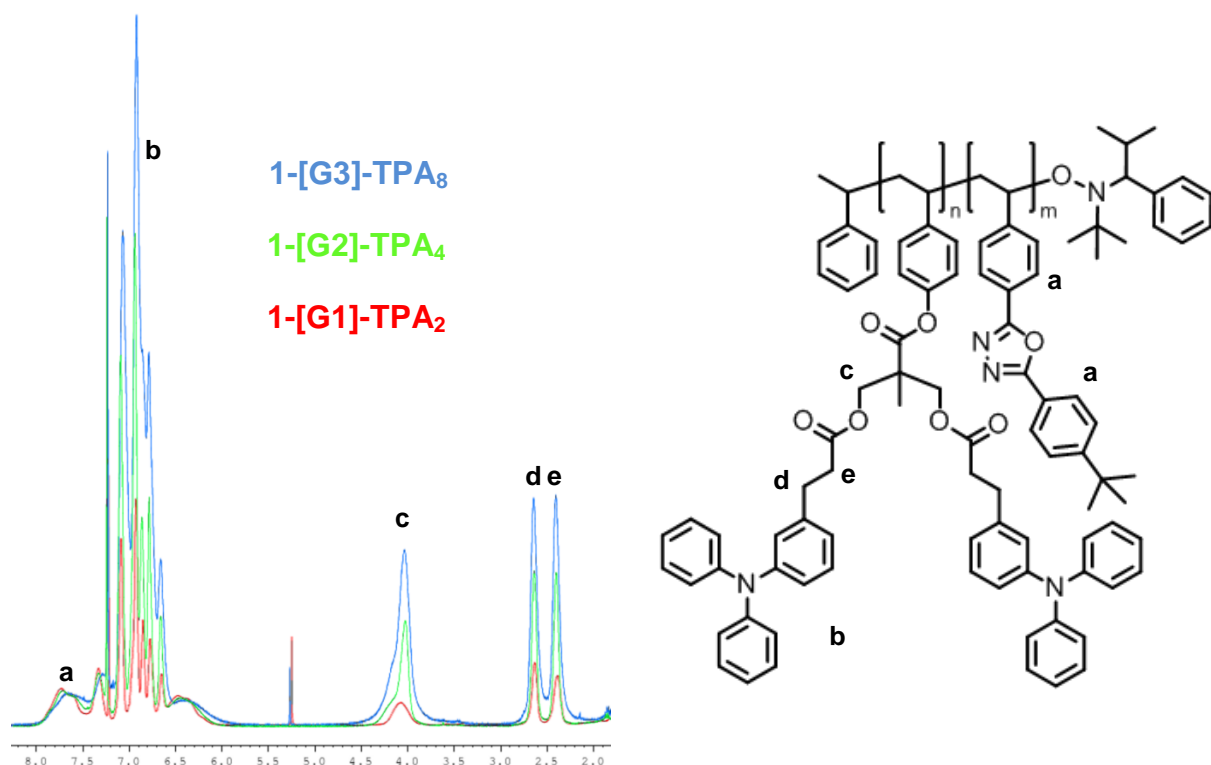
Figure 2.5. Superimposed ^{1}H NMR spectra for all three resulting dedronized linear polymers normalized to the oxadiazole peak a. The peaks corresponding to the triarylamine dendritic material double accordingly with the generations of dendron.

Polymer 5-TMS. To a sealable Whatman reaction vessel was added a mixture of 0.107 g (0.866 mmol) of 4-Trimethylsilyl-1-buten-3-yne, 0.499 g (1.64 mmol) of oxadiazole monomer and 4 mg (30 μmol) of azobisisobutylonitrile (AIBN) in 2.5 mL of benzene. The mixture was stirred vigorously and then purged of oxygen with 5 freeze, pump thaw cycles using argon backfill. The vessel was flame sealed under argon and heated to 60 °C with stirring for 14 h. The resulting viscous solution was then precipitated from hexanes and filtered on a medium frit to yield **5-TMS**. IR (CHCl$_3$): 2962, 2244, 2165, 1615 cm^{-1}. ^{1}H NMR (300 MHz): δ ppm –0.5-0.2 (br, 9n/m), 1.33 (s, 9), 6.2-7.1 (br, 2), 7.3-7.6 (br, 2), 7.6-8.1 (br, 4). n/m = 0.38. THF GPC (UV polystyrene standard) M$_w$ 48 000 PDI 1.8.

Polymer 5. In a round bottomed flask, 190 mg of polymer **5-TMS** was dissolved in 8 mL of tetrahydrofuran (THF). To this solution a mixture of 0.505 g (8.99 mmol) KOH in 2 mL methanol and 0.5 mL water was added. The reaction mixture was heated to 50 °C and stirred for 51 h. The solvent was evaporated and the solid residue was dissolved in a minimum amount of dichloromethane. This was precipitated from hexane and filtered on a medium frit to yield 0.122 g (76%) of **5**. IR (CHCl$_3$): 3306, 2963, 2245, 1615 cm^{-1}. ^{1}H NMR (CDCl$_3$, 400 MHz): δ ppm 1.33 (s, 9), 1.4-2.0 (br, 8), 6.3-7.1 (br, 2), 7.3-7.6 (br, 2), 7.6-8.1 (br, 4). THF GPC (UV polystyrene standard) M$_w$ 45 000 PDI 1.9.

[TAA]$_4$-[G3]-N$_3$. To a round bottomed flask was added 50 mg of **[TAA]$_4$-[G4]-Br**,[22] 2 mg of NaN$_3$ and 1 mL of DMF. The reaction was stirred at room temperature for 24 h. The solution was diluted with 20 mL of water and extracted with three 10 mL portions of CH$_2$Cl$_2$.

The organic phase was dried over MgSO$_4$ and then the solvent evaporated under reduced pressure to yield the product. IR (CDCl$_3$, CHCl$_3$): 3056, 2955, 2929, 2871, 2099, 1678, 1595 cm^{-1}. ^{1}H NMR (400 MHz) δ ppm 0.89 (t, 24 J = 7.3), 0.98 (d, 24, J = 6.6), 1.17 (m, 8), 1.31 (m, 8), 1.44 (m, 16), 1.90 (m, 8), 3.68 (dd, 8), 3.77 (dd, 8), 4.07 (s, 2), 4.91 (m, 28), 6.39 (m, 4), 6.50 (m, 4), 6.53 (m, 10), 6.59 (m, 6), 6.64 (m, 8), 7.00-7.40 (m, 52), 7.52 (m, 4), 7.64-7.73 (m, 8).

References

(1) Liang, C. O.; Helms, B.; Hawker, C. J.; Fréchet, J. M. J. *Chem. Commun.* **2003**, 2524-2525.
(2) Sato, T.; Jiang, D.; Aida, T. *J. Am. Chem. Soc.* **1999**, *121*, 10658-10659.
(3) Pogantsch, A.; Wenzl, F.; List, E.; Leising, G.; Grimsdale, A.; Müllen, K. *Adv. Mater.* **2002**, *14*, 1061-1064.
(4) Marsitzky, D.; Vestberg, R.; Blainey, P.; Tang, B. T.; Hawker, C. J.; Carter, K. R. *J. Am. Chem. Soc.* **2001**, *123*, 6965-6972.
(5) Kimoto, A.; Masachika, K.; Cho, J.; Higuchi, M.; Yamamoto, K. *Org. Lett.* **2004**, *6*, 1179-1182.
(6) Shu, C.; Dodda, R.; Wu, F.; Liu, M. S.; Jen, A. K. *Macromolecules* **2003**, *36*, 6698-6703.
(7) Deng, L.; Furuta, P. T.; Garon, S.; Li, J.; Kavulak, D.; Thompson, M. E.; Fréchet, J. M. J. *Chem. Mater.* **2006**, *18*, 386-395.
(8) Behl, M.; Hattemer, E.; Brehmer, M.; Zentel, R. *Macromol. Chem. Phys.* **2002**, *203*, 503-510.
(9) Helms, B.; Mynar, J. L.; Hawker, C. J.; Fréchet, J. M. J. *J. Am. Chem. Soc.* **2004**, *126*, 15020-15021.
(10) Hawker, C.; Frechet, J. *Polymer* **1992**, *33*, 1507-1511.
(11) Grayson, S. M.; Frechet, J. M. J. *Macromolecules* **2001**, *34*, 6542-6544.
(12) Benoit, D.; Chaplinski, V.; Braslau, R.; Hawker, C. J. *J. Am. Chem. Soc.* **1999**, *121*, 3904-3920.
(13) Benoit, D.; Harth, E.; Fox, P.; Waymouth, R. M.; Hawker, C. J. *Macromolecules* **2000**, *33*, 363-370.
(14) Greczmiel, M.; Strohriegl, P.; Meier, M.; Brutting, W. *Macromolecules* **1997**, *30*, 6042-6046.
(15) Chen, X.; Jankova, K.; Kops, J.; Batsberg, W. *J. Polym. Sci., Part A: Polym. Chem.* **1999**, *37*, 627-633.
(16) Yoshida, M.; Fresco, Z. M.; Ohnishi, S.; Fréchet, J. M. J. *Macromolecules* **2005**, *38*, 334-344.
(17) Malkoch, M.; Malmstrom, E.; Hult, A. *Macromolecules* **2002**, *35*, 8307-8314.
(18) Ihre, H.; Padilla De Jesus, O. L.; Fréchet, J. M. J. *J. Am. Chem. Soc.* **2001**, *123*, 5908-5917.
(19) Rostovtsev, V. V.; Green, L. G.; Fokin, V. V.; Sharpless, K. B. *Angew. Chem. Int. Ed.* **2002**, *41*, 2596-2599.
(20) Huisgen, R. *Angew. Chem. Int. Ed.* **1963**, *2*, 565-598.
(21) Huisgen, R. *Angew. Chem. Int. Ed.* **1968**, *7*, 321-328.
(22) Furuta, P.; Fréchet, J. M. J. *J. Am. Chem. Soc.* **2003**, *125*, 13173-13181.
(23) Lamansky, S.; Djurovich, P.; Murphy, D.; Abdel-Razzaq, F.; Kwong, R.; Tsyba, I.; Bortz, M.; Mui, B.; Bau, R.; Thompson, M. E. *Inorg. Chem.* **2001**, *40*, 1704-1711.
(24) Li, J.; Djurovich, P. I.; Alleyne, B. D.; Yousufuddin, M.; Ho, N. N.; Thomas, J. C.;

Peters, J. C.; Bau, R.; Thompson, M. E. *Inorg. Chem.* **2005**, *44*, 1713-1727.

(25)   Agard, N. J.; Prescher, J. A.; Bertozzi, C. R. *J. Am. Chem. Soc.* **2004**, *126*, 15046-15047.

(26)   Killops, K. L.; Campos, L. M.; Hawker, C. J. *J. Am. Chem. Soc.* **2008**, *130*, 5062-5064.

(27)   Kade, M. J.; Burke, D. J.; Hawker, C. J. *J. Polym. Sci., Part A: Polym. Chem.* **2010**, *48*, 743-750.

(28)   Delorme, D.; Ducharme, Y.; Brideau, C.; Chan, C.; Chauret, N.; Desmarais, S.; Dube; Falgueyret, J.; Fortin, R.; Guay, J.; Hamel, P.; Jones, T. R.; Lepine, C.; Li, C.; McAuliffe, M.; McFarlane, C. S.; Nicoll-Griffith, D. A.; Riendeau, D.; Yergey, J. A.; Girard, Y. *J. Med. Chem.* **1996**, *39*, 3951-3970.

Chapter 3

Effects of Bipolar Diblock Copolymer Host Morphology on Device Performance

Abstract

This chapter discusses the development of bipolar transport polymers as host materials for electroluminescent devices by incorporating electron transporting and hole transporting functionalities into copolymers. The effects of the molecular structure and film morphology of these copolymers on the device performance is studied. Two different copolymers having the same molecular weight (M_n ~ 30 kDa) and same ratio of hole transporting to electron transporting monomers (1:1) were synthesized in the forms of random and diblock copolymers. For the diblock copolymer, pronounced phase segregation forming different nanoscale morphologies was observed, while this was not the case for the random copolymer counterpart under the same thin film preparation conditions. The results of single layer polymer light emitting diodes (PLEDs) show the nanophase separation morphology of diblock copolymers has various effects on the device performance, including lowering charge transport and facilitating the hole-electron recombination leading to much higher quantum efficiency. Using this high triplet energy block copolymer as host material, a high external quantum efficiency of 5.6 % at the brightness of 900 Cd/m^2 was achieved for a single layer PLEDs with a phosphorescent green emitting complex dopant.
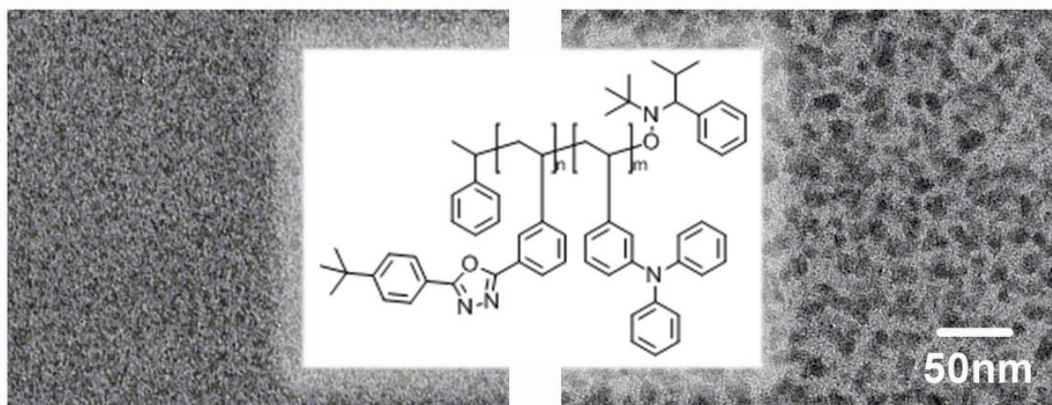
Introduction

Organic light-emitting diodes (OLEDs) have attracted great attention due to their potential application in both flat-panel displays and lighting sources.[1-9] Identifying new materials is of significant importance in realizing high performance OLEDs. To date, there two major kinds of materials that have been widely applied: conducting polymers and small molecular organic materials. An advantage of polymeric materials is their solution processability that offers lower cost and less time for manufacturing, in comparison to vapor deposition of small molecules in high vacuum. However, typical polymer LEDs (PLEDs) only provide fluorescence, which has limited internal quantum efficiencies of 25 %, since only singlet excitons can be utilized.[4] By applying phosphorescent molecules as emitting materials, such as iridium and platinum complexes, 100 % internal quantum efficiencies can be achieved.[5-7,10,11] This is due to the strong spin-orbital coupling of heavy metals that facilitates efficient intersystem crossing and allows complexes to capture both singlet and triplet excitons. Indeed, solution processed highly efficient PLEDs have been demonstrated by physically doping phosphorescent molecules in polymer matrix or chemically bonding them to polymer chains.[12-19]

However, the physical properties of host polymers such as the triplet energy, the charge transport properties and the balance of holes and electrons control various aspects of device behaviour and materials should be judiciously chosen to maximize the device performance. For example, hosts having higher triplet energy over dopants are required to avoid the back energy transfer from the emitters to hosts.[20] To achieve good balance of holes and electrons, both hole and electron transporting functions should be incorporated into the single bipolar host materials. Physically blending one carrier transporting material with another carrier transporting material is a typical technique used to produce this bipolar host matrix. The blend of electron transporting (2-tert-butylphenyl-5-biphenyl-1,3,4-oxadiazol) PBD with the hole transporting poly(N-vinylcarbazole) PVK is a good example, with which as host, efficient single layer green light emitting diodes has been demonstrated with external quantum efficiency at 3.5 %.[12] Since the photophysical and electrical behaviour of polymer films is highly sensitive to aggregation and film morphology[21-31], control of the phase separated morphology of two immiscible polymers is critical for device performance, but difficult to achieve.[21] The devices require fine dispersion of one polymer in another without macrophase separation. Ideally, a bicontinuous morphology with 10-20 nm lengthscale for charge transport and exciton diffusion which has been shown to improve the device performance. However, such a morphology which can be obtained in a kinetically trapped nonequilibrium method, is very difficult to control. In many cases, it can be achieved only in extremely narrow regime of blend composition.[32-34] In contrast to this, a device consisting of random or diblock copolymers does not experience macrophase separation at larger than the micrometer length scale. Of particular interest is that diblock copolymer devices having various morphologies with nanometer lengthscale can be achieved even under equilibrium.[21,35,36] Lastly, very little work has been done in high-triplet host polymers, especially bipolar copolymer systems.

Given the recent progress in living radical polymerization,[37-40] we are able to develop functional polymers with controlled properties and designed architectures. This chapter discusses work in identifying novel bipolar transport polymers as host materials for electroluminescent devices, through incorporating electron transporting and hole transporting functionalities into copolymers. More specifically, demonstrating how the molecular structure of these copolymers affects the film morphology and subsequently the device performance. For the block

copolymers, pronounced phase segregation with nanometer lengthscale has been observed, in contrast to the homogeneous morphology from the random counterparts under the same thin film preparation conditions. The large interfacial area between electron and hole transporting domains in the block copolymer device has a dramatic influence on the charge transport and recombination. Therefore, the interface of block copolymer domains facilitates the hole-electron recombination leading to much higher quantum efficiency than for a random copolymer, while lowering the charge transport at the same time. With optimization, high performance single layer electroluminescent devices with external quantum efficiency up to 5.6 % were achieved. High performance in these devices can be attributed to domain separation mimicking a multilayer structure in a single layer device, where hole transporting and electron transporting moieties self assemble to form large interfacial area for charge recombination.

Results and Discussion

Two copolymers containing hole transporting (HT) triphenylamine (TPA) and electron transporting (ET) oxadiazole (OXA) functionalities (m/n = 1) were synthesized as shown in Scheme 3.1. One is a random copolymer (R-TPA-OXA) having molecular weight (M_n) of 29 kg/mol and PDI of 1.15, and the other is a diblock copolymer (B-TPA-OXA) having M_n of 30 kg/mol and PDI of 1.25. Synthesis of these copolymers has been previously reported.[19] Analysis of these polymers by differential scanning calorimetry (DSC) is shown in Figure 3.1. Only one glass transition temperature (T_g) at 143 °C was observed for the random copolymer (R-TPA-OXA), while two separate T_g at 131 °C and 168 °C were observed for the diblock copolymer (B-TPA-OXA). These two glass transitions occur at roughly the same temperature as in homopolymers of each block, TPA homopolymers ($T_g \sim$ 125 °C) and OXA homopolymers ($T_g \sim$ 182 °C). Equilibrium thin film morphologies of these copolymers were obtained by thermal annealing at 225 °C for 3 days and then at 185 °C for 1 day. The TEM image in the inset of Figure 3.1 shows the lamellar structure of B-TPA-OXA polymers with domain spacing of 24 nm. Hole transporting (TPA) and electron transporting (OXA) components of the block copolymer self assembled to form a layer-by-layer structure. In contrast, such phase separation was not observed for the random copolymer R-TPA-OXA.
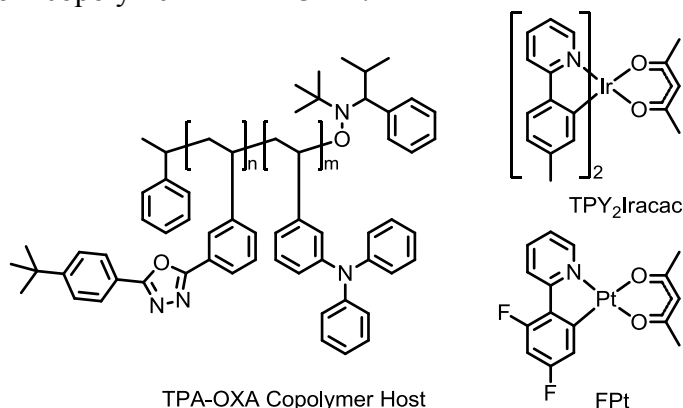
Scheme 3.1. The chemical structures of bipolar copolymers (m/n=1) and two phosphorescent heavy metal complexes.
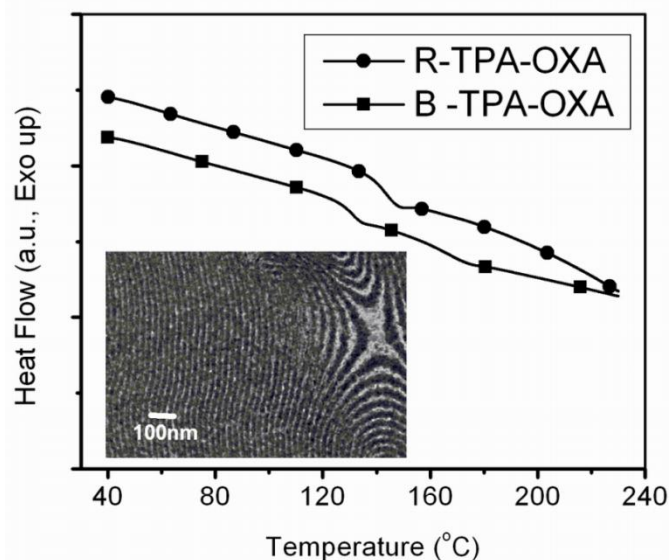
Figure 3.1. DSC of two copolymers: R-TPA-OXA (●) and B-TPA-OXA (■); and the TEM image of thermally treated block copolymer bulk sample showing lamellar structure.

These two HT/ET bipolar copolymers were applied as the host matrix for phosphorescent dopants in polymer LEDs to investigate the effects of polymer composition of these polymers on the device performance. Single layer polymer LEDs were fabricated from chloroform solutions of both copolymers with 8 wt. % green emitting TPY$_2$Iracac doping. A 90 nm thick polymer layer was produced by spincasting the solution on pre-treated indium-tin-oxide (ITO)-coated glass substrate and metal cathodes consisting of 1 nm LiF and 100 nm of Al were vapor deposited in high vacuum chamber at lower than $3\text{-}4\times10^{-6}$ Torr to give the device structure as shown in Figure 3.2.
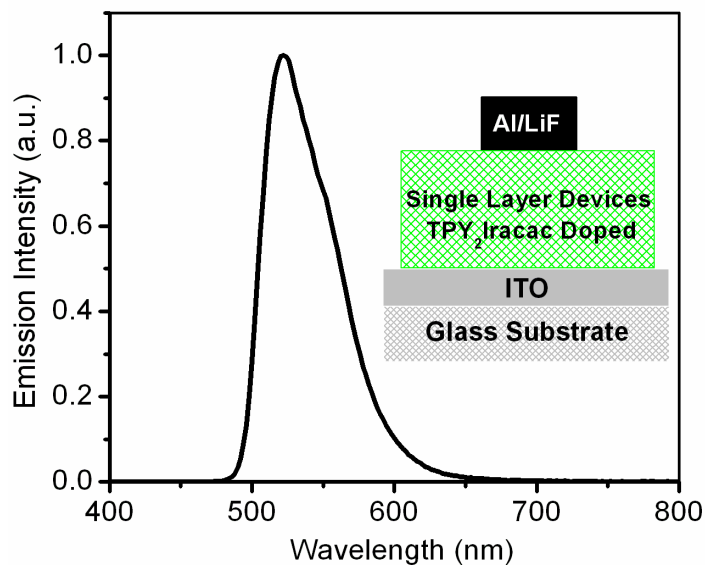
Figure 3.2. The electroluminescent spectrum for a device with structure of ITO/copolymers with 8 wt. % TPY$_2$Iracac dopant (90 nm) /LiF(1nm)/Al(100 nm).

The electroluminescent spectrum of these single layer green phosphorescent devices in Figure 3.2 shows emission purely from TPY$_2$Iracac and the absence of either TPA or OXA emission indicates that the excitons are exclusively localized on the phosphorescent dopants prior to relaxation. Efficient energy transfer from the polymer host to the dopant is not surprising, since the triplet energy of the host (>2.5 eV) is higher than that of the dopant (2.36 eV). Figure 3.3 shows the device characteristics of these two different devices, and Table 3.1 summarizes the device performance. It was found that the R-TPA-OXA device has about one order magnitude higher current density over B-TPA-OXA device at the same voltage. A similar slope (~ 2) was found for the logI-logV plots of the two devices in high-voltage region, which indicates that the transport characteristics in both devices can be well described using space-charge limited current (SCLC) theory in the presence of traps.[41,42] The charge transport is described by

$$j = \frac{9}{8}\varepsilon\mu_{eff}\frac{V^2}{d^3}, \text{ or } I \propto V^2,$$ where ε is the permittivity of the polymer, d is the polymer film

thickness, μ_{eff} is the effective mobility and V is the applied voltage. These two devices not only exhibited different I-V characteristics, but also significant difference in quantum efficiency. As shown in Figure 3.3, 2-3 times higher light output from B-TPA-OXA device over R-TPA-OXA device was observed at the same current density yielding maximum external quantum efficiencies (η_{max}) of 4.6% (at 220 Cd/m^2) and 2.0% (560 Cd/m^2) respectively. Since the polymer chemical compositions, the dopants, and film thicknesses are identical for both devices, we believe that the dramatic difference in device performance is attributed mainly to the film morphology which determines the effective carrier mobility and the carrier recombination.
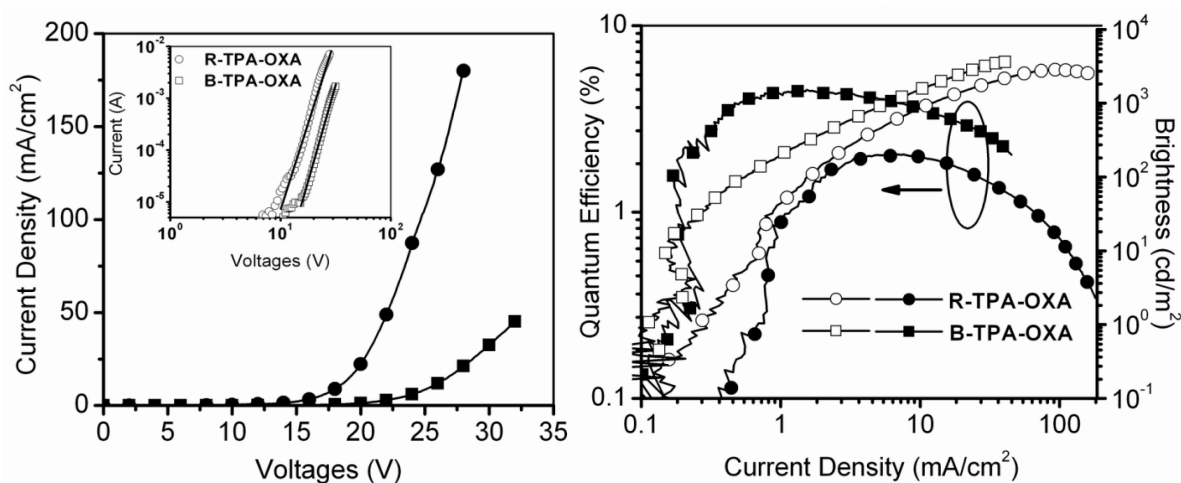
Figure 3.3. I-V characteristics (left), Brightness vs. Current Density and External Quantum Efficiency vs. Current Density (right) for single layer light emitting diodes using TPY$_2$Iracac as guest and copolymers as host from chloroform solutions: R-TPA-OXA (circles: ○●) and B-TPA-OXA (squares: □■).

The difference in morphology for spin-casted thin films was investigated by AFM and TEM. Since the properties of spin-casted films are related to a number of factors, including solvent properties, solvent-polymer interactions, and the spin-casting conditions (speed, temperature, time and so on), thin films were fabricated with both copolymers in the same conditions to evaluate the effects of molecular structure on the film architectures. Figure 3.4a

and 3.4c show the AFM phase images of the surface morphology for thin films from chloroform solutions of R-TPA-OXA and B-TPA-OXA. For random copolymers, the AFM phase image is smooth and featureless, indicating homogeneous morphology without any phase segregation of hole and electron transporting materials. In contrast, two distinct phases were observed in the morphology for block copolymers. The phase separation lengthscale ranges from 20 nm to 30 nm.
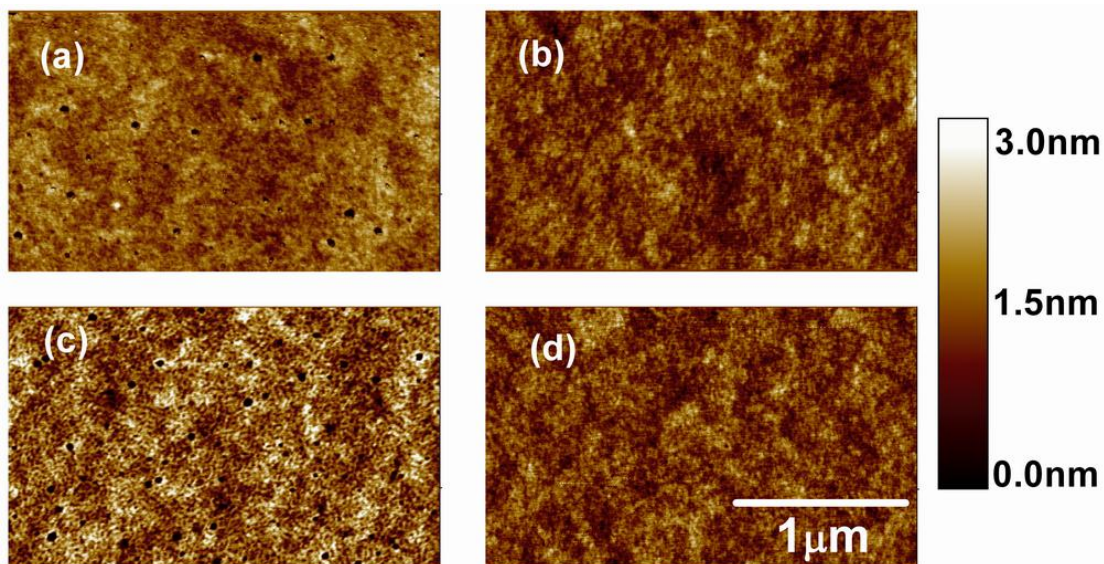
Figure 3.4. Tapping-mode AFM topographic images of thin films: (a) R-TPA-OXA in chloroform, (b) R-TPA-OXA in chlorobenzene, (c) B-TPA-OXA in chloroform, (d) B-TPA-OXA in chlorobenzene.

AFM images of samples from chlorobenzene solutions in Figure 3.4b and 3.4c showed improved film quality with no pin-holes and smaller root-mean-square (RMS) surface roughness of 0.3 nm, as compared to chloroform samples with RMS surface roughness of 0.5 nm. This can be attributed to the slower evaporation of chlorobenzene with a higher boiling point during the film formation. Doping small molecular emitters in both copolymers at 8 wt. % did not change the film morphology. Figure 3.5 shows the TEM images of two copolymers with 8 wt. % TPY$_2$Iracac doping from chlorobenzene solutions. The formation of interfaces by nanophase separation was clearly found in block copolymers, but not in random copolymers. Since charge traveling through a film is a hopping process that is related to the intermolecular overlap of neighbouring molecules,[31] the charge transport behavior in both copolymers can then be schematically described in Figure 3.5. In the random copolymer host, holes and electrons can transport continuously in the TPA phase (HOMO orbital) and in the OXA phase (LUMO orbital) respectively when the traps are filled at high driving voltage. However, the formation of phase segregated domains in the B-TPA-OXA polymer device interrupts carrier transport pathways, leading to less charge transport at the same driving voltage. Such film morphology accompanies the formation of large interfacial area between the two domains of the hole and electron materials, facilitating the recombination of opposite charges as shown in Figure 3.5. This is evident in the device characteristics in Figure 3.4, showing higher light output from block copolymer device than random copolymer device at the same current density.
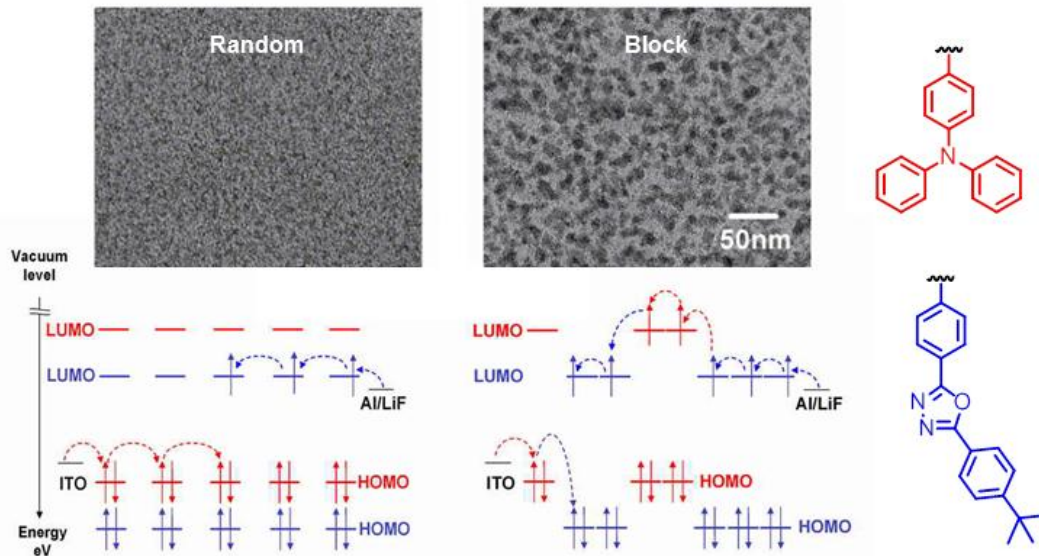
Figure 3.5. TEM images of thin films from chlorobenzene solutions of R-TPA-OXA (left) and B-TPA-OXA (right), and the schemes of charge transport proposed for random copolymers and block copolymers.

We optimized the device performance by modifying the device fabrication conditions, organic solvent and tuning device thickness. Chlorobenzene was used to enhance the film quality of device by allowing more time for the film organization while spincasting. It is well known that carrier leakage and/or charge trapping near the electrodes are invoked as important quenching mechanisms in single-layer polymer LEDs, since the simple structure provides no barrier for either carrier or exciton confinement within the organic layer. Therefore, shifting the recombination zone away from the electrodes and decreasing electrode quenching will improve the device quantum efficiency. Three devices using B-TPA-OXA as host were fabricated with thicknesses of 71 nm, 95 nm, and 125 nm, which correspond to the thickness of 3, 4 and 5 layers of TPA-OXA lamellae. Another 95 nm thick device using R-TPA-OXA was also fabricated for comparison. As is indicated in Figure 3.6, at the same thickness, the device with B-TPA-OXA as host has higher quantum efficiency than that with R-TPA-OXA, consistent with what we observed in devices prepared from chloroform solutions. For B-TPA-OXA devices with increasing device thickness, the current density decreased, turn-on voltage increased and the external quantum efficiency improved. The thicker device produces larger interfacial area between block copolymer domains, facilitating the charge recombination and yielding higher quantum efficiency. However, the reduced current density in a thicker device could lower the probability of charge recombination away from the electrode. Therefore, an optimal thickness was found to be 95 nm for a B-TPA-OXA device which corresponds to 4 layers of TPA-OXA domains. Although the highest quantum efficiency of 5.6 % was achieved for a 125 nm device, the 95 nm B-TPA-OXA with η_{max} = 5.6 % was more likely the best device, when other device characteristics are considered including turn-on voltage, brightness and power efficiency. It is interesting to find a 71 nm device of B-TPA-OXA displayed similar quantum efficiency performance as a 95 nm device of R-TPA-OXA. This can be explained in that more efficient

carrier recombination and higher electrode/polymer interface quenching happen at the same time in the B-TPA-OXA device. From plots of quantum efficiency vs. current density, we found curves for block copolymer devices have a more pronounced rolling off feature than that for random copolymer devices, indicating more triplet-triplet annihilation[43] in the former.
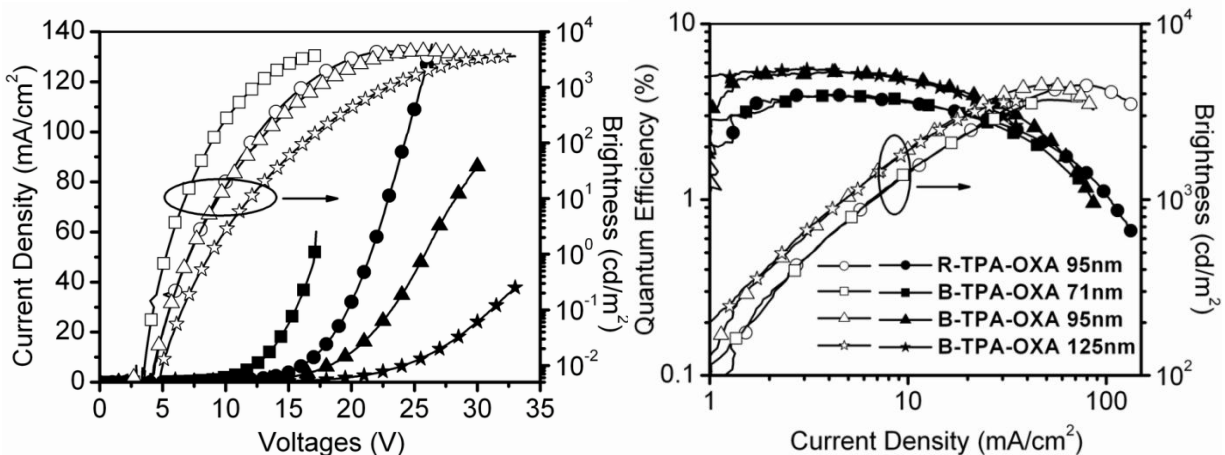
Figure 3.6. I-V Characteristic, Current Density vs. Voltages (left), Brightness vs. Current Density and External Quantum Efficiency vs. Current Density (right) for single layer light emitting diodes using TPY$_2$Iracac as guest and copolymers as host from chlorobenzene solutions in different thickness: R-TPA-OXA 95 nm(circles: ○●), B-TPA-OXA 71 nm (squares: □■), B-TPA-OXA 95 nm (triangles: △▲) and B-TPA-OXA 125 nm (stars: ☆★).

To investigate the dopant's interaction in both copolymers, we fabricated single layer devices with a structure of ITO/8 wt.% FPt doped Copolymers/LiF/Al. Platinum complex FPt was chosen as the dopant due to its pronounced molecular aggregation-dependent red-shifted emission.[8-10;44] Electroluminescent spectra and external quantum efficiencies as a function of current density for these two devices are shown in Figure 3.7. Higher quantum efficiency for B-TPA-OXA device over R-TPA-OXA device was observed, showing the same trend as the results of iridium doped devices in Figure 3.3. In the electroluminescent spectra, the featured platinum dimer/excimer emission peak at 600 nm was clearly observed for the device with B-TPA-OXA as host, but not for device with R-TPA-OXA as host, indicating more FPt aggregation in block copolymer than in random copolymer. This is likely due to the immiscible polymer blocks forming separate coexisting phases which facilitates the aggregation of small molecules out of the polymer hosts. Since device performance usually drops upon dopant aggregation, we believe that the quantum efficiency can be further improved by dispersing small molecules uniformly in bipolar hosts. To achieve this, we are currently investigating three component polymers with covalently bonded phosphorescent emitters.
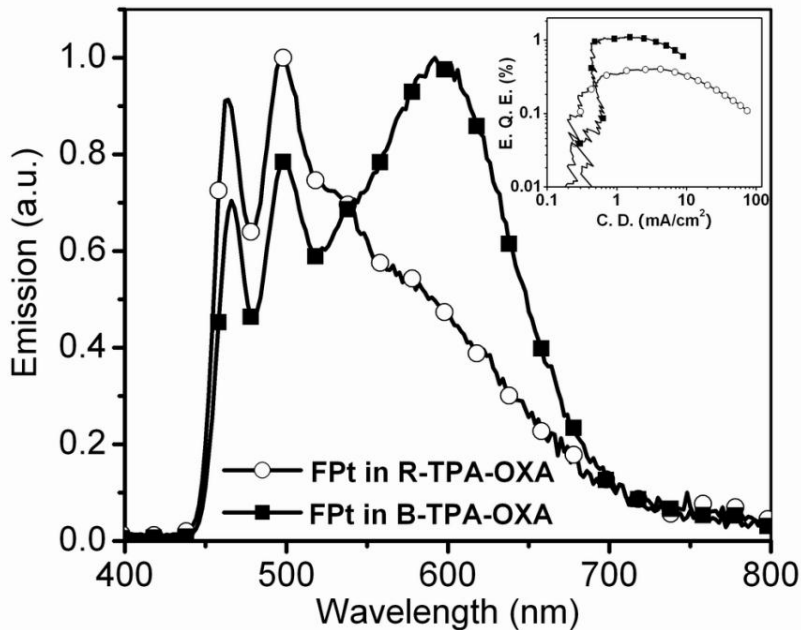
Figure 3.7. The electroluminescent spectra and External Quantum Efficiency vs. Current Density for 8 wt.% FPt doped single layer polymer LEDs using copolymers as host: R-TPA-OXA (○) and B-TPA-OXA (■).

Table 3.1. Summary of devices performance for single layer light emitting diodes using TPY$_2$Iracac as guest and copolymers as host fabricated from chloroform and chlorobenzene solutions.

Single Layer Devices at ~ 95 nm	Random Copolymer R-TPA-OXA		Block Copolymer B-TPA-OXA	
Solvent	Chloroform	Chlorobenzene	Chloroform	Chlorobenzene
Turn-on voltage (0.1 Cdm^{-2})	7.9 V	5.6 V	8.4 V	5.6 V
Maximum E.Q.E./Brightness	2.0 % 560 Cdm^{-2}	3.9 % 600 Cdm^{-2}	4.6 % 220 Cdm^{-2}	5.6 % 900 Cdm^{-2}
Maximum Brightness/Voltage	2850 Cdm^{-2} 24.8 V	4500 Cdm^{-2} 23 V	3800 Cdm^{-2} 32.8 V	4500 Cdm^{-2} 25.5 V
E.Q.E at 800 Cdm^{-2}	2.0 %	3.9 %	4.0 %	5.3 %

Conclusion

This chapter presented a series of experiments studying the effect of molecular structure of bipolar copolymers on the film morphology and device performance. Nonconjugated copolymers containing hole transporting and electron transporting components were studied in random and block copolymer compositions. The morphology of B-TPA-OXA and R-TPA-OXA copolymers prepared in different solvents and thicknesses were characterized by AFM and TEM, showing phase segregated TPA and OXA domains only in the B-TPA-OXA film. This

difference in thin film morphology had a pronounced effect on electroluminescent device performance. Charge transport in the block copolymer was one order of magnitude lower than in the random copolymer resulting from the domain phase separation making transport pathways through the device more circuitous. In consequence the hole/electron recombination is enhanced by 2-3 times for block copolymer over random copolymer, leading to much higher quantum efficiency for single layer polymer light emitting diodes. An external quantum efficiency of 5.6 % for a single layer green electroluminescence was obtained using TPY$_2$Iracac as the guest and B-TPA-OXA copolymer as host. However, the self organization of block copolymer also increased the aggregation of small molecular dopants, leading to increased triplet-triplet annihilation in polymer/dopant phosphorescent devices. In order to overcome this issue covalently bound phosphorescent emitters are discussed in the following chapter along with other beneficial characteristics of this approach.

Experimental

Materials and Film Characterization. The TPA-OXA copolymers studied in this paper are synthesized by living radical polymerization in random and block forms with TPA/OXA=1.[19] Heavy metal complexes were prepared as reported in the literature.[10,11] DSC was performed with a TA DSC Q200. The morphology of bulk sample as well as the thin film of B-TPA-OXA and R-TPA-OXA was investigated by transmission electron microscopy (TEM) and atomic force microscopy (AFM). The B-TPA-OXA polymers were annealed at 225 °C during 3 days, then at 185 °C during 1 day and cooled slowly down to room temperature under vacuum. The bulk sample was microtomed into 50 nm thick film and sequentially stained by RuO$_4$ 0.5% aqueous solution during 25 mins to produce the contrast between TPA and OXA blocks. Samples for morphological study of thin film were prepared under identical condition as the device was prepared. The films were prepared by spincasting from chlorobenzene (40 mg mL^{-1}) onto NaCl substrate and then transferred to the TEM grid by floating it on water. The samples were stained by RuO$_4$ 0.5 % aqueous solution during 25 mins. The morphology of cross-sectioned bulk and thin film samples were observed by FEI Tecnai operated at 200 kV. A Multimode AFM (Veeco) was used in a tapping mode for investigating the 2-dimensional surface topology of the T-TPA-OXA and R-TPA-OXA films on ITO/glass substrate as used for the device fabrication.

Devices Fabrication and Measurement. Prior to device fabrication, ITO on glass substrates were patterned as 2 mm wide stripes with resistivity of 20 Ω/cm. The substrates were cleaned by sonication in soap solution; rinsed with deionized water; boiled in trichloroethylene, acetone, and ethanol for 5 min each; and dried with nitrogen. Finally, the substrates were treated with UV ozone for 10 min. The organic active layer was prepared by spin-casting of solutions at 3000 rpm for 60 s. The solutions were filtered (2 μm poly(vinylidene difluoride) filter) prior to use. The thickness of organic layer was monitored by ellipsometry. After spin casting, a shadow mask with a 2 mm wide stripe was put onto the substrates perpendicular to the ITO stripes. A cathode consisting of 1nm LiF and 100 nm aluminium was deposited at a rate of 0.02 Å/s and 4-5 Å/s respectively. OLEDs were formed at the 2×2 mm squares where the ITO (anode) and Al (cathode) stripes intersect.

The devices were tested in air within 2 h of fabrication. The electrical and optical intensity characteristics of the devices were measured with a Keithly 2400 sourcemeter/2000 multimeter coupled to a Newport 1835-C optical meter, equipped with a UV-818 Si photodetector. Only light emitting from the front face of the device was collected and used in subsequent efficiency calculations. The electroluminescence (EL) spectra were measured on a

PTI QuantaMaster model C-60SE spectrofluorimeter, equipped with a 928 PMT detector and corrected for detector response. The emission was found to be uniform throughout the area of each device.

References

(1)   Tang, C. W.; VanSlyke, S. A. *Appl. Phys. Lett.* **1987**, *51*, 913-915.
(2)   Burroughes, J. H.; Bradley, D. D. C.; Brown, A. R.; Marks, R. N.; Mackay, K.; Friend, R. H.; Burns, P. L.; Holmes, A. B. *Nature* **1990**, *347*, 539-541.
(3)   Kido, J.; Kimura, M.; Nagai, K. *Science* **1995**, *267*, 1332-1334.
(4)   Friend, R. H.; Gymer, R. W.; Holmes, A. B.; Burroughes, J. H.; Marks, R. N.; Taliani, C.; Bradley, D. D. C.; Dos Santos, D. A.; Bredas, J. L.; Logdlund, M.; Salaneck, W. R. *Nature* **1999**, *397*, 121-128.
(5)   Baldo, M. A.; O'Brien, D. F.; You, Y.; Shoustikov, A.; Sibley, S.; Thompson, M. E.; Forrest, S. R. *Nature* **1998**, *395*, 151-154.
(6)   Baldo, M. A.; Thompson, M. E.; Forrest, S. R. *Nature* **2000**, *403*, 750-753.
(7)   Sun, Y.; Giebink, N. C.; Kanno, H.; Ma, B.; Thompson, M. E.; Forrest, S. R. *Nature* **2006**, *440*, 908-912.
(8)   Adamovich, V.; Brooks, J.; Tamayo, A.; Alexander, A. M.; Djurovich, P. I.; D'Andrade, B. W.; Adachi, C.; Forrest, S. R.; Thompson, M. E. *New J. Chem.* **2002**, *26*, 1171-1178.
(9)   D'Andrade, B. W.; Brooks, J.; Adamovich, V.; Thompson, M. E.; Forrest, S. R. *Adv. Mater.* **2002**, *14*, 1032.
(10)   Brooks, J.; Babayan, Y.; Lamansky, S.; Djurovich, P. I.; Tsyba, I.; Bau, R.; Thompson, M. E. *Inorg. Chem.* **2002**, *41*, 3055-3066.
(11)   Lamansky, S.; Djurovich, P.; Murphy, D.; Abdel-Razzaq, F.; Lee, H. E.; Adachi, C.; Burrows, P. E.; Forrest, S. R.; Thompson, M. E. *J. Am. Chem. Soc.* **2001**, *123*, 4304-4312.
(12)   Lamansky, S.; Djurovich, P. I.; Abdel-Razzaq, F.; Garon, S.; Murphy, D. L.; Thompson, M. E. *J. Appl. Phys.* **2002**, *92*, 1570-1575.
(13)   Vaeth, K. M.; Tang, C. W. *J. Appl. Phys.* **2002**, *92*, 3447-3453.
(14)   He, G. F.; Chang, S. C.; Chen, F. C.; Li, Y. F.; Yang, Y. *Appl. Phys. Lett.* **2002**, *81*, 1509-1511.
(15)   Gong, X.; Ostrowski, J. C.; Moses, D.; Bazan, G. C.; Heeger, A. J. *Adv. Func. Mater.* **2003**, *13*, 439-444.
(16)   Gong, X.; Lim, S. H.; Ostrowski, J. C.; Moses, D.; Bardeen, C. J.; Bazan, G. C. *J. Appl. Phys.* **2004**, *95*, 948-953.
(17)   Brunner, K.; van Dijken, A.; Borner, H.; Bastiaansen, J. J. A. M.; Kiggen, N. M. M.; Langeveld, B. M. W. *J. Am. Chem. Soc.* **2004**, *126*, 6035-6042.
(18)   Suzuki, M.; Tokito, S.; Sato, F.; Igarashi, T.; Kondo, K.; Koyama, T.; Yamaguchi, T. *Appl. Phys. Lett.* **2005**, *86*.
(19)   Deng, L.; Furuta, P. T.; Garon, S.; Li, J.; Kavulak, D.; Thompson, M. E.; Fréchet, J. M. J. *Chem. Mater.* **2006**, *18*, 386-395.
(20)   Sudhakar, M.; Djurovich, P. I.; Hogen-Esch, T. E.; Thompson, M. E. *J. Am. Chem. Soc.* **2003**, *125*, 7796-7797.
(21)   Bates, F. S. *Science* **1991**, *251*, 898-905.

(22)   Berggren, M.; Inganas, O.; Gustafsson, G.; Rasmusson, J.; Andersson, M. R.; Hjertberg, T.; Wennerstrom, O. *Nature* **1994**, *372*, 444-446.
(23)   Granstrom, M.; Berggren, M.; Inganas, O.; Andersson, M. R.; Hjertberg, T.; Wennerstrom, O. *Synth. Met.* **1997**, *85*, 1193-1194.
(24)   Nguyen, T. Q.; Kwong, R. C.; Thompson, M. E.; Schwartz, B. J. *Appl. Phys. Lett.* **2000**, *76*, 2454-2456.
(25)   Tan, C. H.; Inigo, A. R.; Fann, W.; Wei, P. K.; Perng, G. Y.; Chen, S. A. *Org. Electron.* **2002**, *3*, 81-88.
(26)   Iyengar, N. A.; Harrison, B.; Duran, R. S.; Schanze, K. S.; Reynolds, J. R. *Macromolecules* **2003**, *36*, 8978-8985.
(27)   Alam, M. M.; Tonzola, C. J.; Jenekhe, S. A. *Macromolecules* **2003**, *36*, 6577-6587.
(28)   Snaith, H. J.; Friend, R. H. *Thin Solid Films* **2004**, *451-52*, 567-571.
(29)   Kim, J. S.; Ho, P. K. H.; Murphy, C. E.; Friend, R. H. *Macromolecules* **2004**, *37*, 2861-2871.
(30)   Xia, Y. J.; Friend, R. H. *Adv. Mater.* **2006**, *18*, 1371.
(31)   Kline, R. J.; McGehee, M. D. *Polym. Rev.* **2006**, *46*, 27-45.
(32)   van Duren, J. K. J.; Yang, X. N.; Loos, J.; Bulle-Lieuwma, C. W. T.; Sieval, A. B.; Hummelen, J. C.; Janssen, R. A. J. *Adv. Func. Mater.* **2004**, *14*, 425-434.
(33)   Smith, A. P.; Smith, R. R.; Taylor, B. E.; Durstock, M. F. *Chem. Mater.* **2004**, *16*, 4687-4692.
(34)   Babel, A.; Jenekhe, S. A. *Macromolecules* **2004**, *37*, 9835-9840.
(35)   Bates, F. S.; Fredrickson, G. H. *Annu. Rev. Phys. Chem.* **1990**, *41*, 525-557.
(36)   Bates, F. S.; Fredrickson, G. H. *Phys. Today* **1999**, *52*, 32-38.
(37)   Matyjaszewski, K. *Chem. Eur. J.* **1999**, *5*, 3095-3102.
(38)   Hawker, C. J.; Bosman, A. W.; Harth, E. *Chem. Rev.* **2001**, *101*, 3661-3688.
(39)   Kamigaito, M.; Ando, T.; Sawamoto, M. *Chem. Rec.* **2004**, *4*, 159-175.
(40)   Moad, G.; Rizzardo, E.; Thang, S. H. *Aust. J. Chem.* **2005**, *58*, 379-410.
(41)   Burrows, P. E.; Shen, Z.; Bulovic, V.; McCarty, D. M.; Forrest, S. R.; Cronin, J. A.; Thompson, M. E. *J. Appl. Phys.* **1996**, *79*, 7991-8006.
(42)   Ma, D. G.; Hummelgen, I. A.; Hu, B.; Karasz, F. E. *J. Phys. D: Appl. Phys.* **1999**, *32*, 2568-2572.
(43)   Baldo, M. A.; Adachi, C.; Forrest, S. R. *Phys. Rev. B: Condens. Matter* **2000**, *62*, 10967-10977.
(44)   Ma, B. W.; Djurovich, P. I.; Thompson, M. E. *Coord. Chem. Rev.* **2005**, *249*, 1501-1510.

Chapter 4

Emitter Organization and Isolation Through Self-Assembly of Diblock Copolymer Morphologies

Abstract

Self-assembly of block copolymers enables rational control of the thin film morphology on the nanoscale. This characteristic can be exploited in the simple preparation of new functional materials for various applications such as organic light emitting diodes (OLEDs). We have previously demonstrated the use of block copolymers for highly efficient solution processed OLEDs, in which the nanophase separation between the hole and electron transporting domains enhances the recombination of charge carries. This approach has other advantages for use in single layer white OLEDs. Efficient electroluminescence across the entire visible spectrum for illumination purposes requires two or more emitters integrated in an OLED. However, these different energy emitters are subject to undesirable fluorescence resonance energy transfer (FRET) in distances up to 10 nm. In order to minimize this energy transfer to achieve simultaneous emission, site isolation has been demonstrated previously as an effective approach using dendrimers. In this chapter, the goal of site isolation using block copolymers consisting of two colored domains, blue emitting hole transporting domain and red emitting electron transporting domains is realized. The domain spacings can be well controlled ranging from 20 – 50 nm by changing the molecular weight. The effect of molecular structure on morphology and device performance is discussed in this chapter.
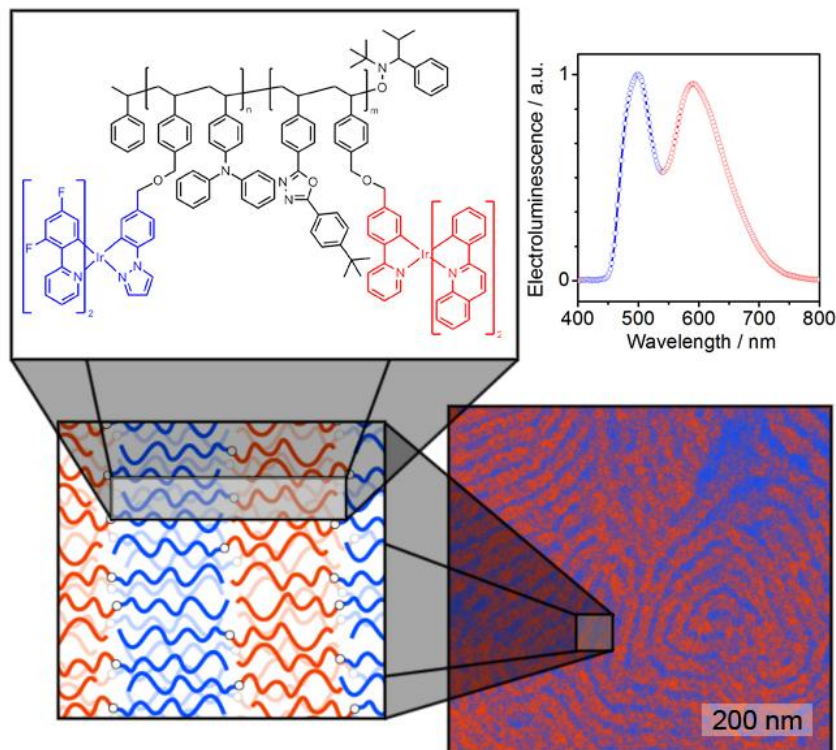
Introduction

White organic light emitting diodes (WOLEDs) have attracted great attention for their potential use in full color displays and solid state lighting applications due to several advantages such as low cost and flexibility. To date, the most efficient WOLEDs have used small phosphorescent molecules in multilayer structured devices prepared by high vacuum vapor deposition. The key issue in these systems is that the phosphorescent emission produced by each individual metal complex Ir(III) or Pt(II),[1,2] is narrow, thus requiring simultaneous emission from more than one color phosphor to illuminate across the visible region. Typically this is achieved through a combination of either three different chromophores emitting blue, green and red; or of two different ones emitting green/blue and orange/red. If more than one phosphorescent emitter is present in a device, the electroluminescent color may be affected by energy transfer between emitters. Vapor deposition enables isolation of the various emitters to minimize this energy transfer and achieve the desired goal of multiple emission using techniques such as patterning,[3] stacking,[4,5] layered isolation[6,7] and exciton management.[8]

Because polymeric materials can be solution-processed, they constitute an interesting option for application in OLEDs due to their potential to reduce cost and increase scalability. Another advantage is that a single polymer chain can bear multiple functional groups each contributing to the tuning of properties. For example, successful demonstrations of polymer WOLEDs have been based on blends of fluorescent polymers,[9] polymers incorporating multiple fluorescent emitters in their side chains[10,11] or their backbone[12,13] and fluorescent polymers doped with small molecule phosphorescent emitters.[14-16] However, these devices are generally fluorescent systems with limited internal quantum efficiencies or doped phosphorescent systems with poor stability. Furthermore, the occurrence of energy transfer limits the amount of low energy dopant that can be incorporated into these polymers, which affects their intrinsic efficiency.[17-19] There have been some efforts to suppress this energy transfer using dendrimers for site isolation,[20,21] but ultimately multilayer structures that can isolate phosphorescent emitters are needed. Unfortunately, this is extremely difficult to achieve with solution processing as the deposition of a layer must not affect any previously deposited layers.

Block copolymers allow hierarchical supramolecular control over the spatial location of their functional component blocks as well as various nanoscale objects.[22-26] This design flexibility has been exploited in the efficient fabrication of novel functional materials such as nanostructured solar cells, photonic bandgap materials, highly efficient catalysts, and high density magnetic storage media.[27-31] Therefore, block copolymers have the unique potential to spontaneously achieve phosphorescent emitter isolation through self-assembly. In this chapter, we have explored their use as active materials for WOLEDs in which phosphorescent emitter isolation can be achieved. We have exploited the use of triarylamine (TPA) oxadiazole (OXA) diblock copolymers (TPA-b-OXA), which have been used as host materials due to their high triplet energy and charge-transport properties enabling a balance of holes and electrons.[32] These coil-coil type TPA-b-OXA diblocks can produce various morphologies with controlled domain spacings ranging from 10 – 50 nm. By incorporating two different colored phosphorescent Ir(III) emitters (green-blue and orange-red emissive pendant styryl heteroleptic Ir(III) complexes) randomly into each different block, we have been able to produce a block copolymer system, (TPA-r-Blue)-b-(OXA-r-Red), which can deliver site isolation of the two emitters. As a result of site isolation these diblock copolymers can be targeted to suppress FRET from high to lower energy emitters, which generally occurs at distances below 10 nm.[33,34] With these block

copolymers, we demonstrate a self-assembled single layer solution processed WOLED that provides improved white color balance, and efficiency. Furthermore, by varying the molecular weight (MW) of (TPA-r-Blue)-b-(OXA-r-Red) and the ratio of blue to red emitters, we have investigated the effect of domain spacing on the electroluminescence spectrum and device performance.

Results and Discussion

Polymers containing heavy metal complexes have been demonstrated previously for similar Ir(III) complexes through incorporation of ancillary ligand then post polymerization complex formation, or through the post polymerization attachment of preformed Ir(III) complexes.[35,36] Unfortunately, these strategies are unsuitable since they do not allow incorporation of different colored emitters preferentially in either block without the development of complex orthogonal connection strategies. Other approaches involving the incorporation of heavy metal complexes within the polymer backbone have been accompanied by a significant alteration of the photophysical properties due to extended π-conjugation of the Ir(III) complex in the polymer.[37,38] To overcome these limitations, two heteroleptic Ir(III) complexes have been synthesized bearing a pendant styrene handle, which enables their polymerization using "living" free radical conditions that do not alter the photophysical properties of the Ir(III) complex (Scheme 4.1). In this study, the heteroleptic Ir(III) complexes, Ir(dfppy)$_2$(tpzs) (**3**) and Ir(pq)$_2$(tpys) (**4**), which are modified versions of FIrpic[39,40] and Ir(pq)$_2$(tpy),[41] were designed such that the polymerizable group is both spatially distant and electronically isolated from the Ir(III) center. The polymerizable ancillary ligands, 1-*p*-tolylpyrazole styrene (tpzs) and 2-*p*-tolylpyridine styrene (tpys) have been chosen for their high triplet energy and thus phosphorescent emission color is dictated by the other two lower energy cyclometallating ligands. As a result, **3** and **4** show phosphorescent emission in the green/blue and orange/red region of the visible spectrum, respectively.
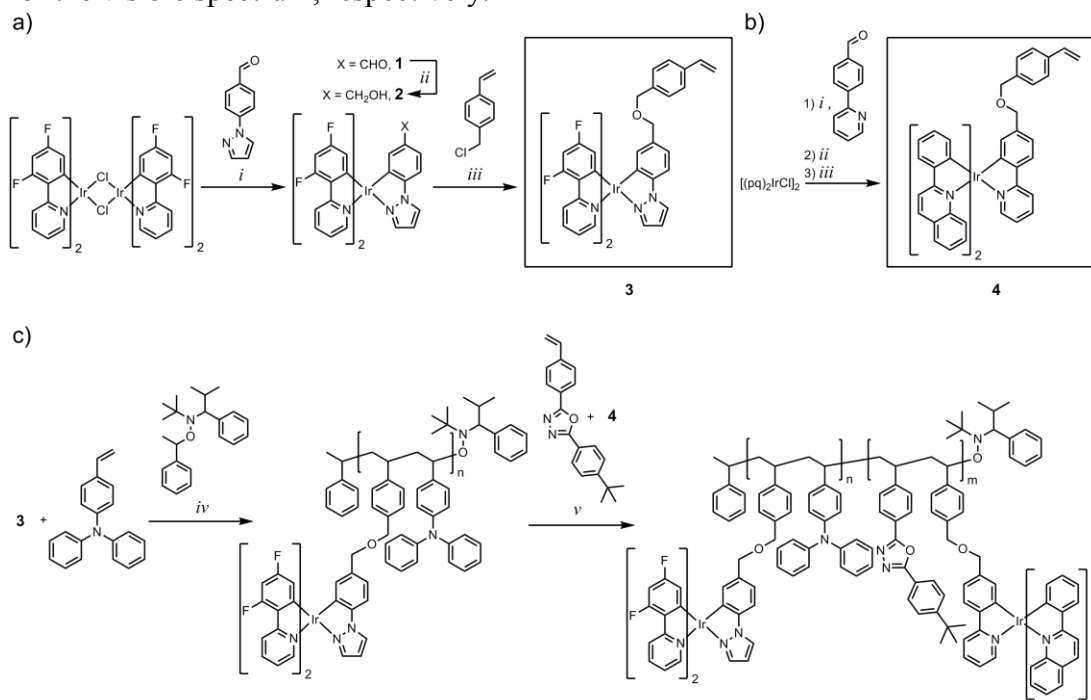
Scheme 4.1. a) Synthesis of iridium monomer Ir(dfppy)$_2$(tpzs) (**3**); b) synthesis of iridium monomer Ir(pq)$_2$(tpys) (**4**); and c) synthesis of diblock copolymers (**5-8**). *i.* diglyme, AgCF$_3$SO$_4$, 95 °C, 24 h; *ii.* 1:1 DCM: ethanol, NaBH$_4$, RT, 24 h; *iii.* THF, KI, KH, 18-crown-6, RT, 24 h; *iv. t*-butylbenzene, argon filled sealed ampule, 6 h.

In this chapter the M$_n$ of the polymers was varied with a wide range from 30 to 150 kDa, but the lengths of the two blocks were kept equal in all cases in order to preserve the morphology at different domain spacings thus enabling a fundamental study of the effect of domain spacing on electroluminescence (EL) and device performance. The target (TPA-r-Blue)-b-(OXA-r-Red) block copolymers **5-8** were synthesized by living radical polymerization as shown in Scheme 1. Diblock copolymers were obtained by first preparing the first block via a random copolymerization of TPA with **3**, followed by addition of the second block in a random copolymerization of OXA with **4**. The resulting polymers contained 10 wt. % of **3** in the TPA block, while the amount of **4** in the OXA block was varied in a series of copolymers to determine the optimal ratio of **3** to **4** (blue to red) emitters leading to white electroluminescence. The weight fraction of **3** (blue monomer) in the TPA block was chosen to avoid triplet-triplet annihilation by high Ir(III) doping while enabling high brightness. The polymers synthesized and used in this chapter are detailed in Table 4.1 and SEC traces are shown in Figure 4.1.
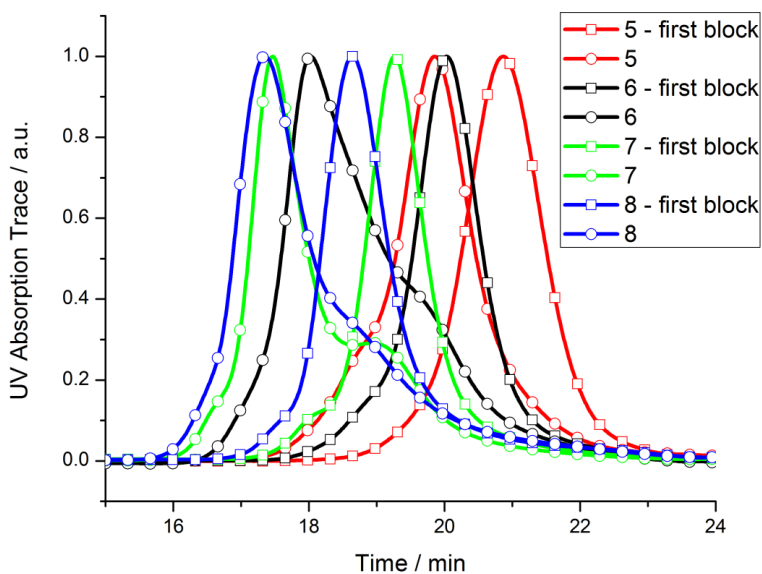

Figure 4.1. SEC traces with UV detector at 254 nm showing the increase in MW for all diblock copolymers.

Table 4.1. Summary of synthesized polymers.

	Sample	MW[a] / kDa	PDI	Blue : Red
5a	(TPA-r-10B)-b-(OXA-r-0.1R)	30	1.2	10 : 0.1
5b	(TPA-r-10B)-b-(OXA-r-0.5R)	30	1.2	10 : 0.5
6a	(TPA-r-10B)-b-(OXA-r-0.5R)	70	1.3	10 : 0.5
6b	(TPA-r-10B)-b-(OXA-r-1R)	70	1.4	10 : 1
7a	(TPA-r-10B)-b-(OXA)	100	1.4	10 : 0
7b	(TPA-r-10B)-b-(OXA-r-0.5R)	100	1.4	10 : 0.5
7c	(TPA-r-10B)-b-(OXA-r-1R)	100	1.4	10 : 1
8a	(TPA-r-10B)-b-(OXA-r-1R)	150	1.4	10 : 1
8b	(TPA-r-10B)-b-(OXA-r-2R)	150	1.5	10 : 2

[a] M_n value measured by SEC MALLS.

A requirement of this study is the absence of compositional drift of the Ir complexes within each of the TPA and OXA block in order to achieve a near random distribution of the Ir(III) complexes through each polymer chain. The weight percent as well as the compositional distribution of the Ir(III) complexes in each block were analyzed by SEC with triple detection (UV at 404 nm, MALS and RI). It was found that the weight fraction of components in the monomer feed matched that in the resulting polymer with even distribution of Ir(III) across the mass range of the polymers (Figure 4.3). ^{1}H NMR analysis in the benzylic proton region (4.0 – 4.5) confirmed polymer incorporation of the Ir(III) monomers, however it was not quantitative at such low signal (Figure 4.10).
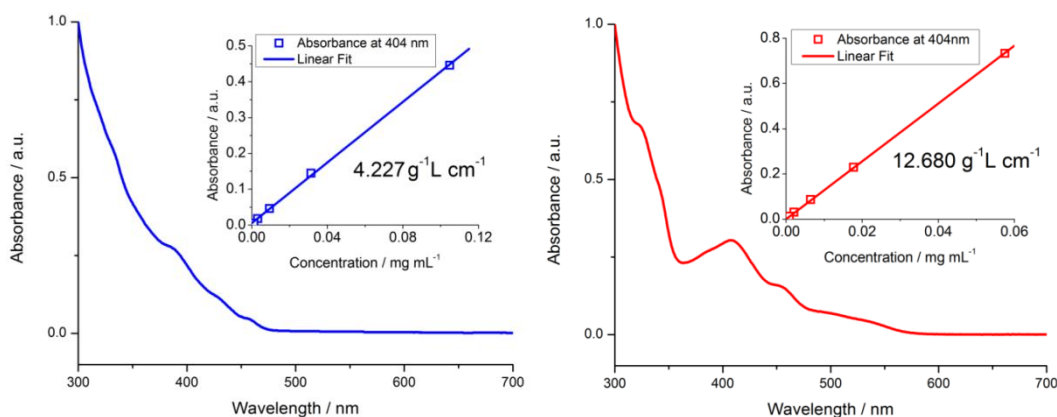

Figure 4.2. Absorbance of monomers **3** (top left) and **4** (bottom left) in THF solution.
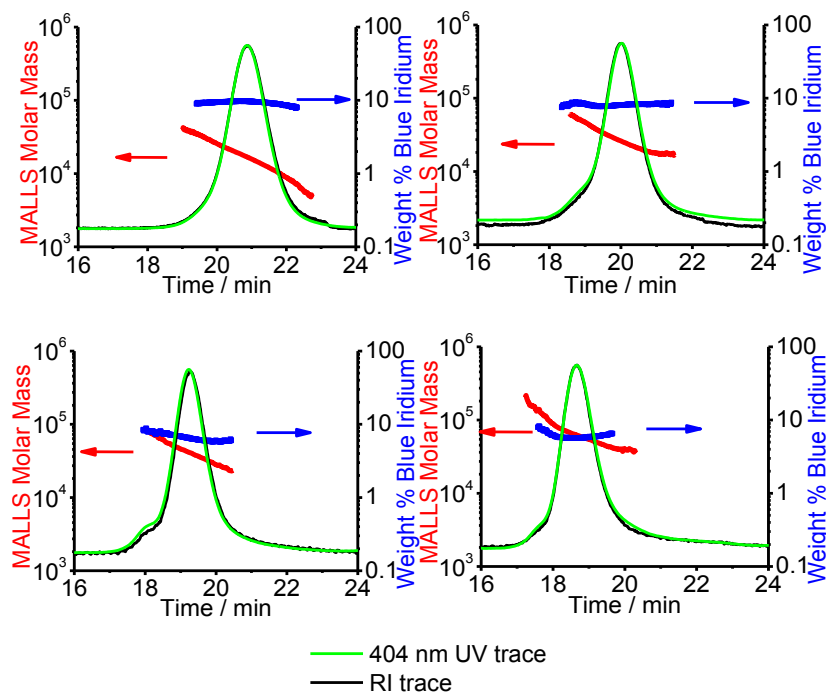
Figure 4.3. SEC traces showing iridium content and distribution by absorption for the range of polymer molecular weights as determined by MALLS. First block for all polymers **5** (top left); first block for all polymers **6** (top right); first block for all polymers **7** (bottom left); first block for all polymers **8** (bottom right).

The use of these copolymers as the single active layer in polymer OLED devices has been explored to investigate the fundamental effect of both MW and the ratio of blue to red Ir(III) complexes (**B:R**) on device performance. Devices were prepared by spin-coating the (TPA-r-Blue)-b-(OXA-r-Red) copolymers from chlorobenzene solution onto ITO substrates, followed by vapor deposition of a LiF/Al electrode. Figure 4.4 shows the electroluminescence (EL) spectra of (TPA-r-Blue)-b-(OXA-r-Red) polymers having various MW and **B:R** ratios. It is clear that increasing MW results in lower emission from the red Ir(III) complex **4**. In particular, a significant decrease in red emission with a concomitant increase in blue emission is seen when the molecular weight is increased from 30 kDa (**5a**) to 70 kDa (**6a**) while keeping the **B:R** ratio constant at 10:0.5. Increasing the MW from 70 kDa (**6a**) to 100 kDa (**7b**) leads to a further decrease in red emission. Figure 4.3b shows a similar trend is same trend for polymers **6b**, **7c**, and **8a** with MW as high 150 kDa containing a higher **B:R** ratio of 10:1. It is clear that the use of larger blocks enables a more balanced dual emission at higher red wt % incorporation.
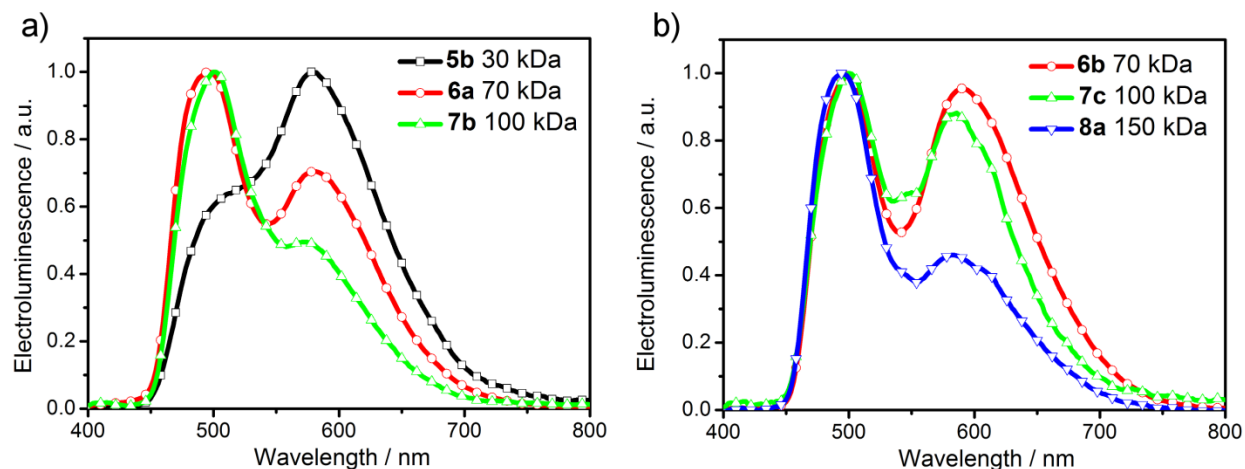
Figure 4.4. Electroluminescence as a function of molecular weight: a) (TPA-r-10 wt % Blue)-b-(OXA-r-0.5 wt % Red) for three polymers (**5b**, **6a**, **7b**) of increasing MW = 30 kDa, 70 kDa and 100 kDa; b) (TPA-r-10 wt % Blue)-b-(OXA-r-1 wt % Red) for three polymers (**6b**, **7c**, **8a**) of increasing MW = 70 kDa, 100 kDa and 150 kDa.
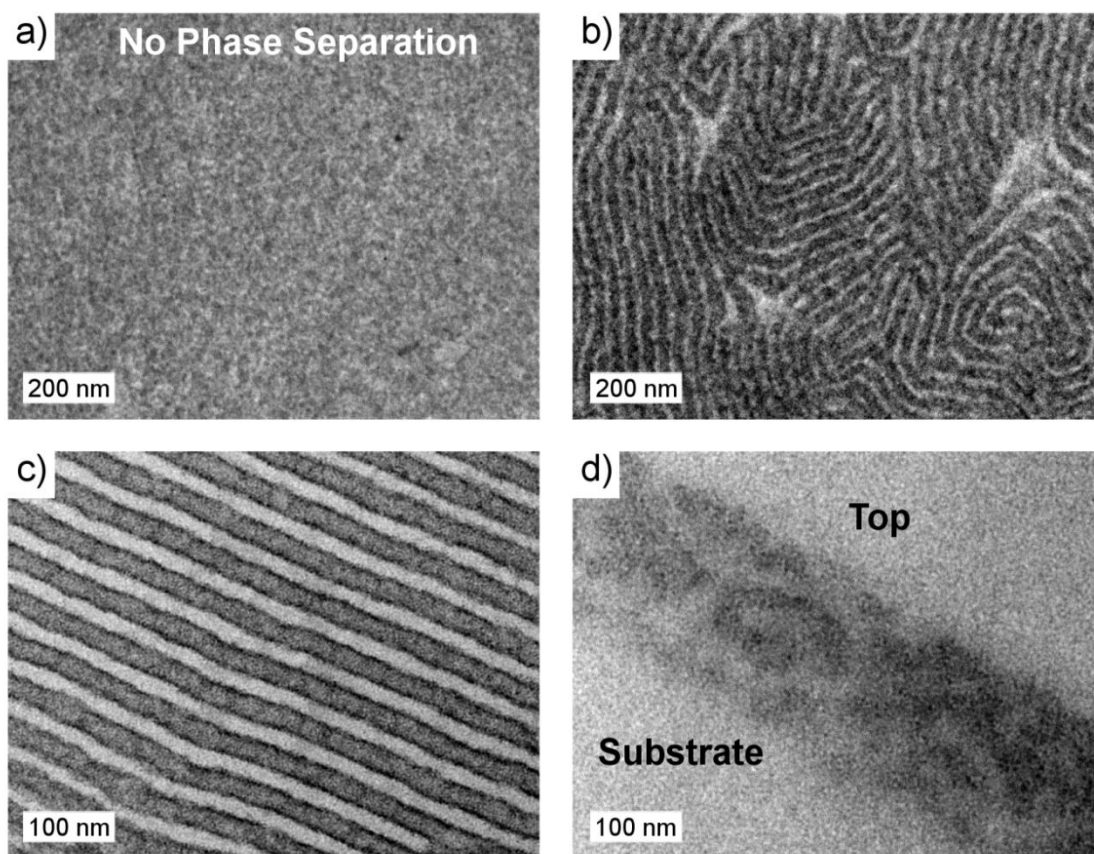
Figure 4.5. TEM images of (TPA-r-Blue)-b-(OXA-r-Red) polymers having different MW at near equilibrium morphologies: a) **5b** MW = 30 kDa B:R =

10:0.5; b) **7c** MW = 100 kDa B:R = 10:1; c) **8b** MW = 150 kDa B:R = 10:2; d) shows the cross-sectional view of polymer **8b** MW = 150 kDa B:R = 10:2 in thin film as spuncast from chlorobenzene solution.

The film morphology of the various (TPA-r-Blue)-b-(OXA-r-Red) copolymers was probed by transmission electron microscopy (TEM) to elucidate the fundamental reason behind the dramatic change in EL with increasing MW. Three different (TPA-r-Blue)-b-(OXA-r-Red) polymers that all show white EL but have different MW values of 30 kDa (**5b**), 100 kDa (**7c**) and 150 kDa (**8b**), respectively, were chosen for this TEM analysis. The samples were annealed at 230ºC for 3 days and slowly cooled and equilibrated at 190ºC for 1 day, which is above the glass transition temperatures of both the TPA (~125 ºC) and OXA (~182 ºC) polymers.[32] Samples were microtomed to produce 50 nm thick films, then stained with RuO_4 vapor to enhance the contrast between the (TPA-r-Blue) and (OXA-r-Red) blocks. The TEM images of Figure 4.5a-c show the morphology of copolymers **5b**, **7c** and **8b**. Of particular interest are the clear nanometer-sized fingerprint features characteristic of a lamellar morphology observed in Figure 4.5b and 4.5c for films of **7c** and **8b** at MW 100 kDa and 150 kDa, respectively. In contrast, copolymer **5b** with its lower MW of 30 kDa shows no domains, indicating that the film is homogeneous and that the blocks are not phase separated. This coincides with the requirement of far less red iridium monomer for the lower molecular weight polymer **5b** to yield the same EL as the phase separated higher molecular weight polymer **7c**. The dramatic difference in EL between **5b** (MW = 30 kDa) and **7d** (MW = 100 kDa) shown in Figure 4.4 can be explained by this contrast in nanoscale morphology where the phase separated domains in **7d** can suppress the energy transfer from blue to red Ir(III) complexes by isolating one from the other. The length scale of domain separation in **7d** (~36 nm) is larger than typical values for dipole induced FRET (~10 nm).[33,34] As MW increases further to 150 kDa, the degree of segregation between the different blocks increases and thus a larger domain spacing of 47 nm is found (Table 4.2). This is consistent with the theoretical prediction $d\sim M_n^{2/3}$ where d is the spacing between lamellar domains.[42] Therefore, on average, the blue Ir(III) complexes are even further segregated from red ones in films of **8b** (150 kDa), thus enabling the use of a higher **B:R** ratio of 10:2 to obtain white electroluminescence. Control experiments confirmed that the morphologies of copolymers containing iridium complexes were same as those without the complexes (TPA-b-OXA), which indicates that incorporation of 10 wt.% Ir (III) monomer has little effect on the chain conformation of the host polymers. Since all EL measurements were made in the form of a thin film spun cast from chlorobenzene, we have also studied the morphology prepared under same conditions. Figure 4.3d shows the cross-sectional view of a thin film of **8b** (TPA-r-Blue)-b-(OXA-r-Red). Clearly, a phase segregated morphology is still observed in the absence of annealing but it is less ordered than the lamellar morphology of annealed samples.
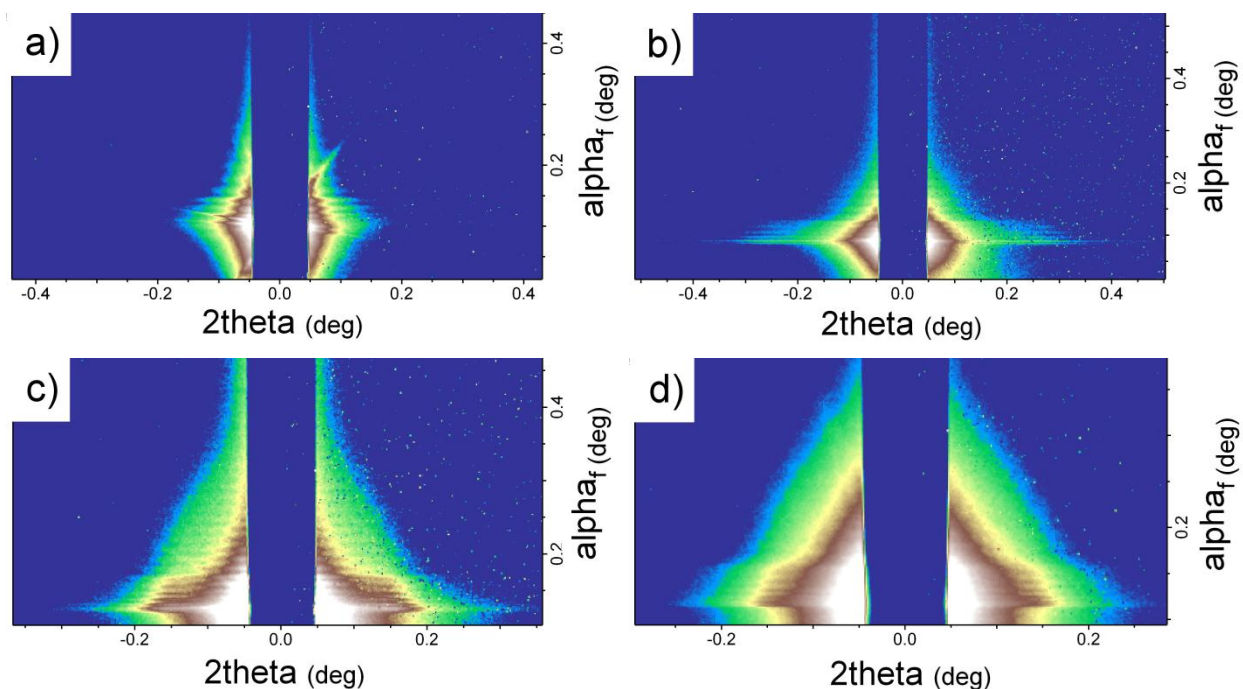
Figure 4.6. Grazing incidence small angle X-ray scattering (GISAXS) yielding calculated domain spacings for thin films of polymers a) **5b**, disordered; b) **6b**, 26.5 nm domain spacing; c) **7b**, 40.7 nm domain spacing; d) **8a**, 48.3 nm domain spacing.

Table 4.2. Observed Domain Spacings.

	Sample	MW[a] / kDa	d (GISAXS)[b] / nm	d (TEM)[c] / nm
5b	(TPA-r-10B)-b-(OXA-r-0.5R)	30	no phase separation	no phase separation
6b	(TPA-r-10B)-b-(OXA-r-1R)	70	26.5	-
7b	(TPA-r-10B)-b-(OXA-r-0.5R)	100	40.7	36
8a	(TPA-r-10B)-b-(OXA-r-1R)	150	48.3	47

[a] M_n value measured by SEC MALLS. [b] as spuncast from chlorobenzene. [c] annealed to equilibrium morphology.

While TEM can reveal the nanoscale morphology of these polymers, it does not provide precise information on domain spacing for the samples as spun cast. More quantitative data can be obtained using grazing incidence small angle X-ray scattering (GISAXS). The domain spacings of films "as spun cast" were obtained as a function of MW from 30 kDa to 150 kDa from peak positions in the in-plane direction of GISAXS images (Table 4.2). In contrast to the homogeneous morphology of copolymer **5b** (MW = 30 kDa), the higher MW copolymers **6b**, **7c**, and **8b** all show phase segregated morphologies with increased domain spacing of 26.5, 40.7, and 48.3 nm, respectively.
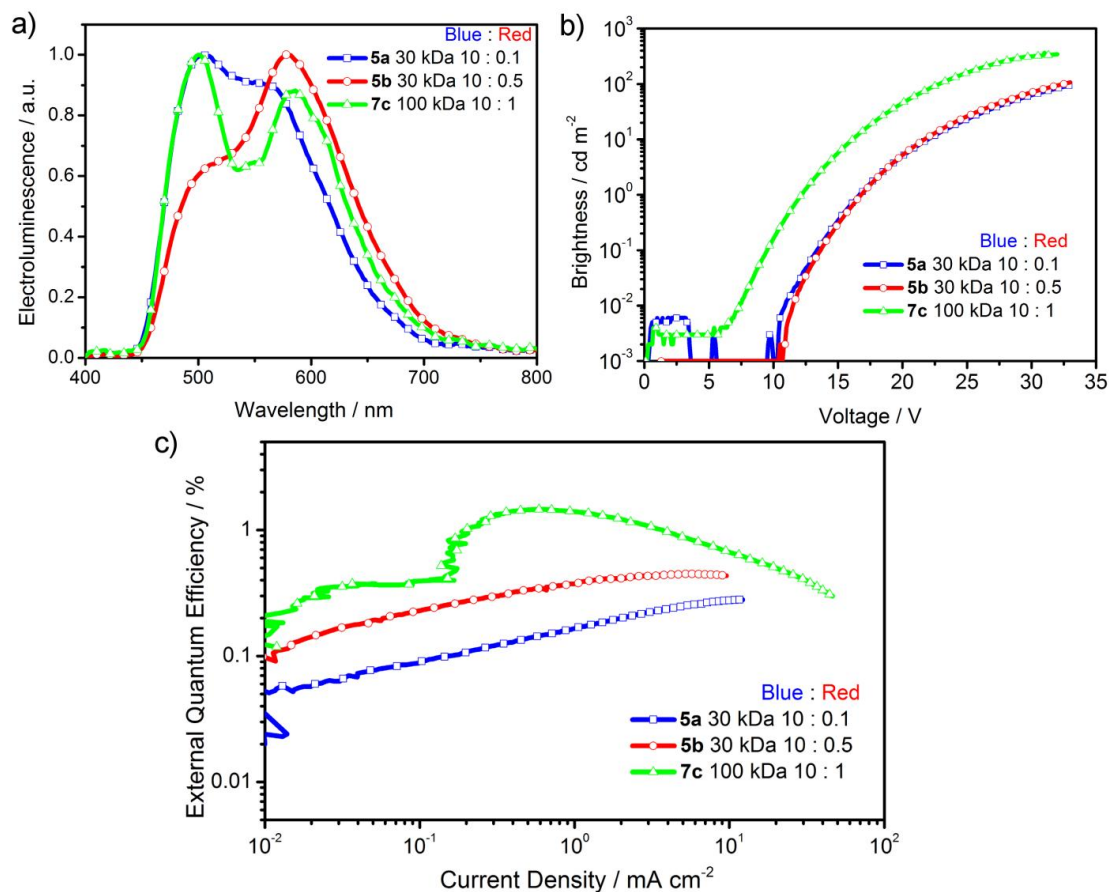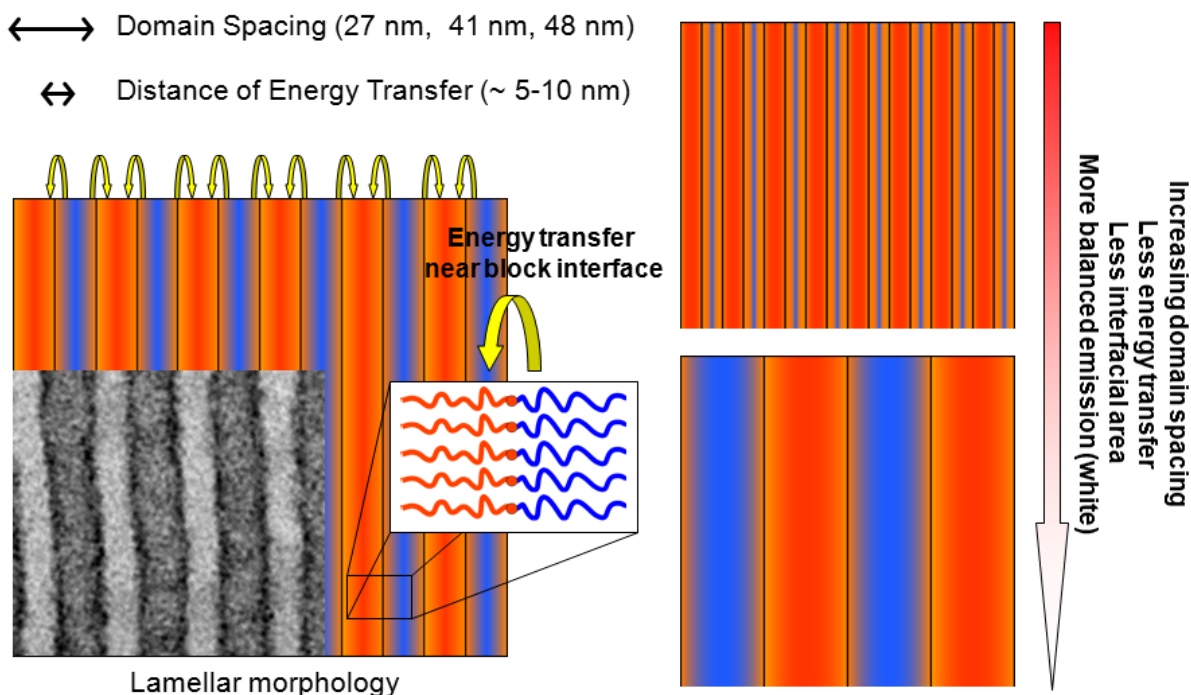
Figure 4.7. Device performance for selected copolymers **5a**, **6b**, **7c** a) Electroluminescence spectra; b) Device brightness; c) External quantum efficiency as a function of current density.

Controlling the nanoscale morphology of the copolymers to obtain phase separated domains is critical to suppress energy transfer from high to low energy dopants by isolating the blue complexes from the lower energy red Ir(III) complexes. The contrast in morphology not only affects the EL, but also other device characteristics. Figure 4.7 shows the device performance for WOLEDs fabricated from (TPA-r-Blue)-b-(OXA-r-Red) **5a**, **5b** (MW = 30 kDa) and **7c** (MW = 100 kDa). To focus on the effects of MW and morphology on WOLED device performance, these polymers were used as the single active layer in a device with no additional material between anode and cathode. While some dual emission can be obtained even in the absence of phase separated morphologies using very high **B:R** ratios (copolymers **5a** and **5b**, Figure 4.7a), a much higher proportion of red emitter may be used if phase separation is achieved as in the higher MW **7c** with its 10:1 **B:R** ratio. This also affects the external quantum efficiency (EQE) of the device (Figure 4.7c) as the higher MW polymer **7c** shows a markedly higher EQE (> 1.5%) for white emission than observed with the lower MW polymers **5a** (EQE ~ 0.3%) and **5b** (EQE ~ 0.4%). The data for device brightness is shown for the three different samples in Figure 4.7b. The device made from the phase separated copolymer **7c** is three times brighter and has lower turn-on voltage than devices made from copolymers **5a** and **5b**. While the absolute value for the brightness of all devices is rather low, due in large part to the poor intrinsic characteristics of the blue emitter, this study demonstrates the effect of phase separation

50

and larger interfacial area on device performance. The large interfacial area between hole and electron transporting domains facilitates hole-electron recombination and thus produces a higher EQE.[32] However, if the MW of the blocks is increased to improve chromophore isolation beyond a certain threshold the interfacial area will decrease thus negating the benefit of site isolation. These competing factors; larger domains providing better emitter isolation, and less interfacial area for recombination are illustrated in Figure 4.8. The majority of energy transfer from blue to red chromophores should be occurring in the 5 – 10 nm distance at the block interface, therefore larger domains yield increased blue emission.

Figure 4.8. The effect of increased domain size on energy transfer and interfacial area for charge recombination.

In order to confirm that the improvement in device performance for the higher MW (TPA-r-Blue)-b-(OXA-r-Red) copolymers may be attributed to the site isolation of the colored chromophores, the copolymer (TPA-r-Blue)-b-OXA (**7a**) was prepared for a control experiment. Copolymer **7a** was identical to the copolymer **7c** in terms of total MW = 100 kDa and was prepared from the same first block containing blue iridium complexes within TPA, however, the OXA block did not include any monomer with the red iridium complex. Instead, the free red Ir(III) emitter small molecule, Ir(pq)$_2$(tpys) (**4**), was added as a dopant into two different solutions of polymer **7a** in chlorobenzene to produce mixtures with **B:R** ratios of 10:0.5 and 10:1. The doped mixtures of **4** into polymer **7a** were spun-cast under identical conditions to produce a single layer device for a comparison to the bichromophoric diblock copolymer polymer **7c** device having the same **B:R** ratio. Figure 4.9 shows the characteristics of three different devices. Device **D1** with a **B:R** ratio of 10:1 showed balanced dual emission while device **D3** prepared from a doped sample shows predominantly red emission at the same **B:R** ratio. In addition, a major portion of blue emission was quenched in device **D2** with an even lower **B:R** ratio of 10:0.5. As seen in Figure 4.9b device **D1** with an EQE value of 1.5% performs significantly better than devices **D2** and **D3** with EQE values of 0.35 % and 0.25 %,

respectively. The EQE values measured for devices **D2** and **D3** are very similar to those measured for low MW copolymers **5a** and **5b** for which no phase separation between the blocks, hence no chromophore site-isolation, was observed.
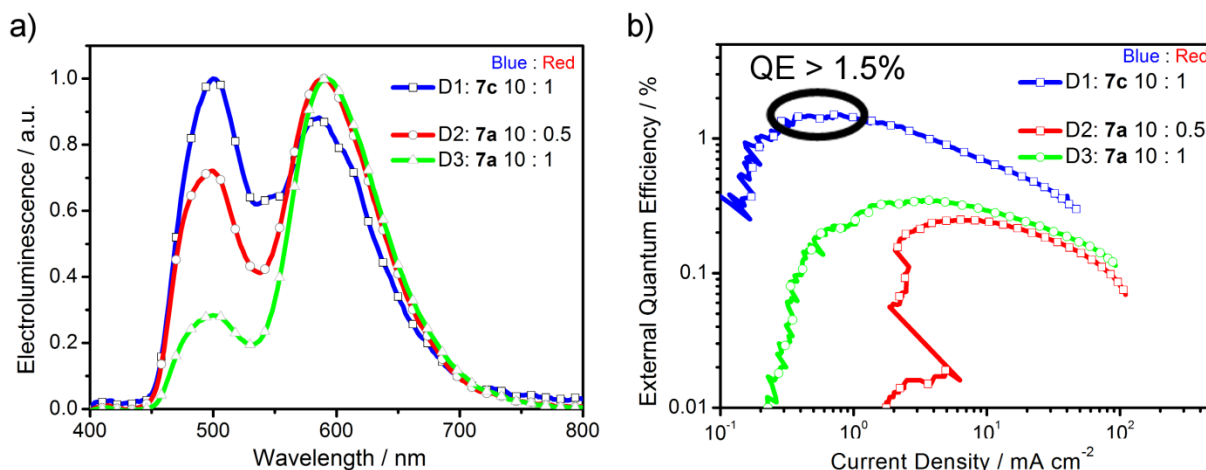
Figure 4.9. Comparison of (TPA-r-Blue)-b-(OXA-r-Red) polymer device to dopant system: a) Electroluminescence spectra; b) EQE of three different devices made of block copolymers having the same MW of 100 kDa, (**D1**: Single polymer system **7c** (MW = 100 kDa, B:R = 10:1), **D2**: Polymer **7a** mixed with red Ir dopants (MW = 100 kDa, B:R = 10:0.5), **D3**: Polymer **7a** mixed with red Ir dopants (MW = 100 kDa, B:R = 10:1)).

Conclusion

It appears that the nanophase separated morphology obtained by increasing block size in (TPA-r-Blue)-b-(OXA-r-Red) copolymers affords the site-isolation of chromophores necessary for improved device performance. While overall performance of these block copolymer may appear to be relatively low, it must be emphasized that this was obtained with an extremely simple solution-cast device constituted of a single active layer directly sandwiched between anode and cathode. Thus the synthetic molecular approach towards site isolation described in this chapter may be extended to other WOLED systems to improve their device efficiency. Since stable, bright, blue emission is still a limiting factor in high performance WOLEDs, this approach towards minimizing blue emission loss by suppressing unnecessary energy transfer to red dopants is versatile and broadly applicable.

Experimental

Device Fabrication and Measurement. ITO coated glass substrates were cleaned through sonication in a soap solution, rinsing with deionized water, boiling in trichloroethylene, acetone, and ethanol then drying under nitrogen. The substrates were then placed under UV ozone for 10 minutes. All diblock copolymer films were prepared directly on top of the ITO substrate by spin-casting at 2000 RPM for 30 seconds from a 40 mg/ml solution of the polymer

in chlorobenzene under inert atmosphere of argon. Following solution deposition of the polymer film a cathode consisting of 1 nm LiF (Aldrich, fused pieces 99.995 %) and 100 nm Al (Alfa Aesar, purity > 99.99 %) was deposited at a rate of 0.2 Å/s and 4 Å/s respectively, in a vacuum chamber below 3×10^{-6} Torr. OLEDs were formed at the 2×2 mm squares where the ITO and Al stripes intersect. The electrical and optical intensity characteristics of the devices were measured with a Keithly 2400 sourcemeter/2000 multimeter coupled to a Newport 1835-C optical meter, equipped with a calibrated UV-818 Si photodetector. Only light emission from the front face of the device was collected and used in subsequent efficiency calculations. The EL spectra were measured on a USB4000 Miniature Fiber Optic Spectrometer.

TEM and GISAXS Measurement. The morphology of bulk sample as well as the thin film of (TPA-r-Blue)-b-(OXA-r-Red) polymers was investigated by TEM and GISAXS measurements. For Figure 4.3a-c, the thick film of (TPA-r-Blue)-b-(OXA-r-Red) polymers was prepared by dropcasting from a 40 mg/ml solution of the polymer in chlorobenzene. Samples were annealed at 230 °C during 3 days, then at 190 °C during 1 day and cooled slowly down to room temperature under vacuum. The bulk sample was microtomed into 50 nm thick film and sequentially stained by RuO_4 0.5 % aqueous solution for 25 mins to produce the contrast between (TPA-r-Blue) and (OXA-r-Red) blocks. A sample for Figure 4.3d was prepared using a slightly higher concentration of polymer to produce a thicker film. The films were prepared by spincasting from chlorobenzene onto NaCl substrate and then transferred to the epoxy substrate. The sample was microtomed into 50 nm thick film, followed by RuO_4 vapor staining for 25 mins. The morphology of cross-sectioned bulk and thin film samples was observed by FEI Tecnai operated at 200 kV. For GISAXS measurements, samples were prepared on Si substrate under identical condition as the devices were prepared. GISAXS measurements were performed on beamline 7.3 at the Advanced Light Source at the Lawrence Berkeley National Laboratory. The scattering profiles were collected on an ADSC Quantum CCD detector. Incidence angle (~0.15 °) was carefully chosen to allow for complete penetration of X-ray into the polymer film. The domain spacings of as-spuncast (TPA-r-Blue)-b-(OXA-r-Red) polymers in a thin film were extracted from scattered peak in in-plane direction of GISAXS images.

General Synthesis. Unless otherwise noted, all reagents were used as received and without further purification, or were prepared according to literature procedures. Chromatography was carried out with Sorbent Technologies silica gel for flash columns, 230-400 mesh. Unless otherwise specified, extracts were dried over $MgSO_4$ and solvents were removed with a rotary evaporator at aspirator pressure. All NMR spectra were measured in either CD_2Cl_2 or $CDCl_3$ with TMS or solvent signals as the standards. High-resolution mass spectrometry (HRMS) was performed with a Micromass ProSpec using fast atom bombardment (FAB). Elemental analyses were performed at the University of California, Berkeley, analytical facility. THF GPC was carried out at 1.0 mL/min. Three PLgel columns (7.5 x 300 mm) were used. The columns had a pore size of 105, 103, and 500 Å, respectively. The particle size was 5 mm. The GPC system consisted of a Waters 510 pump, a Waters 717 autosampler, a Waters 486 UV-Vis detector, a Wyatt DAWN EOS light scattering detector, and a Wyatt Optilab DSP differential refractive index detector. The columns were thermostatted at 35 °C.

TPA and OXA. Both were prepared as previously reported.[43]

Ir Dimers. All cyclometallated Ir(III) chloride dimers were synthesized following the Nonoyama route of refluxing $IrCl_3 \cdot H_2O$ (Strem) with 2 - 2.5 equivalents of the corresponding CN ligand in a 3:1 mixture of 2-ethoxyethanol (Aldrich) and water for 24 hours.[44] Dimers were collected by precipitation into a large excess of water followed by filtration.

Ir(dfppy)₂(pzb) (1). To a round bottom flask was added 3.36 g (2.87 mmol) [Ir(dfppy)$_2$Cl]$_2$ dimer and 1.62 g (6.31 mmol) silver triflate in 60 mL diglyme. This mixture was stirred for 30 minutes at 95 °C under argon followed by addition of 1.09 g (6.33 mmol) 4-pyrazol-1-ylbenzaldehyde (pzb). This solution was stirred at 95 °C for 24 hours under argon then cooled and filtered to remove silver chloride precipitate. The solvent was removed under reduced pressure to yield a dark sludge which was purified on a silica column with dichloromethane eluent (Rf = 0.38). The resulting fractions were concentrated then triturated with excess hexanes and filtered to yield 1.03 g (1.38 mmol) of Ir(dfppy)$_2$(pzb) **1** in 24 % yield as a yellow powder. ^{1}H NMR (400 MHz, CD$_2$Cl$_2$, δ ppm) 6.24 (dd, J = 9.2, 2.4 Hz, 1H), 6.33 (dd, J = 9.3, 2.4 Hz, 1H), 6.40-6.50 (m, 3H), 6.55 (dd, J = 2.7, 2.1 Hz, 1H), 6.98-6.94 (m, 2H), 7.01 (ddd, J = 7.1, 5.6, 1.1 Hz, 1H), 7.17 (d, J = 1.7 Hz, 1H), 7.39 (d, J = 8.2 Hz, 1H), 7.50 (dd, J = 8.2, 1.8 Hz, 1H), 7.55 (dd, J = 5.7, 3.3 Hz, 1H), 7.63 (t, J = 5.5, 5.5 Hz, 2H), 8.18 (d, J = 2.8 Hz, 1H), 8.30 (t, J = 8.2, 8.2 Hz, 2H), 9.70 (s, 1H). HRMS (FAB, m/z): [M]$^+$ calcd for C$_{32}$H$_{19}$N$_4$OF$_4$Ir, 744.112441; found 744.113190. Anal. calcd for C$_{32}$H$_{19}$N$_4$OF$_4$Ir: C, 51.68; H, 2.57; N, 7.53; found: C, 51.88; H, 2.45; N, 7.26.

Ir(dfppy)₂(pzba) (2). To a round bottom flask was added 0.99 g (1.3 mmol) Ir(dfppy)$_2$(pzb) **1** and 51 mg (1.3 mmol) sodium borohydride in 200 mL of a 1:1 mixture of ethanol and dichloromethane. This mixture was stirred for overnight at room temperature then quenched with 50 mL water. This mixture was concentrated under vacuum then extracted with 3 x 100 mL dichloromethane. The organic layers were combined and chromatographed on a flash silica column with 9:1 dichloromethane:ethyl acetate eluent (Rf = 0.60). The solvent was stripped under reduce pressure to yield 815 mg (1.09 mmol) of Ir(dfppy)$_2$(pzba) **2** in 84 % yield as a yellow powder. ^{1}H NMR (400 MHz, CD$_2$Cl$_2$, δ ppm) 4.41 (t, J = 5.8 Hz, 2H), 6.31 (td, J = 9.3, 2.2 Hz, 2H), 6.39 (d, J = 2.4 Hz, 1H), 6.42 (dd, J = 3.6, 2.5 Hz, 1H), 6.45 (d, J = 2.4 Hz, 1H), 6.47 (t, J = 2.3 Hz, 1H), 6.63 (d, J = 1.6 Hz, 1H), 6.86 (d, J = 2.0 Hz, 1H), 6.94 (t, J = 6.5 Hz, 1H), 6.97-7.02 (m, 2H), 7.27 (d, J = 8.1 Hz, 1H), 7.55 (dd, J = 5.7, 3.3 Hz, 1H), 7.62 (t, J = 4.7 Hz, 2H), 7.67-7.74 (m, 1H), 8.09 (d, J = 2.7 Hz, 1H), 8.28 (t, J = 8.5 Hz, 2H); HRMS (FAB, m/z): [M]$^+$ calcd for C$_{32}$H$_{21}$N$_4$OF$_4$Ir, 746.128092; found 746.127570. Anal. calcd for C$_{32}$H$_{21}$N$_4$OF$_4$Ir: C, 51.54; H, 2.84; N, 7.51; found: C, 51.89; H, 2.99; N, 7.33.

**Ir(dfppy)₂(tpzs) (3).** To a flame dried 100 mL round bottom flask was added 147 mg (0.886 mmol) potassium iodide, 180 mg potassium hydride in oil suspension and 58 mg (0.218 mmol) 18-crown-6. The reaction vessel was evacuated for 30 minutes then backfilled with argon. To this vessel was added 5 mL of dry tetrahydrofuran followed by 784 mg (1.05 mmol) of Ir(dfppy)$_2$(pzba) **2** dissolved in 15 mL dry tetrahydrofuran by cannula. To this mixture was added 0.3 mL (21.3 mmol) inhibitor free vinylbenzylchloride by syringe immediately. The solution was allowed to stir under argon in the dark for 24 hours at 30 °C. The reaction was quenched with water then extracted with dichloromethane. The organic layer was combined and chromatographed on a silica column with 1:1 dichloromethane:hexanes eluent (Rf = 0.50) to yield 856 mg (0.993 mmol) Ir(dfppy)$_2$(tpzs) **3** in 95 % yield as a yellow powder. ^{1}H NMR (400 MHz, CD$_2$Cl$_2$, δ ppm) 4.31 (s, 2H), 4.38 (s, 2H), 5.23 (dd, J = 10.9, 0.7 Hz, 1H), 5.76 (dd, J = 17.6, 0.8 Hz, 1H), 6.31 (ddd, J = 9.4, 2.3, 1.4 Hz, 2H), 6.42 (dddd, J = 13.1, 9.1, 2.2, 1.7 Hz, 3H), 6.72 (dd, J = 17.6, 10.9 Hz, 1H), 6.48 (dd, J = 2.6, 2.1 Hz, 1H), 6.65 (d, J = 1.7 Hz, 1H), 6.86 (d, J = 1.9 Hz, 1H), 6.94 (ddd, J = 7.0, 5.6, 1.1 Hz, 1H), 6.97-7.02 (m, 2H), 7.20 (d, J = 8.0 Hz, 2H), 7.27 (d, J = 8.1 Hz, 1H), 7.63 (dd, J = 9.5, 5.7 Hz, 2H), 7.71 (t, J = 7.7 Hz, 2H), 7.37 (d, J = 8.1 Hz, 2H), 8.10 (d, J = 2.6 Hz, 1H), 8.28 (t, J = 6.9 Hz, 2H); HRMS (FAB, m/z): [M]$^+$ calcd for

C$_{41}$H$_{29}$N$_4$OF$_4$Ir, 862.190692; found 862.190840. Anal. calcd for C$_{41}$H$_{29}$N$_4$OF$_4$Ir: C, 57.13; H, 3.39; N, 6.50; found: C, 57.95; H, 3.53; N, 6.31.

Ir(pq)$_2$(tpys) (4). Synthesized under the analogous procedures as for **1** through **3**. ^{1}H NMR (500 MHz, CD$_2$Cl$_2$, δ ppm) 4.13-4.24 (m, 1H), 5.24 (dd, J = 10.9, 0.6 Hz, 1H), 5.78 (dd, J = 17.6, 0.7 Hz, 1H), 6.45 (d, J = 1.6 Hz, 1H), 6.55 (ddd, J = 10.1, 7.8, 1.0 Hz, 2H), 6.70-6.78 (m, 5H), 6.85 (ddd, J = 6.9, 5.5, 1.1 Hz, 1H), 6.91-6.99 (m, 3H), 7.14 (d, J = 8.1 Hz, 2H), 7.24 (ddd, J = 7.8, 6.9, 0.8 Hz, 1H), 7.29 (ddd, J = 7.8, 6.8, 0.9 Hz, 1H), 7.38 (d, J = 8.1 Hz, 2H), 7.44 (d, J = 8.0 Hz, 1H), 7.56-7.62 (m, 2H), 7.69-7.72 (m, 2H), 7.76 (dd, J = 8.0, 1.0 Hz, 1H), 7.78 (d, J = 8.2 Hz, 1H), 7.85 (dd, J = 8.1, 0.8 Hz, 1H), 7.94 (dd, J = 7.9, 1.0 Hz, 1H), 8.01 (d, J = 8.9 Hz, 1H), 8.09 (dd, J = 11.1, 8.9 Hz, 2H), 8.25 (q, J = 8.9 Hz, 2H); HRMS (FAB, m/z): [M+H]$^+$ calcd for C$_{51}$H$_{39}$N$_3$OIr, 902.272255; found 902.270130. Anal. calcd for C$_{51}$H$_{38}$N$_3$OIr: C, 67.98; H, 4.25; N, 4.66; found: C, 68.20; H, 4.13; N, 4.61.

Polymerizations (5-8). First block nitroxide mediated "living" polymerizations were performed by combining triphenylamine (TPA) with Ir(dfppy)$_2$(tpzs) (**3**) at 10 wt. % in *t*-butylbenzene solvent at a concentration of ~1 g mL^{-1} TPA in an ampule with different amounts of alkoxyamine initiator.[45] The ampules were degassed through a minimum of three freeze-pump-thaw cycles then backfilled with argon and sealed with a torch. The ampules were magnetically stirred at 125 °C for 5-6 hours then cooled and opened. The viscous solution was diluted with a minimum amount of dichloromethane then precipitated from hexanes. This process was repeated three times to remove all unconverted monomer. The precipitate polymer was filtered and dried under vacuum. Second block polymerizations were performed by combining the first block with oxadiazole (OXA) and Ir(pq)$_2$(tpys) (**4**) at 0.1, 0.5, 1 and 2 wt. % in *t*-butylbenzene solvent at a concentration of ~1 g mL^{-1} OXA in an ampule. The ampules were degassed as in the procedure for the first block synthesis and polymerized at 125°C for 5-6 hours. The polymer was collected by three precipitations, filtered and dried under vacuum. A summary of polymers is listed in Table 4.1. SEC traces for these polymers are shown in Figure 4.1. ^{1}H NMR for a select polymer is shown in Figure 4.10.
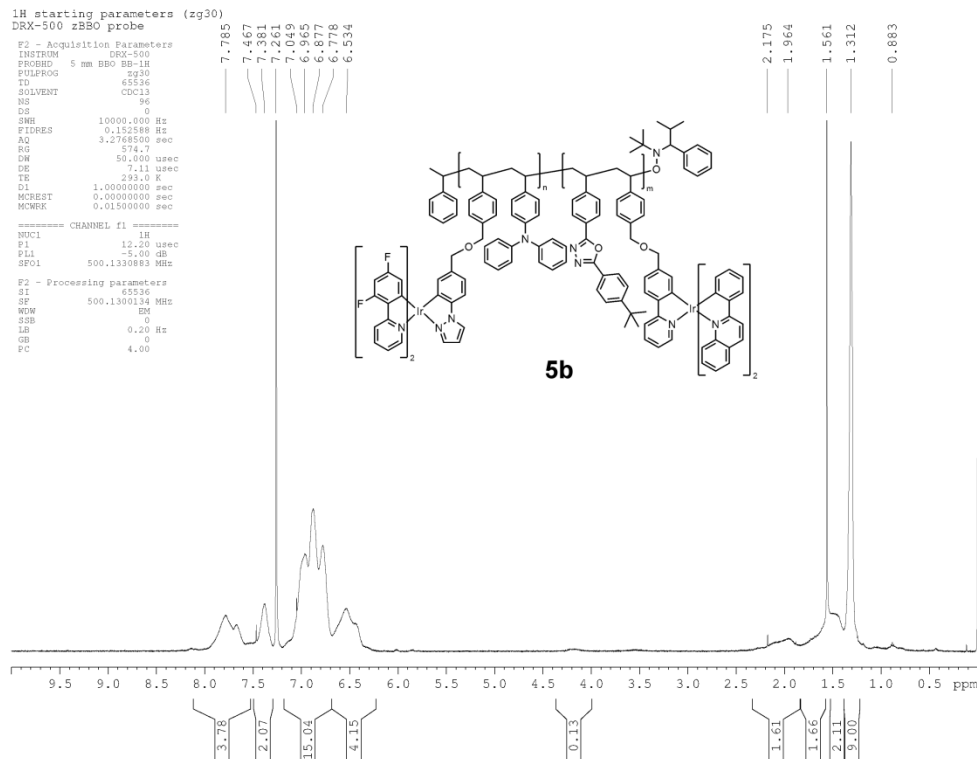
Figure 4.10. A representative ¹H NMR spectrum for the diblock copolymers synthesized. ¹H NMR spectra for all the diblock copolymers appeared very similar, as expected for equal block lengths and varied MW.

References

(1)   Baldo, M. A.; O'Brien, D. F.; You, Y.; Shoustikov, A.; Sibley, S.; Thompson, M. E.; Forrest, S. R. *Nature* **1998**, *395*, 151.

(2)   O'Brien, D. F.; Baldo, M. A.; Thompson, M. E.; Forrest, S. R. *Appl. Phys. Lett.* **1999**, *74*, 442.

(3)   Arnold, M. S.; McGraw, G. J.; Forrest, S. R.; Lunt, R. R. *Appl. Phys. Lett.* **2008**, *92*, 053301.

(4)   Kanno, H.; Holmes, R. J.; Sun, Y.; Kena-Cohen, S.; Forrest, S. R. *Adv. Mater.* **2006**, *18*, 339.

(5)   Parthasarathy, G.; Gu, G.; Forrest, S. R. *Adv. Mater.* **1999**, *11*, 907.

(6)   Sun, Y.; Forrest, S. R. *Appl. Phys. Lett.* **2007**, *91*, 263503.

(7)   Tokito, S.; Lijima, T.; Tsuzuki, T.; Sato, F. *Appl. Phys. Lett.* **2003**, *83*, 2459.

(8)   Y. Sun, N. C. Giebink, H. Kanno, B. Ma, M. E. Thompson, S. R. Forrest, *Nature* **2006**, *440*, 908.

(9)   Berggren, M.; Inganas, O.; Gustafsson, G.; Rasmusson, J.; Andersson, M. R.; Hjertberg, T.; Wennerstrom, O. *Nature* **1994**, *372*, 444.

(10)   Liu, J.; Guo, X.; Bu, L. J.; Xie, Z. Y.; Cheng, Y. X.; Geng, Y. H.; Wang, L. X.; Jing, X. B.; Wang, F. S. *Adv. Func. Mater.* **2007**, *17*, 1917.

(11)   Liu, J.; Xie, Z. Y.; Cheng, Y. X.; Geng, Y. H.; Wang, L. X.; Jing, X. B.; Wang, F. S. *Adv. Mater.* **2007**, *19*, 531.

(12)   Luo, J.; Li, X.; Hou, Q.; Peng, J. B.; Yang, W.; Cao, Y. *Adv. Mater.* **2007**, *19*, 1113.

(13)   Tu, G. L.; Mei, C. Y.; Zhou, Q. G.; Cheng, Y. X.; Geng, Y. H.; Wang, L. X.; Ma, D. G.; Jing, X. B.; Wang, F. S. *Adv. Func. Mater.* **2006**, *16*, 101.

(14)   Chen, F.; Yang, Y.; Thompson, M. E.; Kido, J. *Appl. Phys. Lett.* **2002**, *80*, 2308.

(15)   Shih, P.; Shu, C.; Tung, Y.; Chi, Y. *Appl. Phys. Lett.* **2006**, *88*, 251110.

(16)   Xu, Y.; Zhang, X.; Peng, J.; Niu, Q.; Cao, Y. *Semicond. Sci. Technol.* **2006**, *21*, 1373.

(17)   Liu, J.; Gao, B.; Cheng, Y.; Xie, Z.; Geng, Y.; Wang, L.; Jing, X.; Wang, F. *Macromolecules* **2008**, *41*, 1162.

(18)   Park, M.; Lee, J.; Park, J.; Lee, S. K.; Lee, J.; Chu, H.; Hwang, D.; Shim, H. *Macromolecules* **2008**, *41*, 3063.

(19)   Jiang, J. X.; Xu, Y. H.; Yang, W.; Guan, R.; Liu, Z. Q.; Zhen, H. Y.; Cao, Y. *Adv. Mater.* **2006**, *18*, 1769.

(20)   Freeman, A. W.; Koene, S. C.; Malenfant, P. R. L.; Thompson, M. E.; Fréchet, J. M. J. *J. Am. Chem. Soc.* **2000**, *122*, 12385.

(21)   Furuta, P.; Brooks, J.; Thompson, M. E.; Fréchet, J. M. J. *J. Am. Chem. Soc.* **2003**, *125*, 13165.

(22)   Bockstaller, M. R.; Mickiewicz, R. A.; Thomas, E. L. *Adv. Mater.* **2005**, *17*, 1331.

(23)   Bates, F. S.; Fredrickson, G. H. *Phys. Today* **1999**, *52*, 32.

(24)   Kim, B. J.; Bang, J.; Hawker, C. J.; Kramer, E. J. *Macromolecules* **2006**, *39*, 4108.

(25)   Bang, J.; Kim, S. H.; Drockenmuller, E.; Misner, M. J.; Russell, T. P.; Hawker, C. J. *J. Am. Chem. Soc.* **2006**, *128*, 7622.

(26)   Kim, B. J.; Fredrickson, G. H.; Hawker, C. J.; Kramer, E. J. *Langmuir* **2007**, *23*, 7804.

(27)   Sivula, K.; Ball, Z. T.; Watanabe, N.; Fréchet, J. M. J. *Adv. Mater.* **2006**, *18*, 206.

(28)   Jaramillo, T. F.; Baeck, S. H.; Cuenya, B. R.; McFarland, E. W. *J. Am. Chem. Soc.* **2003**, *125*, 7148.

(29)   Lee, J. I.; Cho, S. H.; Park, S.; S. Kim, S.; Kim, J. K.; Yu, J.; Kim, Y. C.; Russell, T. P. *Nano Lett.* **2008**, *8*, 2315.

(30)   Bockstaller, M. R.; Thomas, E. L. *J. Phys. Chem. B.* **2003**, *107*, 10017.

(31)   Cheng, J. Y.; Ross, C. A.; Chan, V. Z. H.; Thomas, E. L.; Lammertink, R. G. H.; Vancso, G. J. *Adv. Mater.* **2001**, *13*, 1174.

(32)   Ma, B.; Kim, B. J.; Deng, L.; Poulsen, D. A.; Thompson, M. E.; Fréchet, J. M. J. *Macromolecules* **2007**, *40*, 8156.

(33)   Förster, T. *Discuss. Faraday Soc.* **1959**, *27*, 7.

(34)   Turro, N. J. *Modern Molecular Photochemistry*; University Science Books: Sausalito, CA, 1991.

(35)   Furuta, P. T.; Deng, L.; Garon, S.; Thompson, M. E.; Fréchet, J. M. J. *J. Am. Chem. Soc.* **2004**, *126*, 15388.

(36)   Wang, X. Y.; Prabhu, R. N.; Schmehl, R. H.; Weck, M. *Macromolecules* **2006**, *39*, 3140.

(37)   Zhang, K.; Chen, Z.; Zou, Y.; Yang, C.; Qin, J.; Cao, Y. *Organometallics* **2007**, *26*, 3699.

(38)   Langecker, J.; Rehahn, M. *Macromol. Chem. Phys.* **2008**, *209*, 258.

(39)   Adachi, C.; Kwong, R. C.; Djurovich, P.; Adamovich, V.; Baldo, M. A.; Thompson, M. E.; Forrest, S. R. *Appl. Phys. Lett.* **2001**, *79*, 2082.

(40)   You, Y.; Park, S. Y. *J. Am. Chem. Soc.* **2005**, *127*, 12438.

(41)   Seo, J. H.; Kim, I. J.; Kim, Y. K.; Kim, Y. S. *Jpn. J. Appl. Phys.* **2008**, *47*, 6987.

(42)   Bates, F. S.; Fredrickson, G. H. *Annu. Rev. Phys. Chem.* **1990**, *41*, 525.

(43)   Deng, L.; Furuta, P. T.; Garon, S.; Li, J.; Kavulak, D.; Thompson, M. E.; Fréchet, J. M. J. *Chem. Mater.* **2006**, *18*, 386.
(44)   Nonoyama, M. *Bull. Chem. Soc. Jpn.* **1974**, *47*, 767.
(45)   Benoit, D.; Chaplinski, V.; Braslau, R.; Hawker, C. J. *J. Am. Chem. Soc.* **1999**, *121*, 3904.

Chapter 5

Crosslinked Polymer Nanoparticles for Site Isolation of Encapsulated Emitters

Abstract

Polymer particles with nanoscale dimensions are a promising carrier to encapsulate various guest cargos, such as drugs and dyes. The chemical composition and morphology of these particles can be well controlled through synthetic approaches, leading to their use in many applications. The encapsulated guest molecules inside one particle can be isolated from those in other particles by the protective polymer matrix, resulting in minimized interaction between guests in different particles. This characteristic of polymer particles can be exploited in the development of electroactive crosslinked nanoparticles containing various chromophores for application in organic light emitting diodes (OLEDs). Specifically, the energy transfer between different emitters is effectively suppressed due to the site isolation afforded by crosslinked nanoparticles, which is of great interest for white light emitting devices requiring emission from multiple chromophores. This chapter reports an approach to achieving synergetic electroluminescence from different emitters in a single device with the use of crosslinked polymer nanoparticles. This method has a number of advantages over other techniques. The chromophores are covalently bound in the crosslinked nanoparticles allowing them to be dispersed in organic solvent with preserved particle shape and no emitter leaching. This nanoparticle dispersion behaves as a light emitting ink that can be easily converted to thin films via inkjet and roll-to-roll printing techniques. Simultaneous light emission from multiple emitters can be easily realized for a thin film prepared from a mixture of different colored nanoparticles. Thus, the emission color of OLEDs would be easily tuned by simply varying the initial ratio of nanoparticles in the mixture. Finally, the synthesis of these polymer nanoparticles is significantly expedited over that of dendrimers or block copolymers.

White light
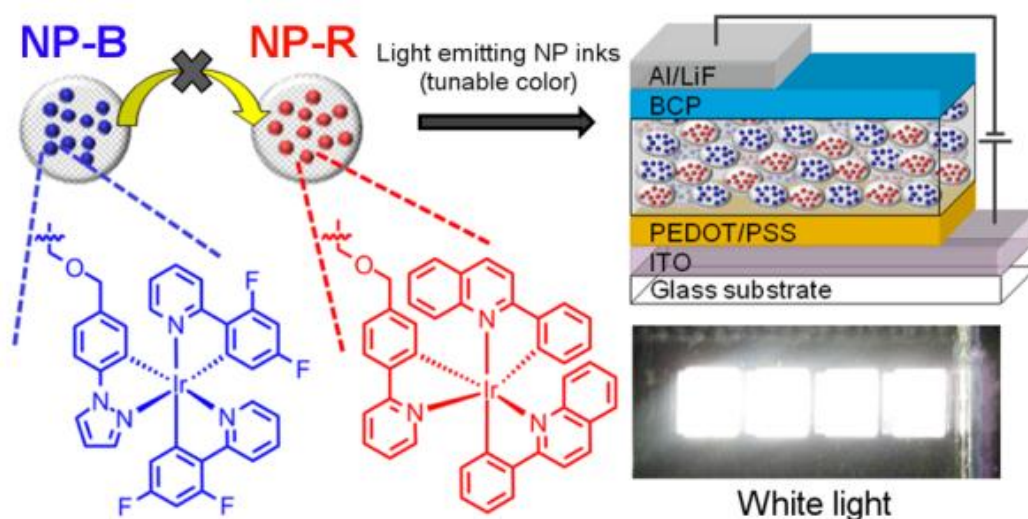
Introduction

Polymeric particles with nanoscale dimensions between 10 and 100 nm provide a promising alternative to encapsulate various guest cargoes.[1,2] The chemical composition and morphology of these nanoparticles can easily be controlled through synthetic approaches. The encapsulated guest molecules inside one nanoparticle are isolated from those in other nanoparticles by the surrounding polymer matrix, resulting in a minimization of interactions between guests in different nanoparticles. This characteristic of discrete polymer nanoparticles, combined with the solution processibility for thin-film fabrication, can be exploited for application in various fields to suppress the undesired interaction of substance or energy between different guest molecules.

Electroluminescent polymers have great potential for their application in organic light emitting diodes (OLEDs), since they allow fabrication of large-area displays and solid state lighting panels via low-cost solution processing techniques.[3-5] To achieve broad emission for solid state lighting, one simple strategy is to incorporate several light emitters with different but complementary emission wavelengths into a single layer in order to achieve synergistic emission.[6] However, doping several emitters into a single layer is generally associated with undesired energy transfer from the high bandgap chromophores to lower bandgap ones, most frequently via Förster and/or Dexter energy transfer[7] occurring over distances of 5-10 nm. These processes can negatively affect color quality, device performance, and stability. As a result, isolating chromophores within appropriately sized polymer domains represents an effective method to minimize this undesirable energy transfer.

Several macromolecular systems have been developed to target the energy transfer problem by site isolating different emitters within dendrimers[8,9] or microphase-separated linear block copolymers.[10,11] While these systems possess well controlled molecular structures and functionalities, a few drawbacks still limit their performance. For example, when dendrimer encapsulated dyes were mixed and cast into a single-layer film, only limited site isolation of the chromophores was observed because of the small size and relative flexibility of the dendrimers. In the case of block copolymers a delicate balance between molecular weight and composition is required in order to achieve optimal nanophase separation. Thus, tuning the emission color using these materials is relatively difficult because adjustments in the dye ratios within the various domains inevitably demand a completely new synthesis of the block copolymers.

In this chapter the use of crosslinked polymer nanoparticles to achieve the site isolation of different encapsulated emitters in a simple OLED consisting of a single emissive layer is demonstrated. Two phosphorescent cyclometalated Ir(III) complexes with different ligands were used as the emitters, which show emission spectra of blue/green (Ir-B) and red/orange (Ir-R).[10-12] These emitters suffer from energy transfer from Ir-B to Ir-R and cannot be simply mixed equally for synergistic emission. Therefore, they were specifically chosen to demonstrate the function of nanoparticles to site isolate the encapsulated emitters. The crosslinked nanoparticles (NP-B and NP-R) with electroactive host composition and covalently bound Ir complexes can be stored in the dry state and easily redispersed in an organic solvent while particle shape is preserved and emitter leaching is prevented. This design is advantageous over non-crosslinked particles, which require storing in an aqueous dispersion and casting from water in order to maintain particle shape.[13-16] These crosslinked nanoparticles dispersed in an organic solvent behave as light emitting "inks" that can easily be converted into thin films via solution casting or spin-coating.

Therefore, the emission color of the electroluminescent device can be readily tuned by varying the initial ratio of nanoparticles in the mixture.
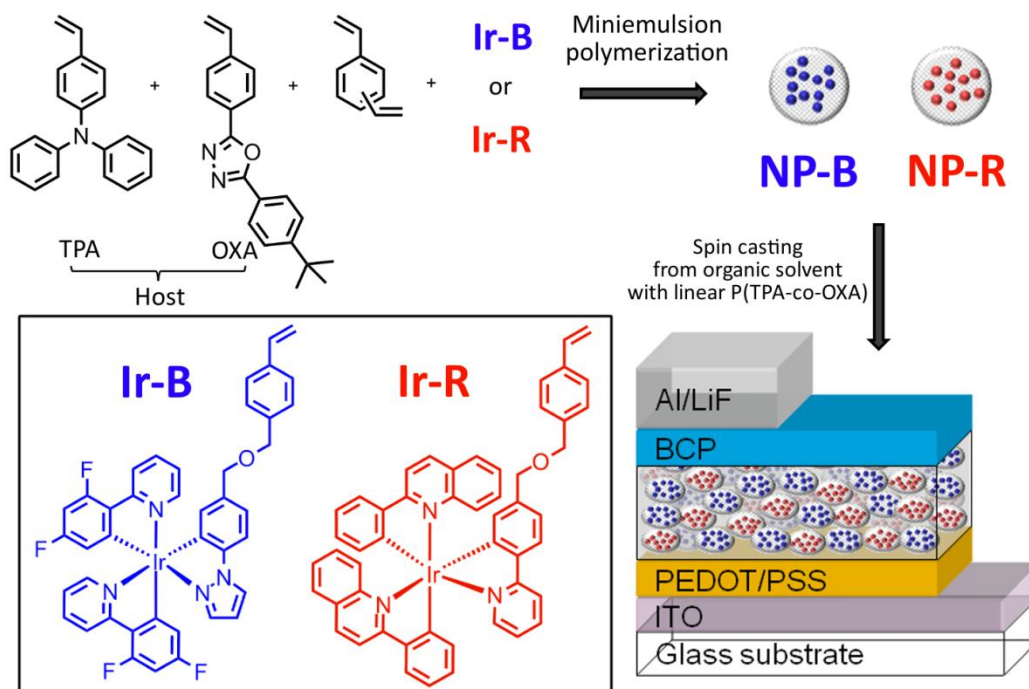

Scheme 5.1. Application of crosslinked nanoparticles for site isolation of iridium chromophores in electroluminescent devices.

Results and Discussion

Crosslinked nanoparticles containing different Ir complexes were synthesized by radical copolymerization of equivalent amounts (by weight) of triarylamine-based monomer[10] (TPA) and oxadiazole-based monomer[10] (OXA) with divinylbenzene used as a crosslinker (8 wt. % vs. total monomers) in a miniemulsion system (Scheme 5.1). Toluene was used as an inert solvent to dissolve the solid monomers and formed a miniemulsion in a solution of sodium dodecyl sulfate (SDS) in water under high-shear sonication. During the polymerization, all of the TPA and Ir monomers were added initially while the OXA monomer was added in two batches. This stepwise addition ensured a more homogeneous incorporation of the monomer units into the polymer chains.[17] The polymerization was initiated by adding the water-soluble initiator $K_2S_2O_8$ into the miniemulsion, and the reaction was stopped after 8 h. The resulting nanoparticles were analyzed by dynamic light scattering (DLS) and showed a hydrodynamic diameter (D_h) of approximately 50 nm in water (Figure 5.2c) which is in agreement with transmission electron microscopy (TEM) analysis (Figure 5.2a). The nanoparticles were purified by dialysis against water to remove most of the surfactant, followed by repeated precipitation in methanol and diethyl ether to remove residual surfactant as well as unreacted monomer and toluene from the nanoparticles. The purified nanoparticles were stored in the dry state under vacuum and could easily be redispersed in an organic solvent. It is important to note that dialysis against water alone can not remove all surfactants since residual amount of surfactant is still necessary to

stabilize the hydrophobic nanoparticles in water. This was confirmed by infrared spectroscopy analysis that detected SDS in the extensively dialyzed nanoparticles. In contrast, no surfactant was found in the nanoparticles after repeated precipitation in methanol.
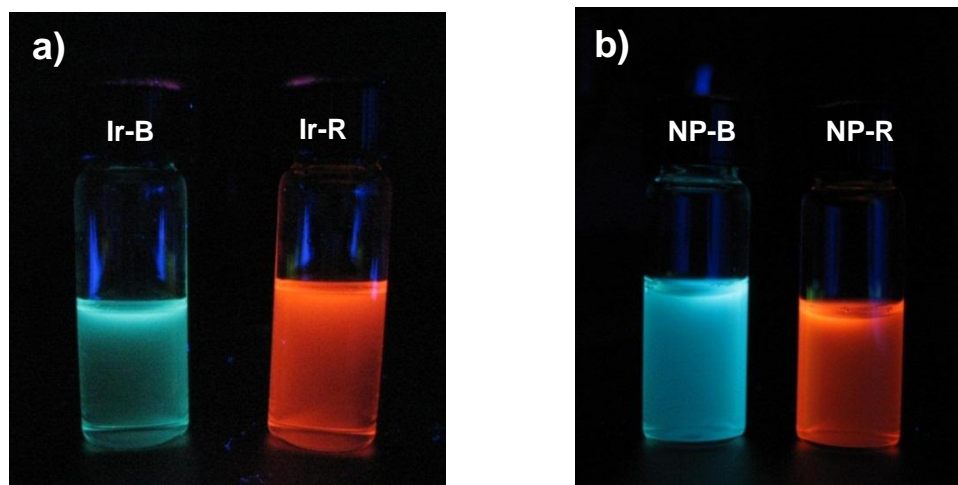
Figure 5.1. Visible photoluminescent images of a) Ir monomers in CHCl$_3$ and b) NP-B and NP-R nanoparticles in water prior to purification.
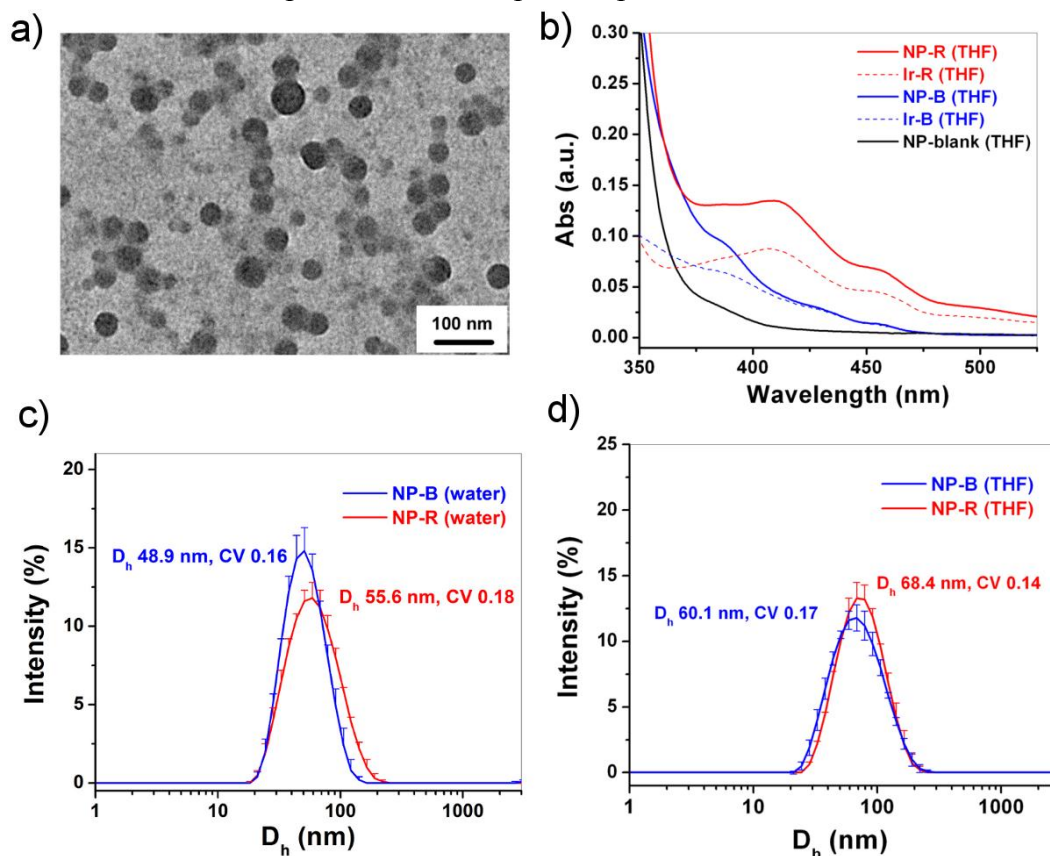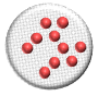

Figure 5.2. a) TEM image of NP-B before purification. b) Absorption spectra of NP-B, NP-R, NP-blank (no Ir), and Ir monomers in THF. c) Size distribution of purified NP-B and NP-R in THF, determined by DLS. d) Size distribution of NP-B and NP-R nanoparticles in water, determined by DLS.

The purified nanoparticles had a diameter of $D_h = 60 - 70$ nm in organic solvents and a narrow size distribution, as determined by DLS (Figure 5.2d). The Ir complexes incorporated into the nanoparticles displayed absorption and emission spectra similar to those of the corresponding monomers in organic solvents. This consistency indicates that the chemical nature of the Ir complexes is preserved during particle synthesis and purification (Figure 5.1). The amount of Ir complex in nanoparticles was determined by measuring the absorbance of nanoparticles in THF. Comparing these results to monomer standard calibrated curves presented in chapter 4 (Figure 4.2) indicated that both nanoparticles contained a similar amount of Ir (approximately 10 wt. %). The particle size, coefficient of variation (CV), and iridium incorporation amounts are listed in Table 5.1.

Table 5.1. Size, CV and iridium monomer loading amounts of NP-B and NP-R.

| NPs	Size D_h (nm)/CV	Iridium in NPs (wt. %)
	60.1/0.17	10.0
	68.4/0.14	9.86
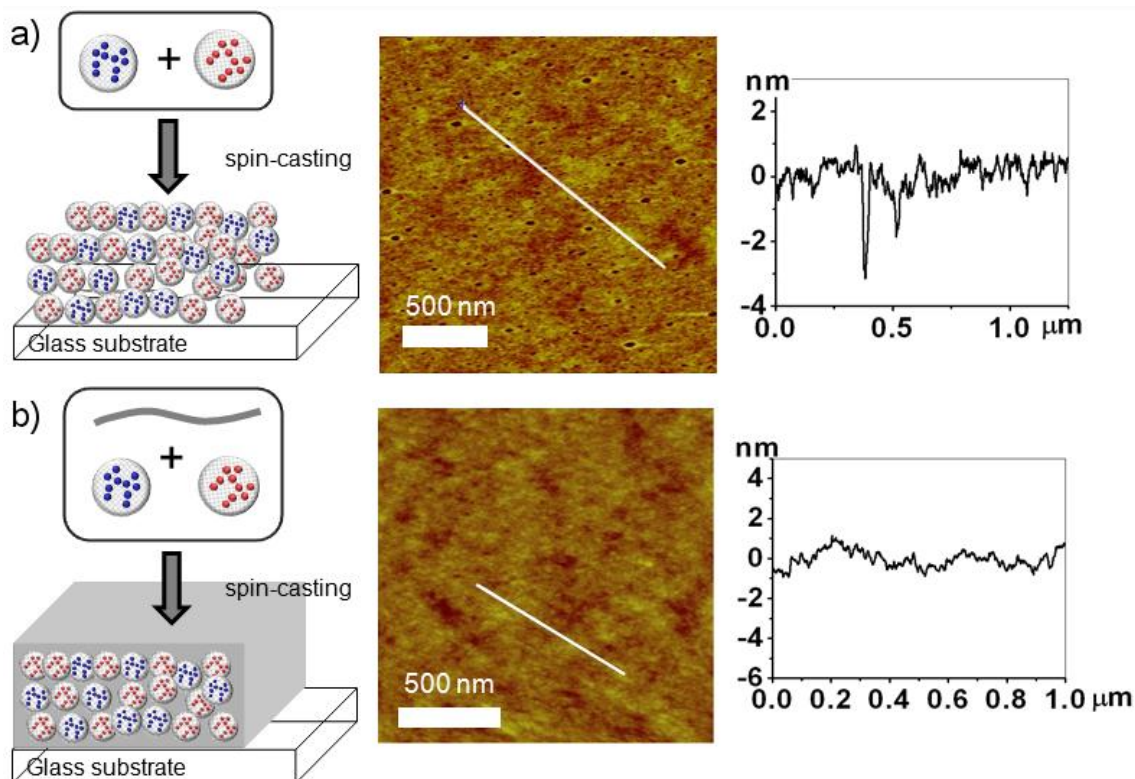
Figure 5.3. a) AFM topographic image of the film cast from the mixture of NP-B and NP-R (wt. ratio as 3:1) *without* linear P(TPA-*co*-OXA) polymer; b) AFM topographic image of the film cast from the mixture of NP-B, NP-R and linear

P(TPA-*co*-OXA) (wt. ratio as 3:1:4) in chlorobenzene (40 mg/ml). The section profiles on the right corresponding to the white line in the AFM image center.
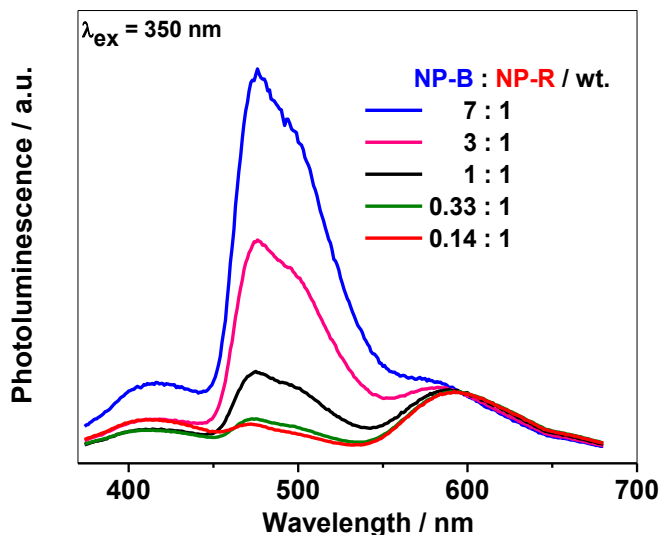

Figure 5.4. Photoluminescence (PL) spectra of polymer films on a glass substrate with varied ratios of NP-B and NP-R, mixed with linear P(TPA-*co*-OXA) polymer. The weight ratio of total nanoparticles to linear polymers was 1:1. The film was prepared by spin casting a 40 mg/ml polymer solution in chlorobenzene (2000 rpm, 40 sec).

Site isolation of the iridium emitters in nanoparticles was first confirmed by the measurement of their photoluminescence in thin films. The results showed a balanced blue and red emission using a 1:1 wt. ratio of blue and red nanoparticles (Figure 5.4). The emissive film on a glass substrate was fabricated by spin casting a blend of nanoparticles and a linear polymer P(TPA-*co*-OXA),[11] with chemical composition similar to that of the nanoparticle host material, from chlorobenzene. In this study, the weight ratio of linear polymer to nanoparticles was kept at 1:1, although the amount of linear polymer could have profound effects on the film morphology and the device performance. While the addition of the linear polymer lowers the effective concentration of iridium emitter in the film, it was found to be critical to minimize the presence of pinholes and yield a smooth film required for device preparation (Figure 5.3). This was determined by atomic force microscopy (AFM) of a film prepared of just solution processed particles (Figure 5.3a). There were noticeable pinholes present in the film which also resulted in a poorly functioning device. Figure 5.3b shows the AFM topographic image of the 65 nm thick film, prepared from a 40 mg/ml solution. The smooth film surface obtained exhibited a root mean square roughness < 0.5 nm, which is favorable for use as an emissive layer in electroluminescent devices.
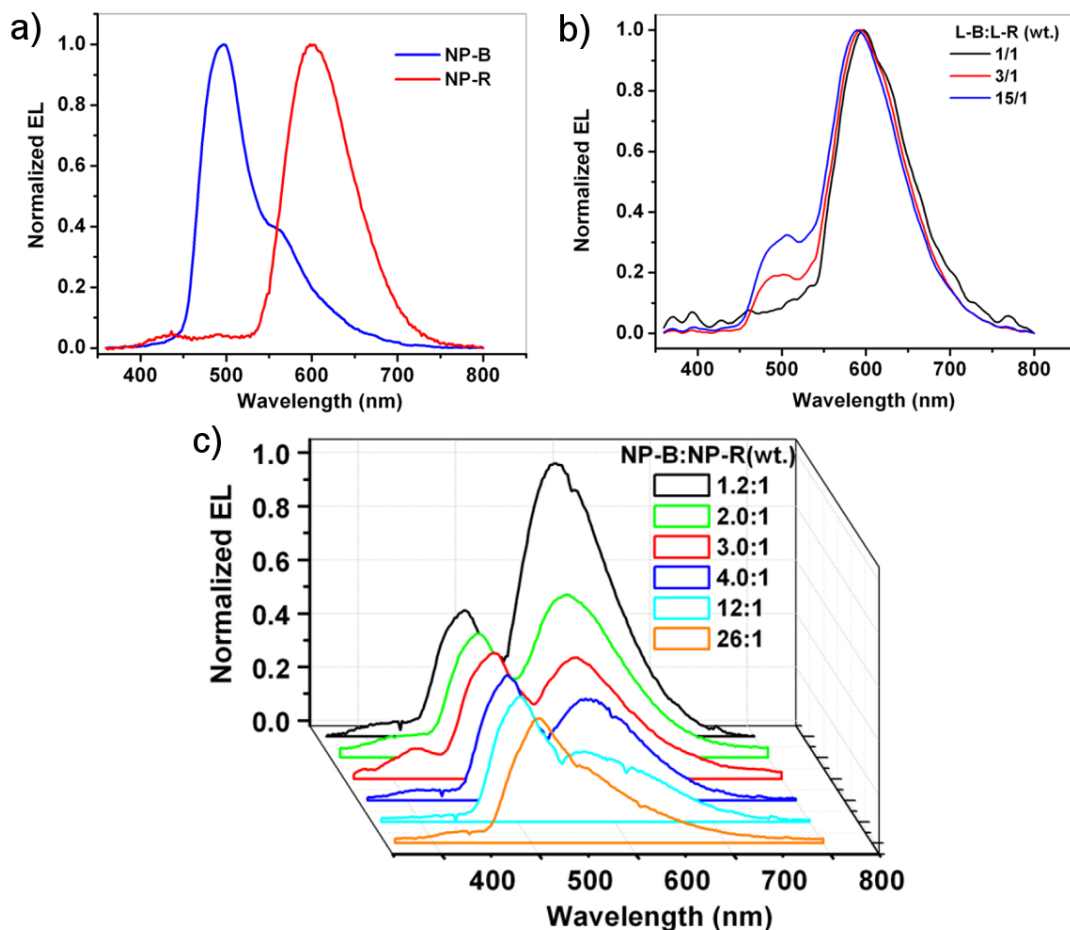
Figure 5.5. a) EL spectra of devices fabricated from single color nanoparticle and equivalent weight amount of linear (TPA-*co*-OXA). b) EL spectra of control devices with varied ratios of blue L-B and red L-R linear polymers. c) EL spectra of devices with varied ratios of NP-B and NP-R, as well as linear P(TPA-*co*-OXA) (wt. ratio as *x:1:(x+1)* with varied *x*).

The electroluminescence (EL) of these crosslinked nanoparticles in solid films was evaluated in a very simple device architecture, glass/ITO/PEDOT:PSS (40 nm)/emissive layer (65 nm)/BCP(40 nm)/LiF(1 nm)/Al(100 nm), where ITO = indium tin oxide, PEDOT:PSS = poly(3,4-ethylenedioxythiophene):poly(styrenesulfonate), and BCP = 2,9-dimethyl-4,7-diphenyl-1,10-phenanthroline. The EL spectra of devices fabricated from either blue or red nanoparticles showed emission peaks around 498 nm and 598 nm, respectively (Figure 5.5a). For the devices made from blends of these two nanoparticles, the EL spectra in Figure 5.5c demonstrate that, as a result of site isolation, color tuning is readily achieved by varying the nanoparticle ratio. The device showed a balanced EL emission (equal peak height of blue and red emission) at a wt. ratio of NP-B to NP-R of 3:1. Further increasing the wt. ratio of NP-B to NP-R resulted in a relatively decreased red emission peak. As control experiments, devices constructed from a mixture of linear copolymers (L-B and L-R) containing similar amounts of Ir complexes showed a dominant red emission even at 15:1 wt. ratio of L-B to L-R, due to the significant energy transfer and charge trapping to the red emitters (Figure 5.5b).
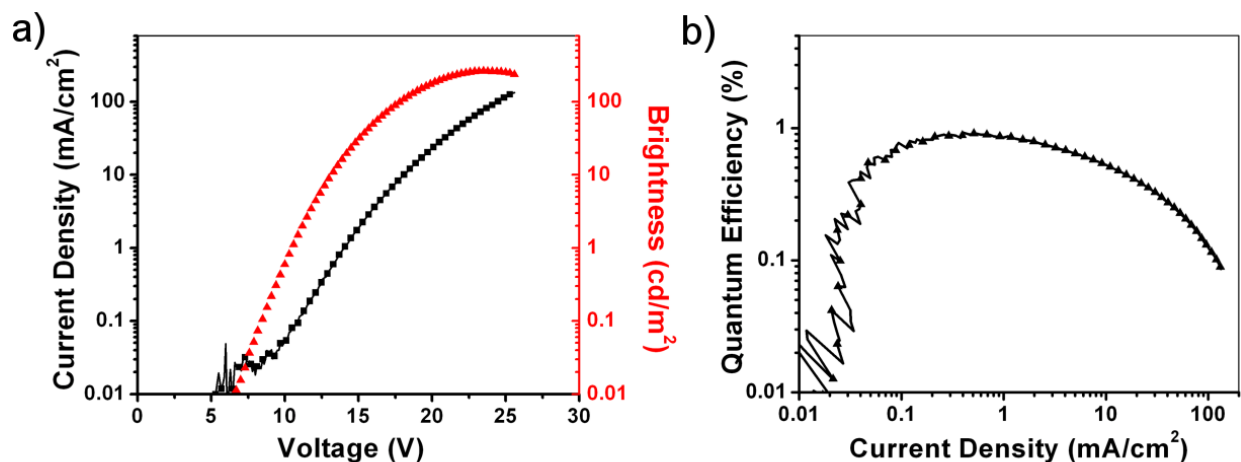
Figure 5.6. a) I-V characteristics and brightness vs. voltages and b) Dependence of external quantum efficiency on current density for single-emissive-layer OLED by using a mixture of NP-B and NP-R, as well as linear P(TPA-*co*-OXA) polymer (wt. ratio as 3:1:4).

The device fabricated from the 3:1 wt. ratio of NP-B to NP-R with a 40 mg/ml concentration of polymer showed a near white emission with Commission Internationale de l'Eclairage (CIE) coordinates of (0.40, 0.42). The turn-on voltage was at 6.7 V and the device had a maximum brightness of 260 cd/m^2 and maximum external quantum efficiency approximately 1 % (Figure 5.6). While the overall performance of our simple, single layer nanoparticle devices is relatively low,[18] this study demonstrates the validity of the approach and the very effective site isolation realized through the novel use of encapsulating nanoparticles leading to the suppression of undesired energy transfer between chromophoric emitters. Using this strategy, device performance could be enhanced by combing improvements in the quantum efficiency of the emitters coupled with an increase in carrier mobilities in order to limit series resistance.[12,19]

Conclusion

This chapter demonstrated a facile and versatile strategy to achieve site isolation of different emitters in one emissive layer by covalently incorporating iridium dyes into electroactive crosslinked nanoparticles. These nanoparticles could easily be dispersed in an organic solvent and behaved as light emitting "inks", providing access to tunable electroluminescence by simple adjustments in the ratio of nanoparticles in the mixture. Using this concept, both higher efficiencies and purer white electroluminescence using three colored nanoparticles should be attainable.

Experimental

Materials. The monomers, including triphenylamine-based monomer (TPA), oxadiazole-based monomer (OXA) and heteroleptic Ir(III) complexes bearing a pendant styrene handle, were synthesized based on published procedures.[10,20] Linear copolymer P(TPA-*co*-OXA) was

synthesized by sequential nitroxide mediated polymerization of TPA and OXA monomers. The weight fraction of these two monomer units in the final polymer was approximately 1:1. Indium tin oxide (ITO)-coated glass sheets were purchased from Thin Film Devices Inc. Poly(3,4-ethylenedioxythiophene):poly(styrenesulfonate) (PEDOT:PSS, Clevios PH) water solution was purchased from H.C. Starck and filtered (PTFE filter 0.45 μm) before use. 2,9-Dimethyl-4,7-diphenyl-1,10-phenanthroline (BCP) (96%) was purchased from Aldrich and was purified in a home-built thermal gradient sublimator before its use for vapor evaporation. Al was purchased from Alfa Aesar (purity >99.99%), and LiF (fused pieces 99.995%) was purchased from Aldrich. Divinylbenzene (DVB, 80%) was purchased from Aldrich and purified twice by passing through a column filled with basic alumina to remove the inhibitor. All other solvents were purchased from Aldrich with the highest purity and used as received.

Preparation of Ir-Containing Nanoparticles by Miniemulsion Polymerization. Crosslinked nanoparticles containing different Ir complexes, NP-B and NP-R, were synthesized by an O/W miniemulsion polymerization. A typical procedure for synthesis of nanoparticles containing blue emitter, Ir-B complex, is briefly described. A solution was prepared by mixing 50 mg TPA, 14 mg OXA, 14 mg Ir-B monomer, 11 μL DVB, 10 μL hexadecane and 0.35 mL toluene in a 5 ml vial. This solution was then added dropwise into a beaker containing 0.27 g of SDS and 45 g of water. The miniemulsion was prepared by sonicating the biphasic mixture in an ice bath for 4 min using a Branson 450 Sonifier with a ½ inch flat tip (an output setting of 7, and a duty cycle of 70%). The prepared miniemulsion was charged into a 250 mL three-neck round flask equipped with a condenser. Under 550 rpm mechanical agitation, the mixture was deoxygenated via nitrogen bubbling for 20 min before the flask was immersed into an oil bath with 70 °C. The polymerization was initiated by addition of deoxygenated 14 mg potassium persulfate initiator water solution (0.4 ml) into the system and the polymerization temperature was kept constant at 70 °C throughout the reaction under nitrogen atmosphere. The reaction became transparent at ca. 0.5 hour due to the polymerization of monomers and evaporation of some toluene solvent. At 1.5 h, a second batch of monomer containing 36 mg OXA in 0.15 ml toluene was emulsified with 0.03 g SDS in 5 mL water. The mixture was deoxygenated before adding into the polymerizing system. Aliquots were taken at timed intervals to measure the particle size by using DLS and the reaction was stop at 8 h. Dialysis against deionized water (dialysis tubing with COMW 100 kDa) was carried out for 5 days (changing deionized water every 12 hours) in order to remove the surfactant and unreacted initiator. The obtained nanoparticles were precipitated from the water by adding small amount of $CaCl_2$ into the system, followed by centrifugation. The nanoparticles were washed twice with methanol to remove the surfactant and washed with diethyl ether to remove the unreacted monomer and hexadecane. Each wash was followed by centrifugation to collect the nanoparticles. The purified nanoparticles were dried and stored in a vacuum desiccator.

Synthesis of Ir-Containing Linear Copolymers by Conventional Free Radical Polymerization in Solution. For the control experiments, linear copolymers L-B and L-R, were synthesized, which had similar chemical compositions and weight fractions of Ir emitters as the crosslinked nanoparticles. A typical procedure for synthesis of linear polymer containing blue Ir-B emitter is described. Into a 5 ml vial was charged with 50 mg TPA, 14 mg OXA, 14 mg Ir-B monomer, and 0.35 mL toluene. This solution was deoxygenated under magnetic stirring (500 rpm) for 20 min before immersing into a 70 °C oil bath. The polymerization was initiated by addition of 14 mg 2,2'-azobisisobutyronitrile with 0.1 ml toluene (deoxygenated) into the system and the polymerization temperature was kept constant at 70 °C under nitrogen atmosphere. At 1.5

h, a second batch of monomer containing 36 mg OXA in 0.15 ml toluene was deoxygenated and added into the polymerizing system. The reaction was stopped after 8 hours by opening the vial and diluting the system with room temperature THF. The polymers were precipitated in hexanes twice before collected and dried under vacuum.

Devices Fabrication and Measurement. ITO-coated glass substrates were cleaned by sequentially boiling in trichloroethylene, acetone, and *2*-propanol for 10 min each followed by drying under nitrogen. The substrates were then treated using a UVOCS ultraviolet/ozone cleaner for 10 min. A thin layer (~ 40 nm) of PEDOT:PSS was spin-coated onto ITO surface (2000 rpm for 40 sec) before being baked at 140 ^{o}C for 10 min. The substrates were transferred into a nitrogen-filled glovebox. The emissive polymer layer with a thickness of ~65 nm was prepared on the top of ITO/PEDOT:PSS by spin casting (2 000 rpm for 40 s) a 40 mg/ml polymer solution in chlorobenzene. The polymer solution contained various ratios of blue and red nanoparticles and the weight ratio of total nanoparticles to linear P(TPA-*co*-OXA) was kept as 1:1. The film was transferred into a thermal evaporator standing in air. A hole blocking layer BCP (40 nm) was deposited at a rate of 1 Å/sec with a base pressure $< 7 \times 10^{-6}$ Torr. After taking the film out of the evaporator and wiping out the BCP on the electrodes, the film was put back in the evaporator to deposit a cathode consisting of 1 nm LiF and 100 nm Al at a rate of 0.2 and 4 Å/sec, respectively. Four OLED devices with 2×2 mm^2 each were formed at the intersections of the ITO anode and the striped Al cathode. The devices were tested in air within 2 h after fabrication. The electrical and optical intensity characteristics of the devices were measured with a Keithly 2400 sourcemeter/2000 multimeter coupled to a Newport 1835-C optical meter, equipped with a UV-818 Si photodetector. Only light emitted from the front face of the device was collected and used in subsequent efficiency calculations. The electroluminescence (EL) spectra were measured on a USB4000 miniature fiber optic spectrometer. The emission was found to be uniform throughout the area of each device.

Characterization. Ground-state UV/vis absorption spectra were measured on a Shimadzu UV-3600 UV-VIS-NIR spectrophotometer. Emission and excitation spectra were obtained using an ISA/SPEX Fluorolog 3.22 equipped with a 450W Xe lamp, double excitation and double emission monochromators, and a digital photoncounting photomultiplier. Slit widths were set to a 3 nm bandpass on both excitation and emission monochromators. Samples for absorbance and emission experiments were measured either in standard 1 cm quartz cells for solution-based sample or in solid film on an untreated glass slide. The polymer film was spin cast from a chlorobenzene solution with 2000 rpm for 40 seconds. All measurements were performed at room temperature.

The size distribution of the nanoparticles dispersing in solvents was determined by dynamic light scattering (DLS) using a Zetasizer Nano-ZS instrument (Malvern Instruments, Malvern, UK). Transmission electron microscopy (TEM) images were measured using a FEI Tecnai 12 microscope operated at 100 kV. Elemental analyses were performed at the micro-mass analytic facility of the University of California, Berkeley. Polymer film thickness was measured by a Veeco Dektak profilometer. Size exclusion chromatography (SEC) was carried out with THF eluent at 1.0 mL/min by using three PLgel columns (7.5 x 300 mm) with a pore size of 10^5, 10^3, and 500 Å, respectively. The particle size in columns was 5 μm and the columns were thermostatted at 35 °C. The SEC system consisted of a Waters 510 pump, a Waters 717 autosampler, a Waters 486 UV-Vis detector, and a Wyatt Optilab DSP differential refractive index detector. The apparent molecular weights and polydispersity (M_w/M_n) were determined with a calibration based on linear polystyrene standards using Empower software from Waters.

Atomic force microscopy (AFM) was performed using a Veeco (Digital Instruments) Multimode microscope with a Nanoscope V controller. Imaging was performed in semi-contact (tapping) mode using Veeco RTESP tips.

References

(1)   Kawaguchi, H. *Prog. Polym. Sci.* **2000**, *25*, 1171.
(2)   Kawa, M.; Fréchet, J. M. J. *Chem. Mater.* **1998**, *10*, 286.
(3)   Burroughes, J. H.; Bradley, D. D. C.; Brown, A. R.; Marks, R. N.; Mackay, K.; Friend, R. H.; Burns, P. L.; Holmes, A. B. *Nature* **1990**, *347*, 539.
(4)   Kido, J.; Shionoya, H.; Nagai, K. *Appl. Phys. Lett.* **1995**, *67*, 2281.
(5)   Mueller, C. D.; Falcou, A.; Reckefuss, N.; Rojahn, M.; Wiederhirn, V.; Rudati, P.; Frohne, H.; Nuyken, O.; Becker, H.; Meerholz, K. *Nature* **2003**, *421*, 829.
(6)   Tanaka, I.; Suzuki, M.; Tokito, S. *Jpn. J. Appl. Phys., Part 1* **2003**, *42*, 2737.
(7)   Kawamura, Y.; Yanagida, S.; Forrest, S. R. *J. Appl. Phys.* **2002**, *92*, 87.
(8)   Freeman, A. W.; Koene, S. C.; Malenfant, P. R. L.; Thompson, M. E.; Fréchet, J. M. J. *J. Am. Chem. Soc.* **2000**, *122*, 12385.
(9)   Furuta, P.; Brooks, J.; Thompson, M. E.; Fréchet, J. M. J. *J. Am. Chem. Soc.* **2003**, *125*, 13165.
(10)   Poulsen, D. A.; Kim, B. J.; Ma, B.; Zonte, C. S.; Fréchet, J. M. J. *Adv. Mater.* **2010**, *22*, 77.
(11)   Ma, B.; Kim, B. J.; Deng, L.; Poulsen, D. A.; Thompson, M. E.; Fréchet, J. M. J. *Macromolecules* **2007**, *40*, 8156.
(12)   Ma, B.; Kim, B. J.; Poulsen, D. A.; Pastine, S. J.; Fréchet, J. M. J. *Adv. Funct. Mater.* **2009**, *19*, 1024.
(13)   Piok, T.; Gamerith, S.; Gadermaier, C.; Plank, H.; Wenzl, F. P.; Patil, S.; Montenegro, R.; Kietzke, T.; Neher, D.; Scherf, U.; Landfester, K.; List, E. J. W. *Adv. Mater.* **2003**, *15*, 800.
(14)   Huebner, C. F.; Carroll, J. B.; Evanoff, D. D.; Ying, Y. R.; Stevenson, B. J.; Lawrence, J. R.; Houchins, J. M.; Foguth, A. L.; Sperry, J.; Foulger, S. H. *J. Mater. Chem.* **2008**, *18*, 4942.
(15)   Christopher, F. H.; Ryan, D. R.; Stephen, H. F. *Adv. Funct. Mater.* **2009**, *19*, 3604.
(16)   Huebner, C. F.; Foulger, S. H. *Langmuir* **2010**, *26*, 2945.
(17)   OXA monomer has an electron-withdrawing group at the 4-position of styryl unit, and is expected to have a higher reactivity than TPA and Ir monomers in radical copolymerization.
(18)   Wu, H.; Zhou, G.; Zou, J.; Ho, C.-L.; Wong, W.-Y.; Yang, W.; Peng, J.; Cao, Y. *Adv. Mater.* **2009**, *21*, 4181.
(19)   Tamayo, A. B.; Alleyne, B. D.; Djurovich, P. I.; Lamansky, S.; Tsyba, I.; Ho, N. N.; Bau, R.; Thompson, M. E. *J. Am. Chem. Soc.* **2003**, *125*, 7377.
(20)   Deng, L.; Furuta, P. T.; Garon, S.; Li, J.; Kavulak, D.; Thompson, M. E.; Fréchet, J. M. J. *Chem. Mater.* **2006**, *18*, 386.

Chapter 6

Cross-linkable Iridium Complexes for Solution Processed Multilayer Devices

Abstract

This chapter outlines the development of a new series of crosslinkable heteroleptic iridium (III) complexes for use in solution processed phosphorescent organic light emitting diodes (OLEDs). With the incorporation of two crosslinkable vinyl benzyl ether groups, these compounds can be fully crosslinked after heating at 180 °C for 30 minutes. The crosslinked films exhibit excellent solvent resistance and film smoothness which enables fabrication of high performance multilayer OLEDs by sequential solution processing of multiple layers. This diversity makes these materials not only suitable for use as hole transporting/electron blocking but also as emissive layers of several colors. These compounds have been applied as effective materials for all-solution processed OLEDs as hole transporting/electron blocking and host material, as well as crosslinkable phosphorescent emitters.
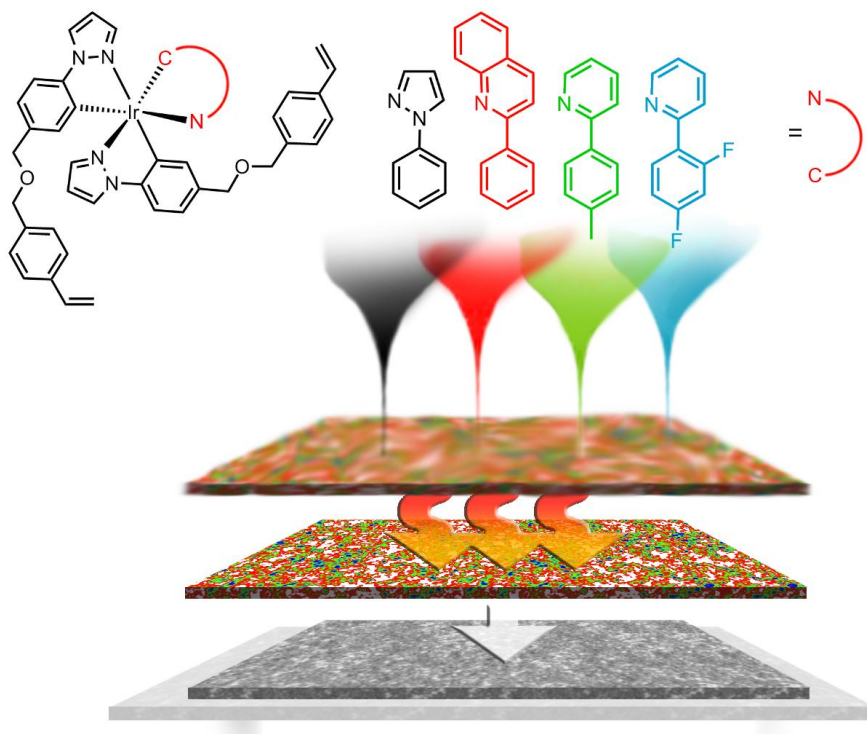
Introduction

Iridium (III) complexes have attracted much attention for their application in organic light emitting diodes (OLEDs).[1-8] As a result of the strong spin-orbital coupling effect of the heavy metal, these complexes are capable of harvesting both singlet and triplet excitons in devices to achieve internal quantum efficiency of 100%, when acting as the emissive material.[9] In addition, iridium (III) complexes can be applied as electron blocking materials, host materials and hole blocking materials,[10,11] since their characteristics and functionality can be controlled by varying the coordinated organic ligands. It has been demonstrated that facial tris-Iridium (III) complexes coordinated with 1-phenylpyrazolyl (PPZ), 2-(4,6-difluorophenyl)pyridyl (DFPPY), 2-(p-tolyl)pyridyl (TPY) and 2-phenylquinolyl (PQ) show different photophysical properties with peak emissions ranging from 400nm to 600nm.[2,4] Among these complexes, facial Ir(PPZ)$_3$ can be used as both host and hole transporting/electron blocking materials because of its high triplet energy (3.4 eV), high LUMO (Lowest Unoccupied Molecular Orbital) level (1.7 eV) and comparable HOMO (Highest Occupied Molecular Orbital) level (5.1 eV) that matches the Fermi level of the ITO electrode (4.7 eV).[10] The other three complexes can be used as phosphorescent emitters to produce highly efficient blue, green and red OLEDs by doping these iridium emitters into appropriate hosts.[2,3] Devices incorporating such species have been fabricated by the high vacuum vapor deposition of small molecules. Typically, a multilayer structure is obtained by high vacuum sequential deposition of an emission layer (EML) sandwiched between the hole transporting and the electron transporting layers (HTL and ETL respectively). Unfortunately, this process of high vacuum vapor deposition of small molecules limits the OLED device size to relatively small areas due to the high fabrication cost of large evaporators or the assembly cost of multiple small device subunits.

Solution processed multilayer OLEDs have been the subject of intense investigation in recent years due their great potential in reducing device fabrication cost without sacrificing the device efficiency. However, the process is non-trivial, since it requires that each deposited layer be resistant to the solvent used in the deposition of subsequent layers.[12] One strategy, which has been developed to overcome the dissolution issues associated with solution processing multilayer structures, is to use materials soluble in orthogonal solvent systems for each individual layer. One of the most frequently used materials is poly(3,4-ethylene dioxythiophene)-poly(styrene sulfonic acid) PEDOT-PSS, which is water soluble and can be used as the HTL, followed by organic soluble iridium complexes containing polymer as the EML, and finally a water soluble copolymer as the ETL.[13] However, the choice of materials available for such trilayer systems is rather limited, thus restricting the range of performance of the resulting OLEDs. Therefore, an elegant alternative strategy involves the development of crosslinkable materials bearing negative photoresist-like properties, which may be crosslinked to form totally insoluble films by light or thermal treatment after a wet chemical deposition. Such materials would therefore enable the sequential deposition of several layers.[14-21] Crosslinkable hole transporting layer materials have been demonstrated successfully in multilayer structured OLEDs. There are also a few reports of crosslinkable emitting materials based on fluorescent conjugated polymers that have limited internal quantum efficiencies of 25%.[16,22] More recently, a crosslinkable phosphorescent material bearing an oxetane moiety, which can be crosslinked cationically upon ultraviolet illumination, has been demonstrated as an efficient orange emitter.[8] While the requirement of a photoinitiator and high energy UV to effect crosslinking might be a concern with regards to materials stability and devices lifetime, these reports do establish the concept of crosslinkable emissive materials,

albeit with limits in device efficiency and scope of emission color. This chapter discusses thermally crosslinked iridium complexes with high thermal stability and varied functionalities that may be used for high efficiency OLED devices.

A series of heteroleptic iridium complexes **1-4** containing two crosslinkable phenylpyrazole vinyl benzyl ester groups, which are able to polymerize at temperatures near 150 °C have been developed. Owing to the rich structure chemistry of iridium (III) complexes, the emission of the complexes can be tuned from the UV region to green and red simply by adjusting the structure of the cyclometallating ligands. The complex (PPZ-VB)$_2$IrPPZ (**1**), with the highest triplet energy >3eV, can perform a variety of functions including hole transport/electron blocking and host material, while the three compounds, (PPZ-VB)$_2$IrDFPPY (**2**), (PPZ-VB)$_2$IrTPY (**3**) and (PPZ-VB)$_2$IrPQ (**4**) can act as emitting dopants in the light emitting layer. By appropriately functionalizing the iridium complexes and tuning their emission energy, optimized materials with desirable electrochemical and photophysical properties can be obtained for application in efficient and fully solution-processed OLEDs. It is believed that this general approach can be easily extended to other metallic ligand systems for high performance solution-processed OLEDs.

Results and Discussion

Synthesis and characterization of functional iridium monomers

Scheme 6.1 shows the design of heteroleptic iridium (III) complexes containing two crosslinkable vinylbenzyl (VB) ether groups. Phenylpyrazole (PPZ) was chosen for its high triplet energy, since the photophysical properties of the complexes would be dictated simply by the judicious choice of the third lower or equal energy cyclometallating ligand.[4,10,23] The synthetic procedure used to prepare these compounds involved four steps. First, cyclometalated Ir(III) μ-chloro-bridged dimer, (PPZ-CHO)$_2$Ir(μ-Cl)$_2$Ir(PPZ-CHO)$_2$, was prepared according to the Nonoyama route, by refluxing IrCl$_3 \cdot n$H$_2$O with 2.2 equiv of 4-pyrazole-1-yl-benzaldehyde in a 3:1 mixture of 2-ethoxyethanol and water for 24 hours.[2,24] Heteroleptic iridium complexes were then obtained by reaction of the chloride bridged dimer with another cyclometalating ligand in the presence of AgCF$_3$SO$_4$ in diglyme at 115 °C for 24 hours.[25] All of the complexes obtained after this second step were the thermodynamically favored facial isomers as confirmed by ^{1}H NMR. Reduction of these iridium complexes with aldehyde-substituted ligands by NaBH$_4$ in a mixture of ethanol and dichloromethane yielded the benzyl alcohol functionalized complexes. Finally, Williamson ether synthesis with vinyl benzyl chloride led to the desired Ir complexes containing two crosslinkable vinylbenzyl ether groups designated as (PPZ-VB)$_2$IrPPZ (**1**), (PPZ-VB)$_2$IrDFPPY(**2**), (PPZ-VB)$_2$IrTPY(**3**) and (PPZ-VB)$_2$IrPQ(**4**), each in an overall yield of *ca.* 20%.
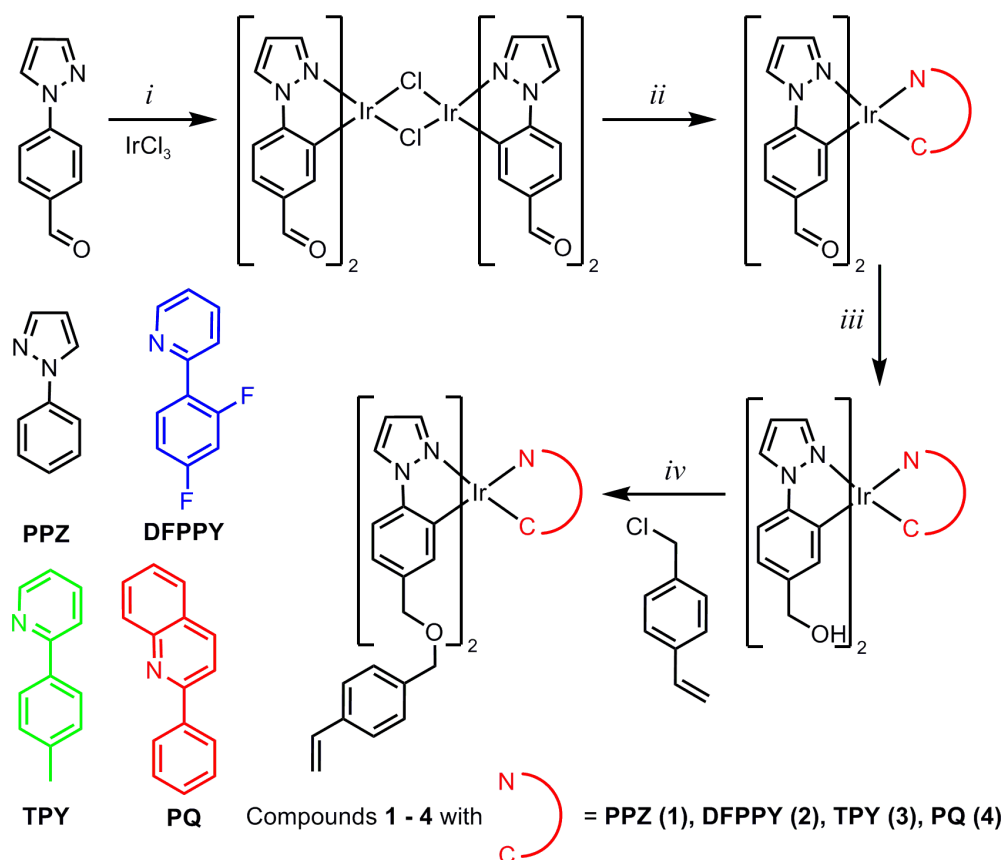
Scheme 6.1. Synthetic scheme and chemical structures of the iridium complexes; reagents used were: *i*, 2-ethoxylethanol: water 3:1, 110 °C, 20h; *ii*, diglyme, AgCF$_3$SO$_4$, 115 °C, 20 h; *iii*, DCM, ethanol, NaBH$_4$, R.T., 24 h; *iv*, THF, KI, KH, 18-crown-6, R.T., 48 h.

Absorption and emission spectra for the four complexes (**1**, **2**, **3** and **4**) dissolved in dichloromethane at room temperature (RT) are shown in Figure 6.1. The spectra show a red shift as the triplet energy of the ligands decreases from PPZ to PQ. No emission at room temperature is seen for compound **1**, which is consistent with a previous observation for the similar facial Ir(PPZ)$_3$.[4] Emission spectra for complexes **2**, **3** and **4** are almost identical to their counterparts without the vinyl benzyl (VB) ether groups reported elsewhere,[23] indicating that the VB group has no significant effect on the photophysical properties of complexes **2**, **3** and **4**. This is not surprising since the VB group is not conjugated the PPZ ligand, thus, the HOMO and LUMO levels are essentially the same for the various compounds before and after functionalized with the VB groups.
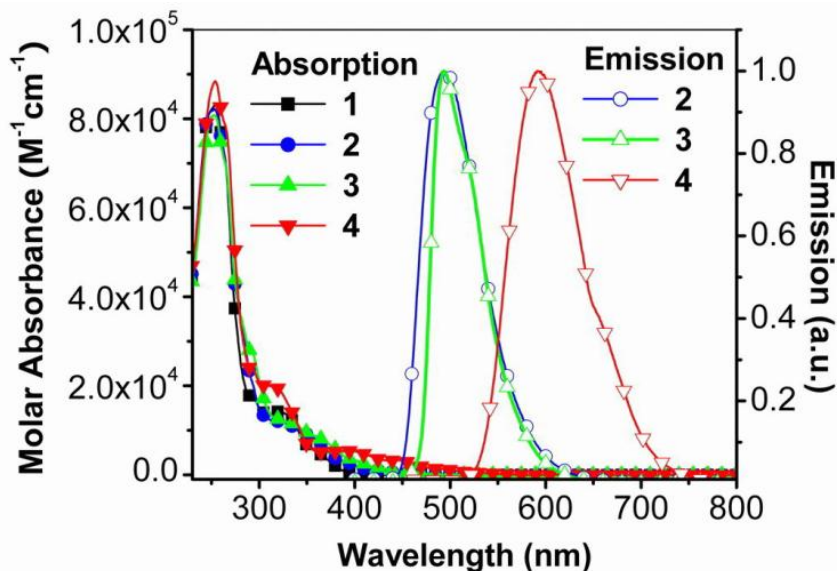
Figure 6.1. The absorption and emission spectrum of compounds **1**-**4** in dichloromethane at RT.

*Crosslinking of functional monomers*

It is well known that styrenic monomers can be polymerized in the bulk at temperatures above 150 °C,[26] and indeed materials containing two vinyl benzyl ether groups and triphenylamine derivative cores have recently been used as efficient thermally crosslinkable hole transporting materials.[21,27] The design of these new complexes takes advantage of this facile thermal crosslinking while preserving the key electronic properties derived from the iridium complex core. The thermal properties of these functional iridium monomers have also been studied. Figure 6.2a shows differential scanning calorimetry (DSC) measurements effected on (PPZ-VB)$_2$IrPPZ(**1**) and (PPZ-VB)$_2$IrDFPPY(**2**). The first scan for compound **1** shows an endothermic peak at ~75 °C and a broad exothermic peak at ~145 °C, which correspond to the crystallization and crosslinking processes, respectively. After isothermal heating at 180 °C for 30 min, the sample was slowly cooled to room temperature and then re-scanned. There was no crystallization peak observed in the second scan, which displayed a broad transition above 200 °C for T_g. A similar behavior was also observed for compound **2**. Such thermal behavior (Figure 6.2b) is in agreement with measurements carried out on other crosslinkable materials bearing two VB groups.[21,27]
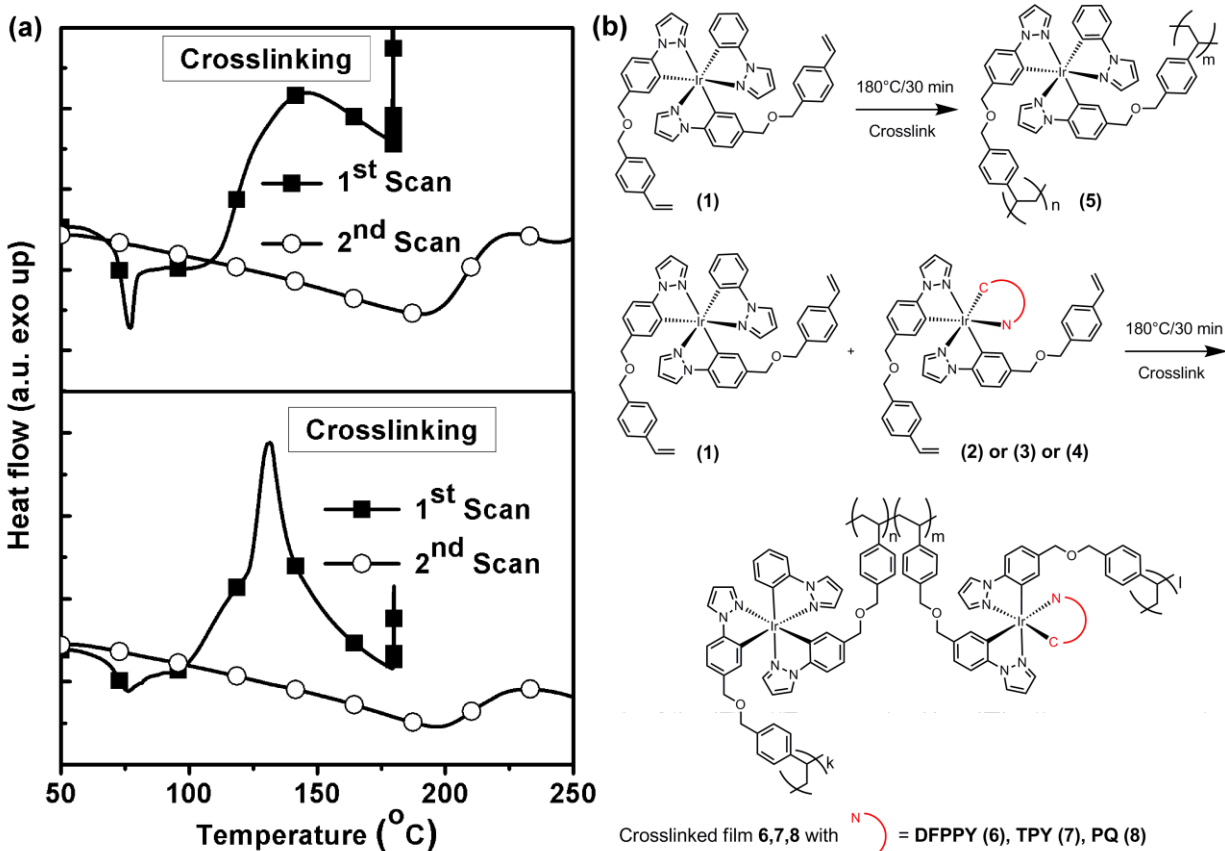
Figure 6.2. a) DSC measurements of **1** and **2**, scan rate of 10 °C/min for both scans; b) crosslinking reaction scheme for a single iridium complex and a host-dopant system

These materials have been investigated as two different types of crosslinked layers: one hole transporting and electron blocking layer (**5**) and three emitting layers (**6**, **7**, **8**). As shown in Figure 6.2b, the blocking layer **5** is based on the crosslinking of pure monomer **1**; while emitting layers **6**, **7**, and **8** were obtained by crosslinking 10 wt. % of monomer **2**, or **3**, or **4** with 90 wt. % of monomer **1**, in which monomer **1** works as host because of its high triplet energy and non-emissive property, and the other three monomers act as emissive dopants. This copolymerization of monomer **2**, or **3**, or **4** with monomer **1** is feasible since they have the same crosslinkable groups and molecular structures. As shown in Figure 6.2a, monomers **1** and **2** have almost identical thermal behaviors. This host-dopant system will therefore effectively prevent the emission self-quenching due to excessive concentration of emitters in the device. The properties of the crosslinked films were studied in terms of absorption, emission, solvent resistance, and film topology using UV/vis spectroscopy, fluorimetry, and atomic force microscopy (AFM). For solvent resistance studies, uniform films were produced on glass substrates through spin-coating of the selected iridium monomers in chlorobenzene solutions. Thin film samples were then thermally treated at 180 °C for 15 and 30 minutes. The results in Figure 6.3a show that the UV/vis absorbance of the films after the 30 minute of thermal treatment followed by washing with chlorobenzene remains the same. In contrast, samples subjected to only 15 minutes of thermal treatment did not reach the required solvent resistance and a reduction in absorption was observed after washing, indicating a loss of material due to dissolution in the wash solvent.

75

Absorption spectra of the films both before and after crosslinking (Figure 6.3a) indicate almost complete transparency in the visible spectrum, making the material suitable for use as a blocking layer on top of the ITO transparent electrode. In addition, as shown in Figure 6.3b, the luminescence properties of the emissive materials in the solid state are almost identical to those of solutions with almost no change in emission energy observed upon crosslinking, suggesting that the crosslinking procedure has no influence on the photophysical properties of the thin films. The surface topology of the polymerized films (both the blocking layer and emitting layers) after thermal crosslinking, a critical feature for optimized device performance, was studied by AFM. Figure 6.3c is the AFM image of crosslinked film **5** on top of ITO, and Figure 6.3d is for crosslinked film **6** on top of the assembly of film **5** on ITO. It was found that both thin films have excellent smoothness with a root-mean-square (RMS) surface roughness of 0.75 nm and 1.29 nm, respectively. These results suggest that films of these crosslinkable iridium complexes provide a good interface with subsequently deposited layers, thus making them suitable for device applications.
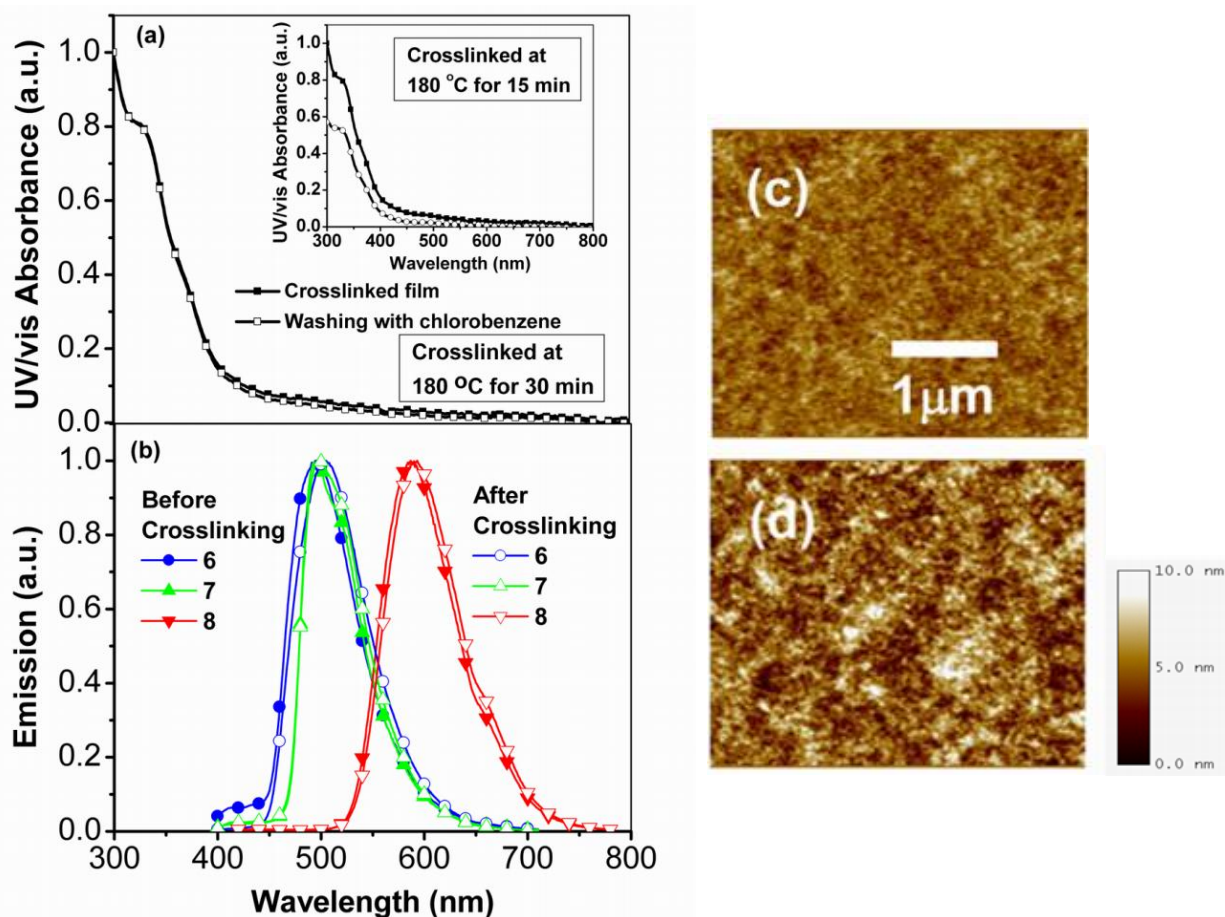
Figure 6.3. a) UV/vis absorbance of the film (**5**), containing pure compound **1**, before (■) and after thermal treatment (□): heating at 180 °C for 30 minutes, followed by thorough solvent rinsing; the inset shows the same data after heating at 180 °C for 15 minutes only. b) Photoluminescent spectra of films (**6**, **7**, **8**), which contain 90 wt. % of compound **1** and 10 wt. % of **2**, **3**, **4**, before thermal crosslinking (filled symbol) and after thermal crosslinking (open symbol). c) AFM of surface topology for the blocking layer (**5**) on top of ITO (RMS 0.75 nm)

after crosslinking and solvent rinsing. d) AFM of surface topology for an emitting layer (**6**) on top of the blocking layer (**5**) after crosslinking and solvent rinsing (RMS 1.29 nm).

Application in OLEDs: crosslinked hole transporting and electron blocking layer

An ideal hole transporting layer (HTL) typically performs multiple ancillary functions including maximizing hole-injection, blocking electron leakage from the emitting layer (EML), and confining excitons within the EML. In order to accomplish this, a material should have a HOMO level comparable to that of the anode, a high LUMO level and a high triplet energy. However, it has proven extremely difficult to obtain a single material fulfilling all of these requirements. Instead, bilayer type HTLs have been applied to provide cascade hole-injection/transport and effective electron-blocking/exciton confinement for solution processed devices.[17,18] The iridium complex discussed here can act as a single crosslinkable hole transporting and electron blocking material **1**. The material is a derivative of facial Ir(PPZ)$_3$, which has triplet energy of 3.4 eV, HOMO of 5.1 eV and LUMO of 1.7 eV. With this multifunctional crosslinkable iridium complex, one can achieve high performing devices with significantly simplified device fabrication at potentially low cost, as one crosslinked film **5** can work as both hole transporting and electron blocking layers.

In order to evaluate the effectiveness of compound **1** as an effective crosslinkable HTL/EBL material (precursor of insoluble film **5)**, we studied three different test configurations of polymer LEDs. Therefore, three devices were fabricated having structure **I** consisting of the following successive layers: ITO/EML/LiF/Al, structure **II** with ITO/**5**/EML/LiF/Al, and structure **III** with ITO/ **5**/EML/Cs$_2$CO$_3$/Al. For device structures **II** and **III**, the 25nm thick crosslinked layer of **5** was prepared on top of ITO by spin coating 12 mg/ml chlorobenzene solutions of **1** followed by thermal treatment at 180 °C for 30 min. The EML (80nm) for all three devices consisted of a polymer host (triphenylamine-oxadiazole block copolymer TPA-b-OXA) doped with 8 wt% of a green emitting iridium complex (TPY$_2$Iracac).[28] The cathodes, either LiF(1nm)/Al(100nm) or Cs$_2$CO$_3$ (3nm)/Al (100nm), were obtained by thermal vapor deposition in a high vacuum chamber (~2×10^{-6} Torr).

Figure 6.4 shows the electroluminescence of the three test polymer LEDs, all involving the pure emission of the green emitting iridium complex dopant.[20,28] Performance of the various devices is shown in Figure 6.5 with the current density-voltage and brightness-voltage characteristics (Fig. 6.5a), as well as external quantum efficiency and power efficiency vs. current density (Fig. 6.5b). Table 6.1 summarizes several important device characteristic values captured from Figure 6.5. As seen in these data, device performance is dramatically improved upon the insertion of blocking layer **5**. As shown in Figure 6.5a, the device with structure **II** has a lower turn-on voltage, a higher current density and a higher brightness at the same bias than the device with structure **I**. Such enhanced performance can be attributed to two major contributions: (i) the high LUMO level of the crosslinked layer, which confines exciton formation to the EML, and blocks electron leakage into the ITO anode (see the schematic energy diagram in the inset of Fig. 6.4); (ii) the crosslinked layer of **5** acts as a cascade layer decreasing the injection barrier between the ITO and the emitting layer, thus affording better hole injection into the emitting layer. Overall, the device with structure **II**, which benefits from the presence of the crosslinked layer of **5** shows a greatly improved external quantum efficiency η_{max} of ~10%, as opposed to η_{max} of ~5 % for the device with structure **I** without the hole transporting/electron blocking layer.

77

Similarly, the power efficiency of the device increases from 3.7 lm/W (for device structure **I**) to 9.0 lm/W (for device structure **II**). Finally, device structure **III** using Cs_2CO_3, instead of LiF, as the electron injection layer to increase electron density in the device[29, 30], shows the lowest turn-on voltage, highest current density and highest brightness at the same bias, with a maximum power efficiency of 14.2 lm/W while maintaining a very high external quantum efficiency, η_{max} ~9.2 %.
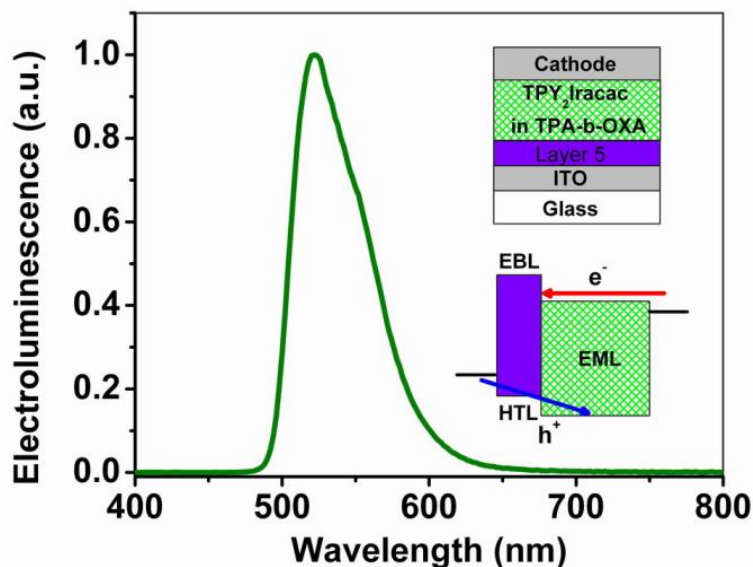
Figure 6.4. The electroluminescent spectrum of devices with three different structures **I**, **II** and **III**; the inset shows the device structures **II** and **III**, as well as the schematic mechanism for the crosslinked film **5** as HTL/EBL.
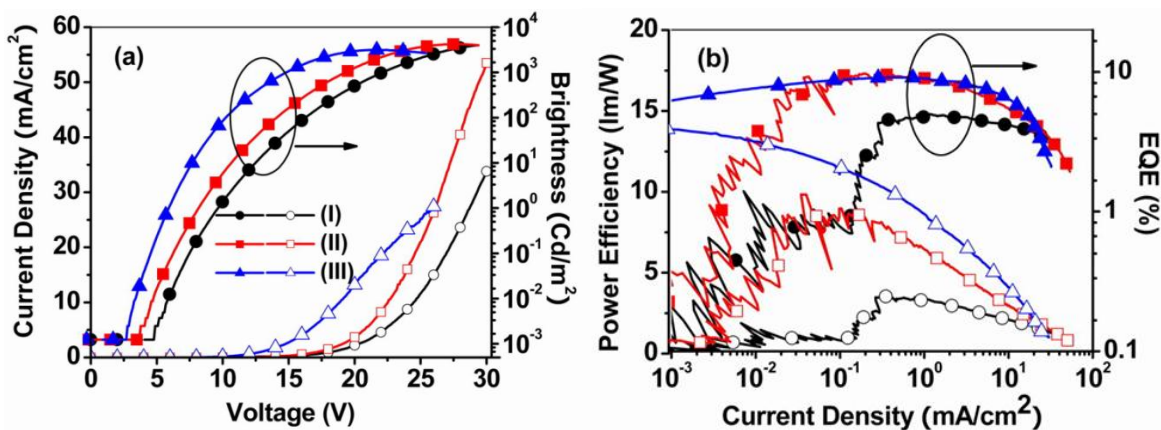
Figure 6.5. (a) Current density - voltage (open symbols) and brightness - voltage (filled symbols) characteristics for device structures **I** (circle), **II** (square) and **III** (triangle). (b) Power efficiency-current density (open symbols) and external quantum efficiency - current density (filled symbols) for those three devices.

78

Table 6.1. Performance data of the devices with structures **I**, **II**, and **III**.

Device	Turn-on voltage (@ 0.1 Cd/m^2)	Maximum E.Q.E., Brightness	Maximum Brightness, Voltage	E.Q.E @ 800 Cd/m^2	Maximum Power Efficiency
I	8 V	5.0 %, 225 Cd/m^2	4000 Cd/m^2, 30 V	4.5 %	3.7 lm/W
II	6.8 V	9.8 %, 125 Cd/m^2	4200 Cd/m^2, 28 V	7.8 %	9.0 lm/W
III	5.1 V	9.2 %, 145 Cd/m^2	3200 Cd/m^2, 22.5 V	8.4 %	14.2 lm/W

Multilayer all solution processed OLEDs

Apart from demonstrating the usefulness of the crosslinked HTL/EBL layer of polymer **5**, it is also desirable to develop a crosslinkable emissive layer. The availability of these two crosslinkable layers would provide access to multilayer monochromatic or near white phosphorescent OLED devices assembled entirely through solution processing as shown in Scheme 6.2.
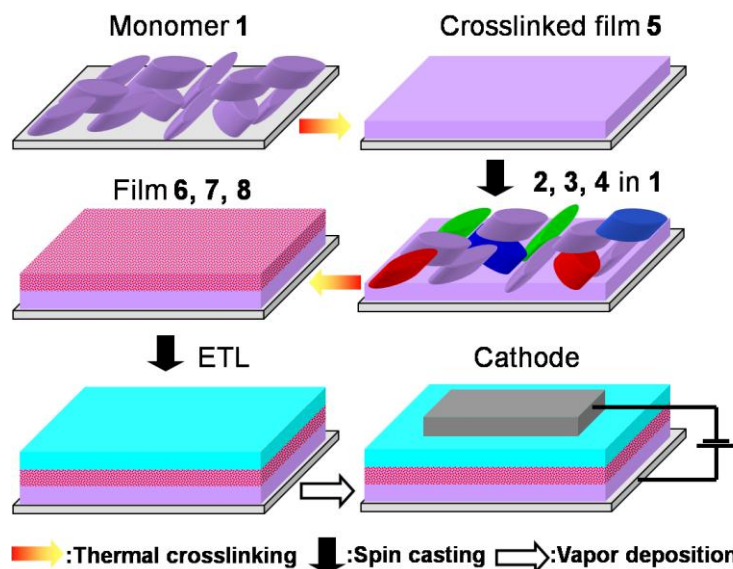

Scheme 6.2. Multilayer structures achieved via full solution processing that involves spin casting and thermal crosslinking.

Monochromatic emitting devices were prepared with the device configuration ITO/**5**/EML (**6**, or **7**, or **8**)/ETL/LiF/Al, in which a layer **5** was prepared on top of ITO as described in the previous sections. Solutions containing 90 wt. % of **1** as host and 10 wt. % of complexes **2**, or **3** or **4** as guest were then spun cast on top of crosslinked **5** and cured at 180 °C for 30 min to form 40 nm thick crosslinked films of **6**, or **7**, or **8**, followed by spin casting of a 40 nm thick electron transporting layer (ETL) of an oxadiazole homopolymer (see its chemical structure in the inset of Figure 6.6), and finally deposition of a cathode (1nm of LiF and 100nm

Al). Figure 6.6 shows the electroluminescent spectra of these three devices, which are almost identical to the photoluminescence spectra of films **6**, **7** and **8** shown previously in Figure 6.3b.

A device with near white emission was also fabricated using emitting layer **9** consisting of 1.5 wt. % of compound **4** (red-emitting) doped into host compound **2** (blue-green emitting). Figure 6.7 shows the near-white electroluminescent spectra with a CIE of (0.41, 0.49) and a CRI of 65, in which the high energy emission originates from compound **2** and the low energy emission from compound **4**. It should be noted that this device shows good color stability at different voltages, because the device operates through exciton formation primarily in the high energy species with energy transfer to low energy species.[5, 31]
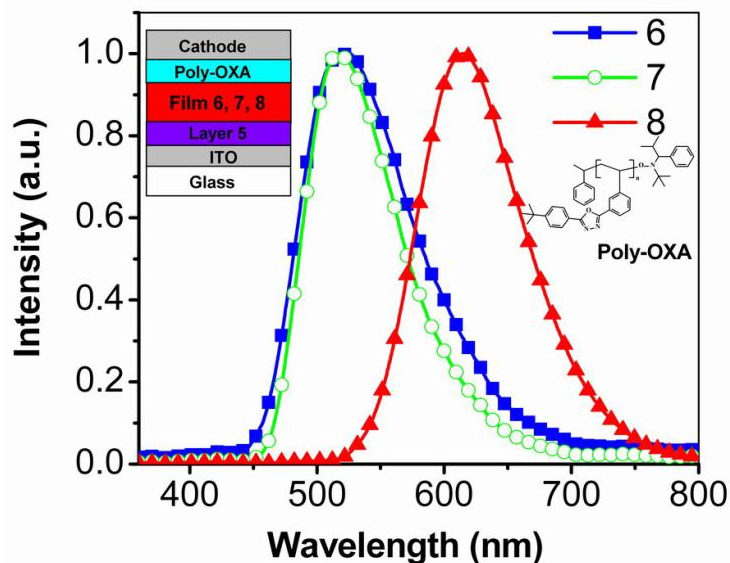

Figure 6.6. The electroluminescent spectra of devices with crosslinked emitting layers **6**, **7** and **8**, which contain compound **1** as host and compound **2**, **3**, and **4** as dopants; the insets show the device structure and the chemical structure of the oxadiazole homopolymer.
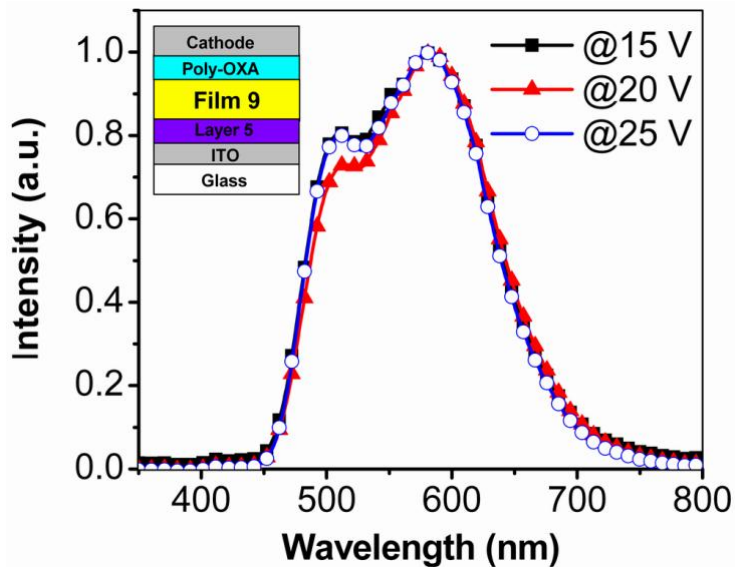
Figure 6.7. The electroluminescent spectra of the device with crosslinked emitting layer **9** (1.5 wt. % of compound **4** in compound **2**) at various driving voltages; the inset shows the device structure.

The device performance of the various monochromatic and near white OLEDs are shown in Figure 6.8. These solution processed devices gave a light output of ~400 cd/m^2 at 20-25 V, with a maximum external quantum efficiencies over 2 %. The relatively low brightness and external quantum efficiency, in comparison to polymer host-iridium dopant devices described above, is likely due to several factors. First, the emission quantum yield of these new complexes with PPZ ligand is lower than that of (TPY)$_2$Iracac. Second, these compounds perform much better as hole transporters than as electron transporters leading to an imbalance between holes and electron while a better balance is achieved in the TPA-OXA host based devices. Overall, while device performance does not yet match the state of art, but these findings validate the strategy of using crosslinkable emitting materials to enable low cost solution processing. Other crosslinkable iridium complexes for improved device performance may prove useful. It is believed that the quantum efficiency of crosslinkable emitters can be improved by using other C^N ligands rather than PPZ and that the charge imbalance issue may be resolved by incorporating iridium complexes with electron transporting moieties.
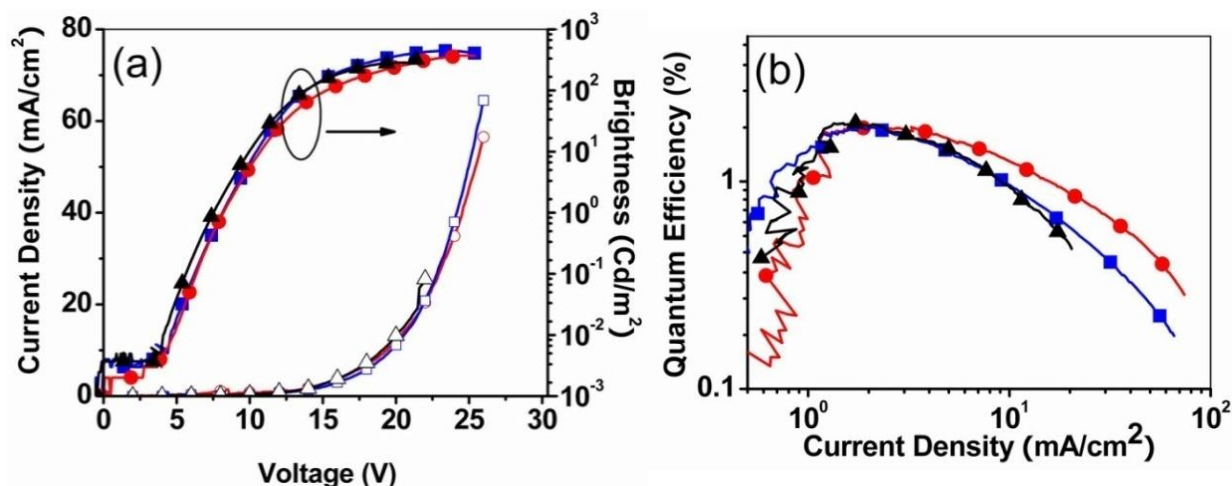
Figure 6.8. (a) Current density - voltage (open symbols) and brightness - voltage (filled symbols) characteristics for monochromatic devices with film **6** (square), film **8** (circle), and near white device with film **9** (triangle). (b) External quantum efficiency - current density for the three devices.

Conclusion

This chapter has discussed the development of a new family of thermally crosslinkable iridium complexes, which can be applied in efficient phosphorescent OLEDs as hole transporting/electron blocking materials, host and emitting materials. The use of two covalently bonded benzyl vinyl ether groups allows the thermal insolubilization of films of these cyclometallated iridium complexes. The excellent solvent resistance and surface smoothness of the fully crosslinked films enables the subsequent solution processing of multilayer structures.

By changing the cyclometallating ligands in these heteroleptic iridium complexes, we have been able to achieve blue-green, red and near-white phosphorescent OLEDs.

Experimental

Materials. Cs_2CO_3 and Al were purchased from Alfa Aesar (Purity > 99.99 %), and LiF (fused pieces 99.995 %) from Aldrich. ITO-coated glass sheets were purchased from Thin Film Devices Inc., green emitting (TPY)$_2$Iracac, TPA-OXA block copolymer host and oxadiazole homopolymer were prepared according to previously reported procedures.[2,32]

Synthesis of crosslinkable iridium complexes. Unless otherwise noted, all reagents were used as received and without further purification, or were prepared according to literature procedures. Chromatography was carried out with Merck silica gel for flash columns, 230-400 mesh. Unless otherwise specified, extracts were dried over $MgSO_4$ and solvents were removed with a rotary evaporator under reduced pressure.

All NMR spectra were measured in either CD_2Cl_2 or $CDCl_3$ with TMS or solvent signals as the standards. High-resolution mass spectrometry (HRMS) was performed with a Micromass LCT using electrospray ionization (ESI) and Micromass ProSpec using fast atom bombardment (FAB). Elemental analyses were performed at the analytical facility of the University of California, Berkeley.

(PPZCHO)₂IrPPZ. *fac-bis(4-Pyrazol-1-yl-benzaldehyde)-(1-phenylpyrazole) iridium (III).* A mixture of [Ir(PPZCHO)$_2$Cl]$_2$ (2.3 g, 2 mmol), phenylpyrazole (1.15 g, 8 mmol), $AgCF_3SO_4$ (1.12 g, 4.4 mmol), and diglyme (20 mL) was purged with nitrogen for 30 minutes before the reaction vessel was sealed and heated to 115°C under continuous stirring for 24 hours. The resulting dark solution was cooled to room temperature (rt) and filtered to remove AgCl. Hexane was added then to the filtrate while under continuous stirring to precipitate the products. The precipitate was then dissolved in dichloromethane and chromatographed on silica gel with dichloromethane as eluent. Ir(PPZ)$_3$ eluted first, followed by (PPZCHO)Ir(PPZ)$_2$, (PPZCHO)$_2$Ir(PPZ) and Ir(PPZCHO)$_3$. (PPZCHO)$_2$Ir(PPZ) was isolated as a light yellow solid in 30% yield. ^{1}H NMR (400 MHz, CD_2Cl_2) δ ppm: 9.73 (s, 1H), 9.69 (s, 1H), 8.19 (dd, J = 4.51, 2.86, 2H), 8.12 (d, J = 2.74, 1H), 7.58-7.50 (m, 2H), 7.43 (dd, J = 10.70, 8.21, 2H), 7.36-7.29 (m, 2H), 7.23 (d, J = 1.81, 1H), 7.02 (d, J = 0.99, 2H), 7.08 (d, J = 2.09, 1H), 7.15 (dd, J = 9.38, 2.02, 1H), 6.81 (dd, J = 7.24, 1.17, 1H), 6.76 (dd, J = 7.44, 1.44, 1H), 6.58 (dd, J = 4.62, 1.90, 2H), 6.53-6.49 (m, 1H).

(PPZCOH)₂IrPPZ. *fac-bis(4-Pyrazol-1-yl-benzylalcohol)-(1-phenylpyrazole) iridium (III).* Compound (PPZCHO)$_2$IrPPZ (0.5 g, 0.74 mmol) was dissolved in 50 mL dichloromethane, addition of a solution of $NaBH_4$ (0.12 g, 3.2 mmol) in 30mL ethanol was accompanied by a color change from bright yellow to colorless. The reaction mixture was stirred at rt for 12 hours and then quenched by the addition of water (200 mL). The resulting solution was extracted twice with CH_2Cl_2 (2×100 mL). The organic layers were combined, washed with water and dried over magnesium sulfate. The solvent was removed to give the target compound (PPZCOH)$_2$IrPPZ in 95% yield.

(PPZ-VB)₂IrPPZ (1). A mixture of (PPZCOH)$_2$IrPPZ (410 mg, 0.6 mmol), KH (30 wt% in oil, 640 mg, 4.8 mmol), KI (200 mg, 1.2 mmol), 18-crown-6 (80 mg, 0.3 mmol), and vinyl benzyl chloride (460 mg, 3 mmol) in THF (30 mL) was stirred at rt for 48 hours. The reaction was quenched by adding water and the resulting solution was then extracted with ethyl acetate/water. The extract was purified by column chromatography over silica gel with a mixture

of dichloromethane and ethyl acetate 19:1 as eluent. The product was isolated as white powder in 60% yield. ^{1}H NMR (500 MHz, CD_2Cl_2) δ ppm 8.06 (s, 3H), 7.34 (t, J = 8.1, 4H), 7.25 (t, J = 7.1, 3H), 7.17 (t, J = 9.0, 4H), 7.03 (d, J = 3.5, 3H), 6.95 (q, J = 8.5, 3H), 6.67-6.82 (m, 6H), 6.46 (s, 3H), 5.76 (d, J = 5.9, 1H), 5.72 (d, J = 5.9, 1H), 5.23 (d, J = 4.8, 1H), 5.21 (d, J = 4.8, 1H), 4.34 (d, J = 3.0, 2H), 4.33, (s, 2H), 4.29 (s, 2H), 4.24 (s, 2H). MS: m/z calcd 914.2920; found 914.2912. CHN Anal. Calcd for $C_{47}H_{41}IrN_6O_2$: C, 61.67; H, 4.52; N, 9.19. Found: C, 61.97; H, 4.26; N, 8.81.

(PPZ-VB)$_2$IrDFPPY (2). The procedure used in the preparation of (PPZVB)$_2$IrPPZ was employed. The product was isolated as yellow green powder in 20% yield. ^{1}H NMR (400 MHz, CD_2Cl_2) δ ppm: 8.30-8.23 (m, 1H), 8.08 (d, J = 2.65, 2H), 7.80-7.75 (m, 1H), 7.73-7.65 (m, 1H), 7.39-7.30 (m, 3H), 7.25 (d, J = 2.90, 2H), 7.17 (dd, J = 11.10, 8.16, 4H), 6.95 (dd, J = 7.31, 4.93, 5H), 6.78-6.64 (m, 5H), 6.51-6.37 (m, 2H), 5.79-5.69 (m, 2H), 5.26-5.17 (m, 2H), 4.30 (dd, J = 23.69, 14.72, 8H). MS: m/z calcd 961.2779; found 961.2772. CHN Anal. Calcd for $C_{49}H_{40}F_2IrN_5O_2$: C, 61.24; H, 4.19; N, 7.29. Found: C, 62.00; H, 4.35; N, 7.08.

(PPZ-VB)$_2$IrTPY (3). The procedure used for the preparation of (PPZVB)$_2$IrPPZ was employed. The product was isolated in 22% yield as a yellow green powder. ^{1}H NMR (400 MHz, CD_2Cl_2) δ ppm: 8.07 (d, J = 1.99, 2H), 7.83 (m, 1H), 7.72-7.52 (m, 3H), 7.39-7.29 (m, 3H), 7.25 (dd, J = 7.96, 4.99, 2H), 7.17 (d, J = 7.98, 4H), 7.02-6.84 (m, 5H), 6.83-6.61 (m, 5H), 6.52-6.39 (m, 2H), 5.73 (dd, J = 17.62, 4.96, 2H), 5.22 (dd, J = 10.85, 4.31, 2H), 4.59-4.00 (m, 8H), 2.08 (s, 3H). MS: m/z calcd 939.3124; found 939.3121. CHN Anal. Calcd for $C_{50}H_{44}IrN_5O_2$: C, 63.95; H, 4.72; N, 7.46. Found: C, 64.22; H, 4.64; N, 7.30.

(PPZ-VB)$_2$IrPQ (4). The procedure described above for the preparation of (PPZVB)$_2$IrPPZ was employed. The product was isolated in 18% as an orange powder. ^{1}H NMR (500 MHz, CD_2Cl_2) δ ppm 8.13 (s, 2H), 8.08 (d, J = 2.7, 1H), 8.03 (d, J = 2.7, 1H), 7.89 (d, J = 7.9, 1H), 7.77 (t, J = 10.0, 2H), 7.33-7.38 (m, 5H), 7.13-7.26 (m, 7H), 6.96-7.02 (m, 3H), 6.86-6.92 (m, 3H), 6.81 (t, J = 7.4, 1H), 6.71 (dt, J = 9.8, 17.5, 2H), 6.58 (s, 1H), 6.54 (s, 1H), 6.47 (t, J = 2.0, 1H), 6.38 (t, J = 2.0, 1H), 5.76 (d, J = 5.7, 1H), 5.73 (d, J = 5.7, 1H), 5.22 (d, J = 5.7, 1H), 5.21 (d, J = 5.7, 1H), 4.29 (s, 2H), 4.26, (s, 2H), 4.24 (s, 2H), 4.22 (s, 2H). MS: m/z calcd 975.3124; found 975.3137. CHN Anal. Calcd for $C_{53}H_{44}IrN_5O_2$: C, 65.28; H, 4.55; N, 7.18. Found: C, 65.41; H, 4.45; N, 6.79.

Optical Measurements. Ground-state UV/vis absorption spectra were measured on either a Cary 50 UV-vis spectrometer or a Cary 500 spectrophotometer. Emission and excitation spectra were obtained using an ISA/SPEX Fluorolog 3.22 equipped with a 450W Xe lamp, double excitation and double emission monochromators, and a digital photon-counting photomultiplier. Slit widths were set to a 2 nm band-pass on both excitation and emission monochromators. Samples for absorbance and emission experiments were measured in standard 1 cm quartz cells. All measurements were performed at room temperature.

Devices Fabrication and Measurement. Indium-tin oxide (ITO)-coated glass substrates were sequentially cleaned by sonication in soap solution; rinsed with deionized water; boiled in trichloroethylene, acetone, and ethanol for 5 minutes each; and dried under nitrogen. Finally, the substrates were treated using a UVOCS ultraviolet/ozone cleaner for 10 mins. The crosslinked layer of **5** was prepared by spin-casting (2000 RPM for 40 seconds) a 12 mg/ml solution of **1** in chlorobenzene on top of the ITO then heating the film at 180 °C for 30 mins. This afforded a 25 nm thick layer of **5** with excellent surface smoothness (RMS roughness of 0.75 nm). The polymer host-iridium guest EML with a thickness of ~80 nm was prepared by spin casting (3000 RPM for 40 seconds) a 32 mg/ml chlorobenzene solution containing 8 wt. % (TPY)$_2$Iracac.

Crosslinked EML of **6**, **7**, or **8** with a thickness of ~30 nm was prepared as described above for **5**. The solutions used to prepare the EML consisted of 90 wt. % of **1** (as host) and 10 wt. % of **2**, or **3**, or **4** (as guest) to produce blue-green and red emissions, respectively. For fully solution processed OLEDs, a 15 mg/ml solution of oxadiazole homopolymer in chlorobenzene was spun cast on top of the EML, working as electron transporting layer (ETL). Once the solution deposition of the various organic films was completed in an inert-atmosphere glove box, a cathode consisting of 1 nm LiF (or 3 nm Cs_2CO_3) and 100 nm Al was deposited at a rate of 0.2 Å/s and 4-5 Å/s respectively, in a vacuum chamber standing in air with a base pressure $< 3 \times 10^{-6}$ Torr. OLEDs were formed in 2×2 mm squares at the intersections of the ITO anode and the striped Al cathode.

The devices were tested in air within 2 hrs after fabrication. The electrical and optical intensity characteristics of the devices were measured with a Keithly 2400 sourcemeter/2000 multimeter coupled to a Newport 1835-C optical meter, equipped with a UV-818 Si photodetector. Only light emitted from the front face of the device was collected and used in subsequent efficiency calculations. The electroluminescence (EL) spectra were measured on a USB4000 Miniature Fiber Optic Spectrometer. The emission was found to be uniform throughout the area of each device.

References

(1)   Baldo, M. A.; Thompson, M. E.; Forrest, S. R. *Nature* **2000**, *403*, 750.
(2)   Lamansky, S.; Djurovich, P.; Murphy, D.; Abdel-Razzaq, F.; Lee, H. E.; Adachi, C.; Burrows, P. E.; Forrest, S. R.; Thompson, M. E. *J. Am. Chem. Soc.* **2001**, *123*, 4304.
(3)   Lamansky, S.; Djurovich, P. I.; Abdel-Razzaq, F.; Garon, S.; Murphy, D. L.; Thompson, M. E. *J. Appl. Phys.* **2002**, *92*, 1570.
(4)   Tamayo, A. B.; Alleyne, B. D.; Djurovich, P. I.; Lamansky, S.; Tsyba, I.; Ho, N. N.; Bau, R.; Thompson, M. E. *J. Am. Chem. Soc.* **2003**, *125*, 7377.
(5)   D'Andrade, B. W.; Holmes, R. J.; Forrest, S. R. *Adv. Mater.* **2004**, *16*, 624.
(6)   Li, J.; Djurovich, P. I.; Alleyne, B. D.; Yousufuddin, M.; Ho, N. N.; Thomas, J. C.; Peters, J. C.; Bau, R.; Thompson, M. E. *Inorg. Chem.* **2005**, *44*, 1713.
(7)   Sajoto, T.; Djurovich, P. I.; Tamayo, A.; Yousufuddin, M.; Bau, R.; Thompson, M. E.; Holmes, R. J.; Forrest, S. R. *Inorg. Chem.* **2005**, *44*, 7992.
(8)   Rehmann, N.; Ulbricht, C.; Kohnen, A.; Zacharias, P.; Gather, M. C.; Hertel, D.; Holder, E.; Meerholz, K.; Schubert, U. S. *Adv. Mater.* **2008**, *20*, 129.
(9)   Baldo, M. A. O'Brien, D. F.; Thompson, M. E.; Forrest, S. R. *Phys. Rev. B: Condens. Matter.* **1999**, *60*, 14422.
(10)   Adamovich, V. I.; Cordero, S. R.; Djurovich, P. I.; Tamayo, A.; Thompson, M. E.; D'Andrade, B. W.; Forrest, S. R. *Org. Electron.* **2003**, *4*, 77.
(11)   Kanno, H.; Ishikawa, K.; Nishio, Y.; Endo, A.; Adachi, C.; Shibata, K. *Appl. Phys. Lett.* **2007**, *90*, 123509.
(12)   Nuyken, O.; Jungermann, S.; Wiederhirn, V.; Bacher, E.; Meerholz, K. *Monatsh. Chem.* **2006**, *137*, 811.
(13)   Gong, X.; Wang, S.; Moses, D.; Bazan, G. C.; Heeger, A. J. *Adv. Mater.* **2005**, *17*, 2053.
(14)   Bacher, A.; Erdelen, C. H.; Paulus, W.; Ringsdorf, H.; Schmidt, H. W.; Schuhmacher, P. *Macromolecules* **1999**, *32*, 4551.
(15)   Bayerl, M. S.; Braig, T.; Nuyken, O.; Muller, D. C.; Gross, M.; Meerholz, K. *Macromol. Rapid Commun.* **1999**, *20*, 224.

(16) Muller, C. D.; Falcou, A.; Reckefuss, N.; Rojahn, M.; Wiederhirn, V.; Rudati, P.; Frohne, H.; Nuyken, O.; Becker, H.; Meerholz, K. *Nature* **2003**, *421*, 829.
(17) Yan, H.; Scott, B. J.; Huang, Q. L.; Marks, T. J. *Adv. Mater.* **2004**, *16*, 1948.
(18) Niu, Y. H.; Liu, M. S.; Ka, J. W.; Jen, A. K. Y. *Appl. Phys. Lett.* **2006**, *88*, 093505.
(19) Zhao, J. L.; Bardecker, J. A.; Munro, A. M.; Liu, M. S.; Niu, Y. H.; Ding, I. K.; Luo, J. D.; Chen, B. Q.; Jen, A. K. Y.; Ginger, D. S. *Nano Lett.* **2006**, *6*, 463.
(20) Ma, B.; Lauterwasser, F.; Deng, L.; Zonte, C. S.; Kim, B. J.; Fréchet, J. M. J.; Borek, C.; Thompson, M. E. *Chem. Mater.* **2007**, *19*, 4827.
(21) Niu, Y. H.; Liu, M. S.; Ka, J. W.; Bardeker, J.; Zin, M. T.; Schofield, R.; Chi, Y.; Jen, A. K. Y. *Adv. Mater.* **2007**, *19*, 300.
(22) Faber, R.; Stasko, A.; Nuyken, O. *J. Macromol. Sci. Part A Pure Appl. Chem.* **2001**, *38*, 353.
(23) Dedeian, K.; Shi, J. M.; Shepherd, N.; Forsythe, E.; Morton, D. C. *Inorg. Chem.* **2005**, *44*, 4445.
(24) Nonoyama, M. *Bull. Chem. Soc. Jpn.* **1974**, *47*, 767.
(25) Beeby, A.; Bettington, S.; Samuel, I. D. W.; Wang, Z. J. *J. Mater. Chem.* **2003**, *13*, 80.
(26) Mayo, F. R. *J. Am. Chem. Soc.* **1968**, *90*, 1289.
(27) Cheng, Y. J.; Liu, M. S.; Zhang, Y.; Niu, Y. H.; Huang, F.; Ka, J. W.; Yip, H. L.; Tian, Y. Q.; Jen, A. K. Y. *Chem. Mater.* **2008**, *20*, 413.
(28) Ma, B.; Kim, B. J.; Deng, L.; Poulsen, D. A.; Thompson, M. E.; Fréchet, J. M. J. *Macromolecules* **2007**, *40(23)*, 8156.
(29) Huang, J. S.; Z. Xu, Y. Yang, *Adv. Funct. Mater.* **2007**, *17*, 1966.
(30) Li, Y.; Zhang, D. Q.; Duan, L.; Zhang, R.; Wang, L. D.; Qiu, Y. *Appl. Phys. Lett.* **2007**, *90*.
(31) Ma, B. W.; Djurovich, P. I.; Garon, S.; Alleyne, B.; Thompson, M. E. *Adv. Funct. Mater.* **2006**, *16*, 2438.
(32) Deng, L.; Furuta, P. T.; Garon, S.; Li, J.; Kavulak, D.; Thompson, M. E.; Fréchet, J. M. J. *Chem. Mater.* **2006**, *18*, 386.